

Unified Micromechanics Theory of Composites

Valeriy A. Buryachenko *

Micromechanics & Composites LLC, Cincinnati, Ohio 45202, USA

Abstract

We consider the matrix composite materials (CM) of either random (statistically homogeneous or inhomogeneous), periodic, or deterministic (neither random nor periodic) structures. CMs exhibit linear or nonlinear behavior, coupled or uncoupled multi-physical phenomena, locally elastic, weakly nonlocal (strain gradient and stress gradient), or strongly nonlocal (strain-type and displacement-type, peridynamics) phase properties. A modified Computational Analytical Micromechanics (CAM) approach introduces an exact Additive General Integral Equation (AGIE) for CMs of any structure and phase properties. This method utilizes a unified iteration solution for static AGIEs, incorporating a new universal training parameter based on body forces with compact support. CAM based on a general integral equation (GIE) and proposed by the author before, is modified by the introduction of the exact AGIE which applies to CMs of any structure and phase properties mentioned above. The unified iteration solution of static AGIEs is adapted to the body force with compact support serving as a fundamentally new universal training parameter. The approach also establishes a critical threshold for filtering out unsuitable sub-datasets of effective parameters through a novel Representative Volume Element (RVE) concept, which extends Hill’s classical framework. This RVE concept eliminates sample size, boundary layer, and edge effects, making it applicable to CMs of any structure and phase properties, regardless of local or nonlocal, linear or nonlinear. Incorporating this new RVE concept into machine learning and neural network techniques enables the construction of any unpredefined surrogate nonlocal operators. The methodology is structured as a modular, block-based framework, allowing independent development and refinement of software components. This flexible, robust AGIE-CAM framework integrates data-driven, multi-scale, and multi-physics modeling, accelerating research in CM of any microtopology and phase properties considered.

Keywords: Microstructures; inhomogeneous material; peridynamics; non-local methods; multiscale modeling

Table of Contents

1. Introduction.....	2
2. Preliminaries.....	6
2.1 Basic equations of peridynamics.....	6
2.2 Volumetric boundary conditions.....	11
2.3 Descriptions of random and periodic structures.....	12
2.4 Some averages	15
3. Decomposition of the material and field parameters.....	16
3.1 Decomposition of the material parameters	16

*buryach@yahoo.com

3.2 Analytical and Computational Micromechanics in LM.....	18
3.3 Modeling of one inclusion inside the infinite matrix.....	19
3.4 General integral equations (GIEs).....	22
4. Solution of nonlinear AGIEs for random structure CMs.....	24
4.1 Iterative solution of AGIE	25
4.2 Effective constitutive law and dataset.....	25
5. Periodic structure CMs.....	29
6. Estimation of field fluctuations and effective energy-based criteria.....	33
7. CMs with other constitutive laws of phases.....	35
7.1 Locally elastic.....	35
7.2 Strongly nonlocal (strain type) model.....	37
7.3 Coupled problems of composites.....	38
7.4 First Strain Gradient Medium.....	40
7.5 Stress-Gradient Elasticity Model.....	41
8. Representative volume element (EVE).....	43
8.1 RVE for CMs subjected to remote homogeneous loading.....	43
8.2 RVE for CMs subjected to inhomogeneous loading....	44
8.3 RVE for CMs subjected to body force with compact support....	46
8.4 RVE for deterministic structure CMs.....	49
8.5 Classification and schematic representation of CAM	52
9. Estimation of a set of surrogate operators	55
10. Conclusion.....	60
References.....	63

1 Introduction

Predicting the behavior of composite materials based on phase properties and microstructure is a fundamental challenge in micromechanics. Stress field estimations rely on solving a basic problem: an inclusion within an infinite homogeneous matrix under a uniform effective field. When constituents exhibit local elasticity, the solution for an ellipsoidal inclusion in a homogeneous field is given analytically by Eshelby’s tensor [164] (see also [371], [510]). For inclusions of arbitrary shapes, various numerical methods have been developed. Finite element analysis (FEA) and truncation methods approximate the infinite medium with an extended sample. Direct modeling of an infinite medium is achieved using boundary integral equation (BIE) methods [314], [79] or volume integral equation (VIE) approaches [53]. Comprehensive reviews of micromechanical methods can be found in [53], [79], [142], [246], [354], and [442].

Conventional micromechanics assumes materials can be treated as a continuum at arbitrarily small scales, with properties and behaviors that are invariant to time and length scales, excluding size effects [231]. However, real material models need to define an “effective” set of properties, approximating microstructural details below a certain resolution [30]. In cases where scales (material and field) are comparable, nonlocal elasticity theory, developed by authors like Kröner, Eringen, Kunin, and Bažant, incorporates lattice theory with classical elasticity to address these intermediate effects (see [160], [163],

[272], [265], [274], [275],[276], as well as [5], [30], [31], [103], [162], [288], [336], [446] see also comprehensive reviews [405], [443], [445]). “Generalized continuum mechanics,” as defined by [337], covers models beyond the Cauchy framework. Generalized continua can be broadly divided into weakly and strongly nonlocal theories. *Weakly nonlocal theories* involve higher-order models where material points have additional degrees of freedom beyond classical translation, such as rotation [116], stretch [162], or higher-order displacement derivatives [196], [197], [346], [347], which were essentially developed later (see, e.g., the comprehensive reviews [5], [30], [376]). The Cosserat theory [116] treats materials as rigid particles with independent rotations, while the micromorphic theory [159], [161] models a material as particles that can move, deform, and rotate. Micromorphic theory generalizes Cosserat and micropolar theories, incorporating microstretch behavior.

Strongly nonlocal elasticity theory explicitly models long-range interactions using convolutions of kinematical variables, which represent the material’s degrees of freedom. This approach contrasts with weakly nonlocal theories, where nonlocality is introduced implicitly through gradients of micro-deformations and coupling variables. In strongly nonlocal theories, stress is an integral functional of strain, with a kernel that weights material properties. Key contributions to this field came from Kröner [266], [270], and Kunin [275] in the 1960s generalized in [163], [276], [388]. These models can be divided into *strain-type* and *displacement-type* (see [163], [266], [270], [274], [275], [278], [388]), with the displacement-type model reducible to the strain-type model [277].

Under certain conditions, strain gradient elasticity can approximate integral non-local theory. Nonlocal microcontinuum mechanics [162], [163] was developed as a more general form of nonlocal mechanics. Eringen [163] presented a unified approach to nonlocal field theories for various media: elastic solids, viscous fluids, electromagnetic solids, and fluids, memory-dependent elastic solids, and media with microstructure. *Peridynamics (PD)*, introduced by Silling [413] and discussed in [337] and [423], is a special displacement-type nonlocal theory that eliminates displacement derivatives. Peridynamics by Silling [413] (see also [41], [136], [240], [328], [366], [414], [422], [423]), revolutionized solid mechanics by replacing local partial differential equations with integral equations that avoid spatial derivatives of displacement. In this approach, the equilibrium at a material point is determined by the sum of internal forces from surrounding points within a defined “horizon.” Unlike classical mechanics, which relies on local interactions, peridynamics uses a *state-based model* (SB) where the deformation at a point is influenced by all bonds within the horizon. This method naturally handles discontinuities like cracks, making it ideal for studying failure and damage propagation. The *bond-based* (BB) peridynamic approach models interactions between pairs of points within a horizon but limits the Poisson’s ratio in isotropic materials to specific values of $\nu = 1/4$ (3D and 2D plane strain) or $\nu = 1/3$ (2D plane stress) [413]. The correspondence model (see [2], [419]) allows peridynamics to replicate the classical elasticity tensor for fully anisotropic materials. Non-ordinary state-based models offer more flexibility but can be unstable, requiring careful numerical methods for accurate results

(see [448] for details). In contrast, the ordinary state-based model [395] overcomes these issues by accurately reproducing any component of the classical continuum mechanics (CCM) elasticity tensor in both 2D and 3D. Tensor-based peridynamics [440] expands on the BB model, enhancing its adaptability for both isotropic and anisotropic materials.

Foundational principles for thermoperidynamic media under uniform volumetric boundary loading were proposed using the linearized bond-based peridynamic approach (see [60], [67], [84]). A key outcome is that the effective behavior of these media can be described by a local effective constitutive equation, similar to classical thermoelasticity [53]. The relationship between effective properties and influence functions, which describe mechanical interactions within the material, highlights how one region's behavior affects others. This is achieved by decomposing local fields into load and residual fields, allowing an energetic definition of the effective elastic moduli. There is a notable similarity between locally elastic composites and peridynamic composites, as both follow principles like Hill's condition and the self-adjoint nature of the peridynamic operator. This allows classical solutions to be extended to nonlocal peridynamic systems, offering a contrast to simplified methods like mixture theory and scale separation hypothesis (see [16], [17], [18], [112], [133], [178], [224], [226], [296], [328], [330], [331], [339], [385], [466], [467], [472], [480]).

The expansion of Local Micromechanics (LM) from classical continuum mechanics (CCM) to nonlocal phenomena (see [60], [67], [79], [93]) is driven by the General Integral Equation (GIE, see [60], [67], [79]) for microinhomogeneous media. This method, also called computational analytical micromechanics (CAM), does not rely on Green's functions or specific constitutive laws, making it more versatile. The GIE significantly improves accuracy in local field estimations and can even lead to correcting the sign of estimations inside inclusions (see [79])

In locally elastic composite materials (CMs) under inhomogeneous loading, effective deformations are governed by nonlocal operators (differential or integral, see [53], [79], [144], [416], [452]), which relate the statistical average of fields at a point to those in the surrounding area. These operators improve material modeling accuracy, especially for inhomogeneous media, nonlinear or nonlocal laws, and coupled processes. The CAM is particularly effective for addressing multiscale and multiphysics problems, enabling precise simulations of small-scale effects by incorporating homogenized surrogate models. This framework provides a robust approach for analyzing random and periodic structure CMs.

The study of periodic structure composites benefits from the regularity of their microstructure, allowing for specialized homogenization techniques [174], [190], [514]. Asymptotic homogenization, introduced by Babuska, analyzes composites where the unit cell is much smaller than the overall material size, approximating the effect of the unit cell on the global response (e.g., [23], [174]). In contrast, computational homogenization explicitly resolves the material's microscopic behavior to determine macroscopic quantities like stress and de-

formation, making it effective for modeling complex behaviors such as nonlinear or inelastic properties (e.g., [262], [334], [439]).

Madenci and colleagues [324] (see also [134], [135], [227], [305],[325], and [453]) advanced computational homogenization by introducing the peridynamic unit cell model, which extends traditional techniques to the peridynamic framework using classical periodic boundary conditions (PBC). The development of volumetric periodic boundary conditions (VPBC) in [70], [72], [79] further generalized these methods for peridynamics. A key innovation in peridynamic homogenization is determining effective material moduli by averaging tractions and displacements along the unit cell boundary [70], [72], [79], offering a simpler, more efficient alternative to methods requiring volume averages of stresses and strains inside the unit cell [182], [185], and [227]. The latter methods are more complex and less general because they require differentiating displacement fields, which may lack smoothness.

The representative volume element (RVE) is crucial for accurately predicting the macroscopic properties of heterogeneous materials. The correct RVE size ensures proper representation of microstructural heterogeneity while avoiding boundary or size effects. Hill's classical definition [216] requires macroscopically homogeneous boundary conditions and defines the effective behavior with a tensor of moduli. RVE size determination involves balancing the capture of microstructural heterogeneities with scale separation, achieved when $a \ll \Lambda \ll L$ (see Subsection 2.3 for details). The smallest size at which properties stabilize is the appropriate RVE. The concept of statistically equivalent representative volume element (SERVE) uses image-based modeling to generate accurate computational domains, with further details found in [26], [251], [334], [352], [365], and others. When the scale separation hypothesis is violated, statistically homogeneous fields no longer apply, leading to nonlocal coupling between stress and strain averages, mediated by a tensorial kernel. This requires using an effective elastic operator in integral form. Nonlocal operators include strongly nonlocal methods (strain type and displacement type, peridynamics) and weakly nonlocal models like strain- or stress-gradient methods. Micromechanics helps bridge coupled scales governed by nonlocal constitutive equations. Instead of classical effective moduli [216], effective nonlocal operators, often in integral or differential form, are required, prompting a redefinition of the representative volume element (RVE). This applies to both random ([138], [139], [140]) and periodic ([13], [263], [264], [425]) composites. The RVE concept is crucial for analyzing nonlocal effects from inhomogeneous fields, material nonlocality, and inclusion interactions.

Machine learning (ML) and neural network (NN) techniques have significantly advanced nonlocal operator theory, improving generality and flexibility. Early work by Silling [417] and [486] (later expanded upon in [488]) used Direct Numerical Simulations (DNS) for the construction of surrogate integral operators. Recent developments include nonlocal neural operators that map function spaces [285], [306], and various NN architectures like DeepONet, PCA-Net, and Fourier Neural Operators (FNO) [194], [228]. Peridynamic Neural Operator (PNO) was proposed in [238] and subsequently extended to the the Het-

erogeneous Peridynamic Neural Operator (HeteroPNO) in [239]. Additionally, Physics-Informed Neural Networks (PINNs) embed physical laws directly into the neural network as constraints (see [117], [205], [209], [221], [252], [259], [382], and [387]). Combining neural operators with PINNs enables modeling complex systems with nonlinearities, heterogeneity, and nonlocality [170], [194], [454].

However, despite the power of ML and NN techniques, they often neglect crucial micromechanical factors like size scale, edge effects, and RVE, important for both linear and nonlinear materials. To overcome this, the proposed CAM generates new compressed datasets for complex material structures (whether random, periodic, or deterministic), using a novel RVE concept that doesn't depend on constitutive laws or surrogate operator forms. Instead, it focuses on field concentration factors within material phases. These datasets, incorporating the new RVE concept, must be used with any ML or NN methods predicting nonlocal surrogate operators, ensuring accurate predictions by eliminating size scale, boundary, and edge effect issues.

The structure of the paper is as follows: Section 2 offers a concise overview of peridynamic theory, tailored to support the subsequent analysis. It includes a discussion on the statistical representation of composite microstructures and describes the volumetric homogeneous displacement loading conditions, alongside certain field averages. Section 3 introduces the decomposition of both material and field parameters. General Integral Equations (GIEs) and Additive GIEs are considered, incorporating either statistical average fields or fields induced in an infinite matrix by a body force with compact support., respectively. Iterative solutions of AGIE are presented for either random or periodic structure CMs in Sections 4 and 5, respectively. Estimation of field fluctuations and effective energy-based criteria are presented in Section 6. AGIEs and datasets are considered in Section 7 for CMs with locally elastic, weakly nonlocal (strain gradient and stress gradient), and strongly nonlocal (strain-type) properties. Classical RVE concepts generalized to nonlocally elastic media are considered in Section 8. A novel RVE concept is introduced specifically for cases involving a body force with compact support. By applying translation averaging to the GIE solutions for periodic structure CMs, statistical averages of fields are derived. Section 9 leverages the body force with compact support as a training parameter to develop a suite of surrogate effective operators of any predefined form for CMs with either random, periodic, or deterministic structures and a wide class of phase properties.

2 Preliminaries.

2.1 Basic equations of peridynamics

One considers a linear elastic medium occupying an open simply connected bounded domain $w \subset \mathbb{R}^d$ with a smooth boundary Γ_0 and with an indicator function W and space dimensionality d ($d = 1, 2, 3$). The domain w with the boundary Γ^0 consists from a homogeneous matrix $v^{(0)}$ and a statistically homogeneous field $X = (v_i)$ of heterogeneity v_i with indicator functions, V_i and

bounded by the closed smooth surfaces Γ_i ($i = 1, 2, \dots$). It is presumed that the heterogeneities can be grouped into phases $v^{(q)}$ ($q = 1, 2, \dots, N$) with identical mechanical and geometrical properties. The basic equations of local thermoelasticity of composites are considered

$$\nabla \cdot \boldsymbol{\sigma}(\mathbf{x}) = -\mathbf{b}(\mathbf{x}), \quad (2.1)$$

$$\boldsymbol{\sigma}(\mathbf{x}) = \mathbf{L}(\mathbf{x})\boldsymbol{\varepsilon}(\mathbf{x}) + \boldsymbol{\alpha}(\mathbf{x}), \quad \text{or} \quad \boldsymbol{\varepsilon}(\mathbf{x}) = \mathbf{M}(\mathbf{x})\boldsymbol{\sigma}(\mathbf{x}) + \boldsymbol{\beta}(\mathbf{x}), \quad (2.2)$$

$$\boldsymbol{\varepsilon}(\mathbf{x}) = [\nabla \otimes \mathbf{u} + (\nabla \otimes \mathbf{u})^\top]/2, \quad \nabla \times \boldsymbol{\varepsilon}(\mathbf{x}) \times \nabla = \mathbf{0}, \quad (2.3)$$

where \otimes and \times are the tensor and vector products, respectively, and $(\cdot)^\top$ denotes a matrix transposition. It is presumed that the body force density (forcing term) $\mathbf{b}(\mathbf{x})$ is self-equilibrated and vanished outside some loading region B^b :

$$\int \mathbf{b}(\mathbf{x}) = \mathbf{0}, \quad \mathbf{y} \notin b(\mathbf{0}, B^b) := \{\mathbf{y} \mid |\mathbf{y}| \leq B^b\}, \quad (2.4)$$

where $b(\mathbf{x}_i, B^b)$ is the ball of radius B^b centered at $\mathbf{x}_i = \mathbf{0}$. $\mathbf{L}(\mathbf{x})$ and $\mathbf{M}(\mathbf{x}) \equiv \mathbf{L}(\mathbf{x})^{-1}$ are the known phase stiffness and compliance tensors. $\boldsymbol{\beta}(\mathbf{x})$ and $\boldsymbol{\alpha}(\mathbf{x}) = -\mathbf{L}(\mathbf{x})\boldsymbol{\beta}(\mathbf{x})$ are second-order tensors of local eigenstrains and eigenstresses. In particular, for isotropic phases, the local stiffness tensor $\mathbf{L}(\mathbf{x})$ is presented in terms of the local bulk $k(\mathbf{x})$ and shear $\mu(\mathbf{x})$ moduli and:

$$\mathbf{L}(\mathbf{x}) = (dk, 2\mu) \equiv dk(\mathbf{x})\mathbf{N}_1 + 2\mu(\mathbf{x})\mathbf{N}_2, \quad \boldsymbol{\beta}(\mathbf{x}) = \beta^t \theta \boldsymbol{\delta},$$

$\mathbf{N}_1 = \boldsymbol{\delta} \otimes \boldsymbol{\delta}/d$, $\mathbf{N}_2 = \mathbf{I} - \mathbf{N}_1$ ($d = 2$ or 3) whereas $\boldsymbol{\delta}$ and \mathbf{I} are the unit second-order and fourth-order tensors; $\theta = T - T_0$ denotes the temperature changes with respect to a reference temperature T_0 and β^t is a thermal expansion. For all material tensors \mathbf{g} (e.g., $\mathbf{L}, \mathbf{M}, \boldsymbol{\beta}, \boldsymbol{\alpha}$) the notation $\mathbf{g}_1(\mathbf{x}) \equiv \mathbf{g}(\mathbf{x}) - \mathbf{g}^{(0)} = \mathbf{g}_1^{(m)}(\mathbf{x})$ ($\mathbf{x} \in v^{(m)}$, $m = 0, 1$) is exploited. The upper index $^{(m)}$ indicates the components, and the lower index i shows the individual heterogeneities; $v^{(0)} = w \setminus v$, $v \equiv \cup v_i$, $V(\mathbf{x}) = \sum V_i(\mathbf{x})$, and $V_i(\mathbf{x})$ are the indicator functions of v_i , equals 1 at $\mathbf{x} \in v_i$ and 0 otherwise, ($i = 1, 2, \dots$). Substitution of Eqs. (2.2) and (2.4) into Eq. (2.1) leads to a representation of the equilibrium equation (2.1) in the form

$${}^L \tilde{\mathcal{L}}(\mathbf{u})(\mathbf{x}) + \mathbf{b}(\mathbf{x}) = \mathbf{0}, \quad {}^L \tilde{\mathcal{L}}(\mathbf{u})(\mathbf{x}) := \nabla[\mathbf{L}\nabla\mathbf{u}(\mathbf{x}) + \boldsymbol{\alpha}(\mathbf{x})], \quad (2.5)$$

where ${}^L \tilde{\mathcal{L}}(\mathbf{u})(\mathbf{x})$ is an elliptic differential operator of the second order.

In this section, a summary of the linear peridynamic model introduced by Silling [413] (see also [294], [328], [418], [422], [423]) is presented. An equilibrium equation is free of any derivatives of displacement (contrary to Eq. (2.5)) and presented in the following form

$$\tilde{\mathcal{L}}(\mathbf{u})(\mathbf{x}) + \mathbf{b}(\mathbf{x}) = \mathbf{0}, \quad \tilde{\mathcal{L}}(\mathbf{u})(\mathbf{x}) := \int \mathbf{f}(\mathbf{u}(\hat{\mathbf{x}}) - \mathbf{u}(\mathbf{x}), \hat{\mathbf{x}} - \mathbf{x}, \mathbf{x}) d\hat{\mathbf{x}}, \quad (2.6)$$

where \mathbf{f} is a *bond force density* whose value is the force vector that the point located at $\hat{\mathbf{x}}$ (in the reference configuration) exerts on the point located at

\mathbf{x} (also in the reference configuration); the third argument \mathbf{x} of \mathbf{f} (2.6) can be dropped for the homogeneous media. Equations (2.5₁) and (2.6₁) have the same form for both local and peridynamic formulation with the different operators (2.5₂) and (2.6₂). Because of this, the superscripts $L(\cdot)$ will correspond to the local case.

The relative position of two material points in the reference configuration $\boldsymbol{\xi} = \hat{\mathbf{x}} - \mathbf{x}$ and their relative displacement $\boldsymbol{\eta} = \mathbf{u}(\hat{\mathbf{x}}) - \mathbf{u}(\mathbf{x})$ are connected with the relative position vector between the two points in the deformed (or current) configuration $\boldsymbol{\eta} + \boldsymbol{\xi}$. Only points $\hat{\mathbf{x}}$ inside some neighborhood (horizon region) $\mathcal{H}_{\mathbf{x}}$ of \mathbf{x} interact with \mathbf{x} :

$$\mathbf{f}(\boldsymbol{\eta}, \boldsymbol{\xi}, \mathbf{x}) \equiv \mathbf{0} \quad \forall \hat{\mathbf{x}} \notin \mathcal{H}_{\mathbf{x}}. \quad (2.7)$$

The vector $\boldsymbol{\xi} = \hat{\mathbf{x}} - \mathbf{x}$ ($\hat{\mathbf{x}} \in \mathcal{H}_{\mathbf{x}}$) is called a *bond* to \mathbf{x} , and the collection of all bonds to \mathbf{x} form the horizon region $\mathcal{H}_{\mathbf{x}}$. Without a loss of generality, it is assumed that a shape of $\mathcal{H}_{\mathbf{x}}$ is spherical: $\mathcal{H}_{\mathbf{x}} = \{\hat{\mathbf{x}} : |\hat{\mathbf{x}} - \mathbf{x}| \leq l_{\delta}\}$ and a number l_{δ} , called the *horizon*, does not depend on \mathbf{x} . The properties of $\mathbf{f}(\boldsymbol{\eta}, \boldsymbol{\xi}, \mathbf{x})$ are considered in [413].

Peridynamic states introduced by Silling [419] (for a more detailed summary, see [423]) are the functions acting on bounds. There are scalar, vector, and modulus states producing the scalars, vectors, and 2nd order tensors, respectively. $\underline{\mathbf{T}}[\mathbf{x}]\langle \boldsymbol{\xi} \rangle$ and $\underline{\mathbf{T}}[\hat{\mathbf{x}}]\langle -\boldsymbol{\xi} \rangle$ are the *force vector states* at \mathbf{x} and $\hat{\mathbf{x}}$, which return the force densities associated with $\boldsymbol{\xi}$ and $-\boldsymbol{\xi}$, respectively. In the ordinary state-based peridynamics being considered, $\underline{\mathbf{T}}[\mathbf{x}]\langle \boldsymbol{\xi} \rangle$ is parallel (in contrast with the non-ordinary model) to the deformation vector state and the equilibrium Eq. (2.6) is expressed through the force vector states as (see for details [419], [423])

$$\tilde{\mathcal{L}}(\mathbf{u})(\mathbf{x}) + \mathbf{b}(\mathbf{x}) = \mathbf{0}, \quad \tilde{\mathcal{L}}(\mathbf{u})(\mathbf{x}) := \int \{\underline{\mathbf{T}}[\mathbf{x}]\langle \boldsymbol{\xi} \rangle - \underline{\mathbf{T}}[\hat{\mathbf{x}}]\langle -\boldsymbol{\xi} \rangle\} d\hat{\mathbf{x}}. \quad (2.8)$$

A small displacement state \mathbf{u} when

$$\mathbf{l} := \sup_{|\boldsymbol{\xi}| \leq l_{\delta}} |\boldsymbol{\eta}(\boldsymbol{\xi})| \ll l_{\delta}. \quad (2.9)$$

is considered. Force vector state

$$\underline{\mathbf{T}} = \underline{\mathbf{T}}^0 + \mathbb{K} \bullet \underline{\mathbf{U}}. \quad (2.10)$$

is expressed through the *modulus state* \mathbb{K} . Here, the operation of *dot product* \bullet of two vector states $\underline{\mathbf{A}}, \underline{\mathbf{B}}$ and a double state $\underline{\mathbb{D}}$ are introduced as

$$\begin{aligned} \underline{\mathbf{A}} \bullet \underline{\mathbf{B}} &= \langle \underline{\mathbf{A}}\langle \boldsymbol{\xi} \rangle \cdot \underline{\mathbf{B}}\langle \boldsymbol{\xi} \rangle \rangle^{\mathcal{H}_{\mathbf{x}}} = \int_{\mathcal{H}_{\mathbf{x}}} \underline{\mathbf{A}}\langle \boldsymbol{\xi} \rangle \cdot \underline{\mathbf{B}}\langle \boldsymbol{\xi} \rangle d\boldsymbol{\xi}, \\ (\underline{\mathbb{D}} \bullet \underline{\mathbf{B}})_i \langle \boldsymbol{\xi} \rangle &= \int_{\mathcal{H}_{\mathbf{x}}} \underline{\mathbb{D}}_{ij} \langle \boldsymbol{\xi}, \boldsymbol{\zeta} \rangle \cdot \underline{\mathbf{B}}_j \langle \boldsymbol{\zeta} \rangle d\boldsymbol{\zeta}. \end{aligned} \quad (2.11)$$

Hereafter $\langle(\cdot)\rangle^{\mathcal{H}_{\mathbf{x}}}$ denotes the average over the horizon region $\mathcal{H}_{\mathbf{x}}$ with the center \mathbf{x} .

A linearized model for pure mechanical loading ($\boldsymbol{\beta} \equiv \mathbf{0}$) can be written from (2.8₂) as described by Silling [414]

$$\tilde{\mathcal{L}}(\mathbf{C}, \mathbf{u})(\mathbf{x}) + \mathbf{b}(\mathbf{x}) = \mathbf{0}, \quad (2.12)$$

$$\tilde{\mathcal{L}}(\mathbf{C}, \mathbf{u})(\mathbf{x}) := \int_w \mathbf{C}(\mathbf{x}, \mathbf{q})(\mathbf{u}(\mathbf{q}) - \mathbf{u}(\mathbf{x})) dV_{\mathbf{q}}, \quad (2.13)$$

where the integrand in Eq. (2.10) vanishing at $|\mathbf{x} - \mathbf{q}| \geq 2l_{\delta}$ may be non-null at $l_{\delta} < |\mathbf{x} - \mathbf{q}| < 2l_{\delta}$. The kernel with the following symmetries holds for any \mathbf{x} and \mathbf{q} :

$$\mathbf{C}^{\top}(\mathbf{x}, \mathbf{q}) = \mathbf{C}(\mathbf{q}, \mathbf{x}). \quad (2.14)$$

Thermoelastic cases ($\boldsymbol{\beta} \neq \mathbf{0}$) were considered in [328], [33], [257], [329]. Fully coupled thermo-mechanical PD theory was proposed in [368], [477].

For subsequent convenience, one introduces a vector-valued function $\tilde{\mathbf{f}} : \mathbb{R}^d \times \mathbb{R}^d \rightarrow \mathbb{R}^d$ by

$$\tilde{\mathbf{f}}(\mathbf{p}, \mathbf{q}) = \begin{cases} \mathbf{f}(\mathbf{u}(\mathbf{p}) - \mathbf{u}(\mathbf{q}), \mathbf{p} - \mathbf{q}, \mathbf{q}), & \text{if } \mathbf{p}, \mathbf{q} \in w, \\ \mathbf{0}, & \text{otherwise,} \end{cases} \quad (2.15)$$

which is presumed to be Riemann-integrable. Then, one can define the ‘‘peridynamic stress’’ $\boldsymbol{\sigma}(\mathbf{z})$ at the point \mathbf{z} as the total force that all material points $\hat{\mathbf{x}}$ to the right of \mathbf{z} exert on all material points to its left (see e.g., [79], [294], [424], [457]). For dD cases ($d = 1, 2, 3$)

$$\boldsymbol{\sigma}(\mathbf{x}) = \mathcal{L}^{\sigma}(\mathbf{u}), \quad (2.16)$$

$$\mathcal{L}^{\sigma}(\mathbf{u}) := \frac{1}{2} \int_S \int_0^{\infty} \int_0^{\infty} (y+z)^{d-1} \tilde{\mathbf{f}}(\mathbf{x} + y\mathbf{m}, \mathbf{x} - z\mathbf{m}) \otimes \mathbf{m} dz dy d\Omega_{\mathbf{m}}. \quad (2.17)$$

Here, S stands for the unit sphere, and $d\Omega_{\mathbf{m}}$ denotes a differential solid angle on S in the direction of any unite vector \mathbf{m} . It was proved [298] that the peridynamic stress is the same as the first Piola-Kirchhoff static Virial stress which offers a simple and clear expression for numerical calculations of peridynamic stress.

The equilibrium Eqs. (2.8), (2.21) and (2.16) of ordinary state-based PD are considered. When the interactions between material points are only pairwise, the equilibrium equations are reduced to the bond-based PD equations. One of the simplest nonlinear is the proportional microelastic material model [418]

$$\mathbf{f}^{\text{bond}}(\boldsymbol{\eta}, \boldsymbol{\xi}, \mathbf{x}) = f(|\boldsymbol{\eta} + \boldsymbol{\xi}|, \boldsymbol{\xi})\mathbf{e}, \quad f(|\boldsymbol{\eta} + \boldsymbol{\xi}|, \boldsymbol{\xi}) = c(\boldsymbol{\xi})s, \quad (2.18)$$

$$\mathbf{e} := \frac{\boldsymbol{\eta} + \boldsymbol{\xi}}{|\boldsymbol{\eta} + \boldsymbol{\xi}|}, \quad s := \frac{|\boldsymbol{\eta} + \boldsymbol{\xi}| - |\boldsymbol{\xi}|}{|\boldsymbol{\xi}|}, \quad (2.19)$$

where s denotes the bond stretch (also called bond strain) which is the relative change of the length of a bond, and c is referenced as the ‘‘bond constant’’. Although this model is linear in terms of the bond stretches, it is nonlinear in terms of displacements; thermoelastic cases ($\boldsymbol{\beta} \neq \mathbf{0}$) were considered in [33], [257], [328], [329]. A nonlinear model in terms of bond stretches (at $\boldsymbol{\beta} \equiv \mathbf{0}$)

$$f(|\boldsymbol{\eta} + \boldsymbol{\xi}|, \boldsymbol{\xi}) = c(\boldsymbol{\xi})[s + 3s^2/2 + s^3/2] \quad (2.20)$$

is considered in [236]. The potential role of employing a nonlinear peridynamic kernel in predicting the onset of fractures has been explored in [128] (see also [114], [115]).

A linearized version of the theory (for small displacement) for a microelastic homogeneous material (2.21) takes the form ($\forall \boldsymbol{\eta}, \boldsymbol{\xi}$)

$$\mathbf{f}^{\text{bond}}(\boldsymbol{\eta}, \boldsymbol{\xi}, \mathbf{x}) = \mathbf{f}_{\text{lin}}^{\text{bond}}(\boldsymbol{\eta}, \boldsymbol{\xi}, \mathbf{x}) = \mathbf{C}^{\text{bond}}(\boldsymbol{\xi}, \mathbf{x})\boldsymbol{\eta}, \quad (2.21)$$

Here, the material’s *micromodulus* function \mathbf{C} contains all constitutive information and its value is a second-order tensor given by

$$\mathbf{C}^{\text{bond}}(\boldsymbol{\xi}, \mathbf{x}) = \frac{\partial \mathbf{f}(\mathbf{0}, \boldsymbol{\xi}, \mathbf{x})}{\partial \boldsymbol{\eta}} \quad \forall \boldsymbol{\xi}. \quad (2.22)$$

Substitution of Eq. (2.21) into Eq. (2.6) leads to the equilibrium equation

$$\tilde{\mathcal{L}}(\mathbf{C}^{\text{bond}}, \mathbf{u})(\mathbf{x}) + \mathbf{b}(\mathbf{x}) = \mathbf{0}, \quad (2.23)$$

$$\tilde{\mathcal{L}}(\mathbf{C}^{\text{bond}}, \mathbf{u})(\mathbf{x}) := \int \mathbf{C}^{\text{bond}}(\mathbf{x}, \mathbf{q})(\mathbf{u}(\mathbf{q}) - \mathbf{u}(\mathbf{x})) dV_{\mathbf{q}}. \quad (2.24)$$

For consistency with Newton’s third law, the micromodulus function \mathbf{C} for the homogeneous materials must be symmetric to its tensor structure as well as to arguments

$$\mathbf{C}^{\text{bond}}(\mathbf{x}, \mathbf{q}) = \mathbf{C}^{\text{bond}}(\mathbf{q}, \mathbf{x}) = (\mathbf{C}^{\text{bond}})^{\top}(\mathbf{x}, \mathbf{q}) \quad \forall \mathbf{x}, \mathbf{q}, \quad (2.25)$$

where the properties of \mathbf{C}^{bond} are discussed in detail in Silling [54] (see also [10, 33]). For example, for the micromodulus functions with the step-function and triangular profiles,

$$\mathbf{C}(\boldsymbol{\xi}) = \mathbf{C}V(\mathcal{H}_{\mathbf{x}}), \quad \mathbf{C}(\boldsymbol{\xi}) = \mathbf{C}(1 - |\boldsymbol{\xi}|/l_{\delta})V(\mathcal{H}_{\mathbf{x}}), \quad (2.26)$$

respectively, where $V(\mathcal{H}_{\mathbf{x}})$ is the indicator function of $\mathcal{H}_{\mathbf{x}}$. The peridynamic solution of Eq. (2.23) with \mathbf{C} described by Eq. (2.26) is investigated in detail by both numerical and analytical methods in 1D (see [43], [342], [424], [457]), 2D (see [224], [225]), and 3D cases [343], [458].

For bond-based peridynamics, the stress representation (2.17) can be recast in terms of displacements

$$\begin{aligned} \mathcal{L}^{\sigma}(\mathbf{C}, \mathbf{u}) : &= \frac{1}{2} \int_S \int_0^{\infty} \int_0^{\infty} (y+z)^{d-1} \mathbf{C}^{\text{bond}}((y+z)\mathbf{m}, \mathbf{x} - z\mathbf{m}) \\ &\times [\mathbf{u}(\mathbf{x} + y\mathbf{m}) - \mathbf{u}(\mathbf{x} - z\mathbf{m})] \otimes \mathbf{m} dz dy d\Omega_{\mathbf{m}}. \end{aligned} \quad (2.27)$$

It is interesting that equilibrium Eqs. (2.22) and (2.23) formally coincide, although the kernels $\mathbf{C}(\mathbf{x}, \mathbf{q})$ (2.23) and $\mathbf{C}^{\text{bond}}(\mathbf{x}, \mathbf{q})$ (2.21) are conceptually different with different symmetry properties (2.15) and (2.25), respectively. Moreover, in the state-based version, the maximum interaction distance between the points is $2l_\delta$ whereas this distance in bond-based peridynamics coincides with the horizon l_δ . However, this similarity provides a possibility to reformulate the results obtained before for the linear bond-based peridynamic micromechanics (see for details [79] and [93]) to their counterparts for the linear ordinary state-based ones.

2.2 Volumetric boundary conditions

Owing to nonlocality, the equilibrium equation (2.6) is combined with a “boundary” condition, used as a volumetric constraint in the so-called interaction domain w_Γ (in opposite to the local case where the boundary conditions are imposed directly at the bounding surface $\Gamma^{(0)}$, see for details [413], [256]; i.e., the nonlocal boundary w_Γ is a d -dimensional region unlike its $(d-1)$ -dimensional counterpart Γ^0 in local problems. The interaction domain w_Γ contains points \mathbf{y} not in w interacting with points $\mathbf{x} \in w$. The most popular shape for w_Γ with prescribed either the forces or displacements is a boundary layer of thickness given by $2l_c$ (see [322]): $w_\Gamma = \{w \oplus \mathcal{H}_0\} \setminus w$, where $w \oplus \mathcal{H}_0$ is the Minkowski sum w ($\mathcal{A} \oplus \mathcal{B} := \cup_{\mathbf{x} \in \mathcal{A}, \mathbf{y} \in \mathcal{B}} \{\mathbf{x} + \mathbf{y}\}$); then w is the internal region of \overline{w} (see [413]).

It is presumed that \overline{w} is considered as a cutting out of a macrodomain (containing a statistically large number of inclusion’s realization) from the random heterogeneous medium covering the entire space \mathbb{R}^d . Then, the Dirichlet, or Neumann volumetric boundary conditions (VBC, see [145]), [340]) are called homogeneous volumetric loading conditions if there exist some symmetric constant tensors either $\boldsymbol{\varepsilon}^{w_\Gamma}$ or $\boldsymbol{\sigma}^{w_\Gamma}$ such that

$$\mathbf{u}(\mathbf{x}) = \mathbf{h}(\mathbf{y}) = \boldsymbol{\varepsilon}^{w_\Gamma} \mathbf{y}, \quad \forall \mathbf{y} \in w_{\Gamma u} = w_\Gamma, \quad (2.28)$$

$$\tilde{\boldsymbol{\mathcal{L}}}(\mathbf{x}) = -\mathbf{g}(\mathbf{y}) = -\boldsymbol{\sigma}^{w_\Gamma} \mathbf{n}(\mathbf{y}), \quad \forall \mathbf{y} \in w_{\Gamma \sigma} = w_\Gamma, \quad (2.29)$$

respectively. There are no specific restrictions on the smoothness and shape of Γ_0 , which is defined only by the convenience of representation. It should be mentioned that in the LM, the analogs of the VBC (2.28) and (2.29) (at the nonlocality vanishing $l_\delta \rightarrow 0$) are the homogeneous boundary conditions (also called the kinematic uniform boundary conditions (KUBC) and static uniform boundary conditions (SUBC), respectively)

$$\mathbf{u}(\mathbf{y}) = \boldsymbol{\varepsilon}^{w_\Gamma} \mathbf{y}, \quad \forall \mathbf{y} \in \Gamma_{0u} = \Gamma_0, \quad (2.30)$$

$$\mathbf{t}(\mathbf{y}) = \boldsymbol{\sigma}^{w_\Gamma} \mathbf{n}(\mathbf{y}), \quad \forall \mathbf{y} \in \Gamma_{0\sigma} = \Gamma_0, \quad (2.31)$$

correspond to the analyses of the equations for either strain or stresses, respectively, which are formally similar to each other. However, in peridynamic micromechanics, a primary unknown variable is displacement (rather than stresses), and, because of this, the VBC (2.28) is assumed.

Seemingly to the volumetric boundary domain w_{Γ_i} , we introduce a volumetric interface boundary (called also interaction interface, see [399], [10]) $v_{\Gamma_i} = v_{\Gamma_i}^+ \cup v_{\Gamma_i}^-$ where $v_{\Gamma_i}^+$ and $v_{\Gamma_i}^-$ are the boundary layers (internal and external, respectively) divided by the geometric boundary Γ_i and have a thickness expressed through the horizon as $2l_\delta$. The geometrical boundaries of the boundary layers $v_{\Gamma_i}^+$ and $v_{\Gamma_i}^-$ are Γ_i^+ and Γ_i^- , respectively. For a general form of the inclusion v_i the external volumetric interface Γ_i^- can be expressed through the Minkowski sum $\Gamma_i^- = \{v_i \oplus 2\mathcal{H}_0\} \setminus v_i$, where $2\mathcal{H}_0 := \{\mathbf{x} \mid \mathbf{x}/2 \in \mathcal{H}_0\}$. A nonlocal closure of the inclusion $v_i^l := v_i \oplus 2\mathcal{H}_0$ (with an indicator function $V_i^l(\mathbf{x})$) is called an *extended inclusion* while $v^l := \cup v_i^l$ ($i = 1, 2, \dots$) (with the indicator function $V^l(\mathbf{x}) = \sum_i V_i^l(\mathbf{x})$) stands for the extended inclusion phase. In so doing $v^{l(0)} := w \setminus v^l \subset v^{(0)}$ is called a *truncated matrix*.

In the simplest case, a micromodulus of interaction interface of the inclusion v_i (see, e.g. [10], [11], [418]) is presented as an average value of the material properties at two material points connecting dissimilar materials ($V^{(0)}(\mathbf{x}) + V_i(\hat{\mathbf{x}}) = V^{(0)}(\hat{\mathbf{x}}) + V_i(\mathbf{x}) = 1$)

$$\mathbf{C}^i(\mathbf{x}, \hat{\mathbf{x}}) = [\mathbf{C}^{(0)}(\mathbf{x}, \hat{\mathbf{x}}) + \mathbf{C}_i(\mathbf{x}, \hat{\mathbf{x}})]/2 \quad (2.32)$$

although more sophisticated models of interaction interface properties (see, e.g., [324], [286], see for references [39]), can be incorporated into the general subsequent representations. In particular, a variation of $\mathbf{C}^i(\mathbf{x}, \hat{\mathbf{x}})$ was presented in [324] and [379] in a spirit of the functionally graded materials theory described in, e.g. [53].

2.3 Descriptions of random and periodic structures of the composite microstructures

We consider a popular group of composites, called matrix composites, which consists of a continuous matrix phase reinforced by isolated inhomogeneities of various shapes. Three material length scales (see, e.g., [442], [497]) are considered: the macroscopic scale L , characterizing the extent of w , the microscopic scale a , related with the heterogeneities v_i , and the horizon l_δ . Moreover, one supposes that the applied field varies on a characteristic length scale Λ . The limit of our interests for both the material scales and field one are either

$$L \geq \Lambda \geq a^{\text{int}} \geq a \geq l_\delta \quad \text{or} \quad L \gg \Lambda \gg a^{\text{int}} \geq a \gg l_\delta, \quad (2.33)$$

$$L \geq \Lambda \geq |\Omega_{00}| \geq l_\delta \quad \text{or} \quad L \gg \Lambda \gg |\Omega_{00}| \gg l_\delta, \quad (2.34)$$

where the inequalities (2.33₂) and (2.34₂) are called a scale separation hypotheses. The inequalities (2.33) correspond to the case of random structure CMs, where a^{int} stands for the scale of long-range interactions of inclusions (e.g. $a^{\text{int}} = 6a$). The inequalities (2.34) describe the scale representations for periodic structure CMs, where Ω_{00} is a unite cell (see for details Subsection 2.4), and, for shortening, we use $|\Omega_{00}|$ instead of linear $|\Omega_{00}|^{1/d}$.

The random quantities of the statistically homogeneous random fields (see, e.g. [79], [332]) are described by a conditional probability density $\varphi(v_i, \mathbf{x}_i | v_1, \mathbf{x}_1$

for finding a heterogeneity of type i with the center \mathbf{x}_i in the domain v_i , with the fixed heterogeneities v_1 centered at \mathbf{x}_1 . The notation $\varphi(v_i, \mathbf{x}_i; v_1, \mathbf{x}_1)$ denotes the case $\mathbf{x}_i \neq \mathbf{x}_1$. We have $\varphi(v_i, \mathbf{x}_i; v_1, \mathbf{x}_1) = 0$ (since heterogeneities cannot overlap) for values of \mathbf{x}_i placed inside the some domain v_1^0 called “excluded volumes”, where $v_1^0 \supset v_1$ with indicator function V_1^0 is the “excluded volumes” of \mathbf{x}_i with respect to v_1 , and $\varphi(v_i, \mathbf{x}_i; v_1, \mathbf{x}_1) \rightarrow \varphi(v_i, \mathbf{x}_i)$ as $|\mathbf{x}_i - \mathbf{x}_m| \rightarrow \infty$, $m = 1, \dots, n$ (since no long-range order is assumed). $\varphi(v_i, \mathbf{x})$ is a number density, $n^{(k)} = n^{(k)}(\mathbf{x})$ of component $v^{(k)} \ni v_i$ at the point \mathbf{x} and $c^{(k)} = c^{(k)}(\mathbf{x})$ is the concentration, i.e. volume fraction, of the component $v_i \in v^{(k)}$ at the point \mathbf{x} : $c^{(k)}(\mathbf{x}) = \langle V^{(k)} \rangle(\mathbf{x}) = \bar{v}_i n^{(k)}(\mathbf{x})$, $\bar{v}_i = \text{mes} v_i$ ($k = 1, 2, \dots, N$; $i = 1, 2, \dots$), $c^{(0)}(\mathbf{x}) = 1 - \langle V \rangle(\mathbf{x})$. Additionally to the average $\langle (\cdot) \rangle(\mathbf{x})$, the notation $\langle (\cdot) | v_1, \mathbf{x}_1 \rangle(\mathbf{x})$ will be used for the conditional average taken for the ensemble of a statistically homogeneous set $X = (v_i)$ at the point \mathbf{x} , on the condition that there is heterogeneity at the point \mathbf{x}_1 and $\mathbf{x}_i \neq \mathbf{x}_1$. The notation $\langle (\cdot) | v_1, \mathbf{x}_1 \rangle(\mathbf{x})$ is exploited for the additional condition $\mathbf{x} \notin v_1$. In a general case of *statistically inhomogeneous* media with the homogeneous matrix (e.g., for so called *Functionally Graded Materials*, FGM) the conditional probability density is not invariant with respect to translation, that is, the microstructure functions depend on their absolute positions [381]:

$$\begin{aligned} \varphi(v_i, \mathbf{x}_i; v_1, \mathbf{x}_1) &= \varphi(v_i, \mathbf{x}_i; v_1, \mathbf{x}_1 + \mathbf{x}), \quad (\forall \mathbf{x} \in R^d) \\ \varphi(v_i, \mathbf{x}_i; v_1, \mathbf{x}_1) &\neq \varphi(v_i, \mathbf{x}_i; v_1, \mathbf{x}_1 + \mathbf{x}), \quad (\exists \mathbf{x} \in R^d). \end{aligned} \quad (2.35)$$

for statistically homogeneous and inhomogeneous media, respectively.

Of course, any deterministic (e.g. periodic) field of inclusions v with the centers $\mathbf{x}_\alpha \in \Lambda$ can be presented by the probability density $\varphi(v_i, \mathbf{x}_i)$ and conditional probability density $\varphi(v_i, \mathbf{x}_i; v_j, \mathbf{x}_j)$ expressed through the δ functions ($\mathbf{x}_\alpha \in \Lambda$)

$$\begin{aligned} \varphi(v_i, \mathbf{x}_i) &= \sum_{\alpha} \delta(\mathbf{x}_i - \mathbf{x}_\alpha), \\ \varphi(v_i, \mathbf{x}_i; v_j, \mathbf{x}_j) &= \sum_{\alpha} \delta(\mathbf{x}_i - \mathbf{x}_\alpha) - \delta(\mathbf{x}_i - \mathbf{x}_j). \end{aligned} \quad (2.36)$$

In more detail, a periodic structure of CM is considered. For simplicity of notations for periodic media, we consider 2D cases $w = \cup \Omega_{ij}$ ($i, j = 0, \pm 1, \pm 2, \dots$) with the square unit cells Ω_{ij} and the centers of the unite cells $\Lambda = \{\mathbf{x}_{ij}\}$. Let a representative unit cell Ω_{00} with the corner points \mathbf{x}_{kl}^c ($k, l = \pm 1$) has the boundary $\Gamma^0 = \cup \Gamma_{ij}^0$ where the boundary partition $\mathbf{x}_{ij}^0 \in \Gamma_{ij}^0$ separates the UCs Ω_{00} and Ω_{ij} ($i = 0, \pm 1, j = \pm(1 - |i|)$, see Fig. 19.2 in [79]). A representative volume element (or the unit cell, UC) Ω_{00} is deformed in a repetitive way as its neighbors. The position vectors $\mathbf{x}_{ij}^0 \in \Gamma_{ij}^0$ or $\mathbf{x}_{kl}^0 \in \Gamma_{kl}^0$ are presented by the corner points \mathbf{x}_{mn}^c ($i = 0, \pm 1, j = \pm(1 - |i|), k = -i, l = -j, m, n = \pm 1$); e.g., $\mathbf{x}_{ij}^0 = \mathbf{x}_{kl}^0 + \mathbf{x}_{1,-1}^c - \mathbf{x}_{-1,-1}^c$ for the $i = 1, j = 0$. N field points \mathbf{x}_i ($i = 1, \dots, N$) in the central cube $\Omega_{00} = \{[-l^\Omega, l^\Omega]^d\}$ are periodically reflected as \mathbf{x}_i^α into the neighboring cubes Ω_α , where $\alpha = (\alpha_1, \dots, \alpha_d) \in Z^+$, and $\alpha_i = 0, \pm 1$ ($i = 1, \dots, d$).

A volumetric unit cell boundary $\Omega_\Gamma = \Gamma^+ \cup \Gamma^-$ contains the boundary layers Γ^+ and Γ^- (internal and external, respectively) separating by the geometric boundary Γ^0 and having a thickness given by the horizon l_δ (the UC Ω_{00} with some parts of the internal and external volumetric boundaries is presented in Fig. 1). For a general form of the UC Ω_{00} the external volumetric boundary Γ^- can be expressed through the Minkovski addition $\Gamma^- = \{\Omega_{00} \oplus \mathcal{H}_0\} \setminus \Omega_{00}$ with the partitions $\Gamma_\alpha^- = \Gamma^- \cap \Omega_\alpha$ (if $|\alpha_1| + \dots + |\alpha_d| = d - 1$) and $\Gamma_\alpha^{c-} = \Gamma^- \cap \Omega_\alpha$ (if $|\alpha_1| + \dots + |\alpha_d| = d$); for $d = 3$ and $|\alpha_1| + |\alpha_2| + |\alpha_3| = 1$, the case $\Gamma^- \cap \Omega_\alpha$ corresponds to the edges. For $\mathbf{x} \in \Omega_{00}$ and $\mathcal{H}_\mathbf{x} \subset \Omega_{00}$ (i.e. $\mathbf{x} \notin \Gamma^+$), we don't need to take the interaction of the opposite volumetric boundaries into account. However, for $\mathbf{x} \in \Gamma^+$, some points of the family $\mathbf{y} \in \mathcal{H}_\mathbf{x}$ don't fall into the UC $\mathbf{y} \notin \Omega_{00}$ that required establishment of the tying constraints linking both the position points and the fields of the opposite volumetric boundaries Γ^+ and Γ^- . If the source point $\mathbf{x}_p + \boldsymbol{\xi} \in \Omega_\alpha$ ($\boldsymbol{\xi} \in \mathcal{H}_p$) then the peridynamic counterpart of the local periodic boundary conditions (PBC) called *volumetric periodic boundary conditions* (VPBC, see [71], [79]) represent periodic displacements and antiperiodic tractions. So, the homogeneous VBC at the remote boundary (2.28) is equivalent to the VPBC

$$\mathbf{u}(\mathbf{x}_p + \boldsymbol{\xi}) = \mathbf{u}(\mathbf{x}_p + \boldsymbol{\xi} - 2\boldsymbol{\alpha}^l) + 2\boldsymbol{\varepsilon}^{w\Gamma} \boldsymbol{\alpha}^l, \quad (2.37)$$

$$\mathbf{t}(\mathbf{x}_\alpha^0) = -\mathbf{t}(\mathbf{x}_\gamma^0), \quad (2.38)$$

where $\boldsymbol{\gamma} = -\boldsymbol{\alpha}$ and \mathbf{x}_α^0 are defined analogously to \mathbf{x}_{ij}^0 . The VPBCs (2.37) and (2.38) coincide with the classical PBC

$$\mathbf{u}(\mathbf{x}_p) = \mathbf{u}(\mathbf{x}_p - 2\boldsymbol{\alpha}^l) + 2\boldsymbol{\varepsilon}^{w\Gamma} \boldsymbol{\alpha}^l, \quad (2.39)$$

$$\mathbf{t}(\mathbf{x}_\alpha^0) = -\mathbf{t}(\mathbf{x}_\gamma^0) \quad (2.40)$$

only for $l_\delta = 0$. The VPBC (2.37) and (2.38) were proposed in [71], [79] for any peridynamic constitutive laws of phases; it was applied to CMs with both the bond-based peridynamic properties of constituents [71], [79] and non-ordinary state-based [182] peridynamic properties of phases. For the general forcing term (2.4) (instead of VBC (2.28)), analogs of VPBC (2.37) and (2.38) are not defined.

The VPBC (2.37) was proposed for the case that the inclusion v_i does not intersect the boundary Γ^0 of the UC Ω^{00} . So, for $\text{dist}(v_i(\mathbf{x}), \Gamma^0) \geq l_\delta^{(0)}$ (for $\forall \mathbf{x} \in v_i$ and $\forall v_i \subset \Omega_{00}$) and $l_\delta^{(1)} \leq l_\delta^{(0)}$, the VPBC (2.37) holds. However, if the inclusion v_i does not intersect the boundary Γ^0 of the UC Ω^{00} then the VPBC (2.37) should be corrected by replacement of $\boldsymbol{\xi} \in \mathcal{H}_p$ by $\boldsymbol{\xi} \in \mathcal{H}_p^{0+1}$, where \mathcal{H}_p^{0+1} is a horizon region with the radius $l_\delta^{(0)} + l_\delta^{(1)}$. Micromodulus $\mathbf{C}(\mathbf{x}, \hat{\mathbf{x}})$ corresponding to the points $\mathbf{x} = \mathbf{x}_p$ and $\hat{\mathbf{x}} = \mathbf{x}_p + \boldsymbol{\xi}$ is given by the formula

$$\mathbf{C}(\mathbf{x}, \hat{\mathbf{x}}) = \begin{cases} \mathbf{C}^{(1)}(\mathbf{x}, \hat{\mathbf{x}}), & \text{for } \mathbf{x}, \hat{\mathbf{x}} \in v, \\ \mathbf{C}^{(0)}(\mathbf{x}, \hat{\mathbf{x}}), & \text{for } \mathbf{x}, \hat{\mathbf{x}} \in v^{(0)}, \\ \mathbf{C}^i(\mathbf{x}, \hat{\mathbf{x}}), & \text{for } \mathbf{x} \in v, \hat{\mathbf{x}} \in v^{(0)} \text{ or } \mathbf{x} \in v^{(0)}, \hat{\mathbf{x}} \in v, \end{cases} \quad (2.41)$$

where the bonds connecting points in the different materials are characterized by micromodulus \mathbf{C}^i , which can be chosen such that, e.g. (2.37). Although there are no technical issues with the correction of discretized peridynamic equation in the extended interface $\mathbf{x} \in v_\Gamma$, it is helpful to assume for simplicity only that the peridynamic operator in the extended interface (fuzzy interface, i.e. not sharp as it would be in a local formulation) is described by Eq. (2.6) with the constant horizon and micromodulus (2.41) determined as an average value of the micromoduli in the matrix and inclusion (2.32). The adaptive grid refinement technique was proposed in [42] for analysis of peridynamic problems in the vicinity of the interface that involves a variable horizon size.

It should be mentioned that the most attractive tool of ML and NN techniques in PM of periodic structure CMs is using a general case of forcing term (2.4) as a training parameter (see Subsection 4.7). Then solution periodicity is lost and PBC (2.39) (and VPBC (2.37)) cannot be fulfilled. This problem of correction of PBC (2.39) even in LM is not solved for the general case of forcing term (2.4). However, this challenge is effortlessly surmounted in Subsection 8.3.

2.4 Some averages

In the case of statistically homogeneous random functions $\mathbf{f}(\mathbf{x})$, the ergodicity condition is assumed when the spatial average is estimated over one sufficiently large sample and statistical mean coincide for both the whole volume w and the individual constituent $v^{(k)}$ ($k = 0, 1, \dots, N$):

$$\langle \mathbf{f} \rangle = \{ \mathbf{f} \} \equiv \lim_{w \uparrow \mathbb{R}^d} |w|^{-1} \int_w \mathbf{f}(\mathbf{x})(\mathbf{x}) d\mathbf{x}, \quad (2.42)$$

$$\langle \mathbf{f} \rangle^{(k)} = \{ \mathbf{f} \}^{(k)} \equiv \lim_{w \uparrow \mathbb{R}^d} |w|^{-1} \int_w \mathbf{f}(\mathbf{x})(\mathbf{x}) V^{(k)} d\mathbf{x}, \quad (2.43)$$

were $|w| = \text{mes } w$. Under the Gauss theorem, the volume averages by integrals over the corresponding boundary are expressed. In particular, for the homogeneous boundary conditions either (2.28) or (2.29) the mean value $\{ \boldsymbol{\varepsilon} \}$ or $\{ \boldsymbol{\sigma} \}$ of $\boldsymbol{\varepsilon}$ or $\boldsymbol{\sigma}$ coincide with $\boldsymbol{\varepsilon}^{w_\Gamma}$ and $\boldsymbol{\sigma}^{w_\Gamma}$ (see, e.g. [79]).

The volume averages of the strains and stresses inside the extended inclusion v_i^l can be presented by the averages over the external inclusion boundary Γ_i^- by the use of Gauss's theorem

$$\langle \boldsymbol{\varepsilon} V^l \rangle = \boldsymbol{\varepsilon}^{l(1)} = \boldsymbol{\varepsilon}^{l\omega(1)} := \frac{1}{\bar{w}} \sum_i \int_{\Gamma_i^-} \mathbf{u}(\mathbf{s}) \otimes \mathbf{n}(\mathbf{s}) d\mathbf{s}, \quad (2.44)$$

$$\langle \boldsymbol{\sigma} V^l \rangle = \boldsymbol{\sigma}^{l(1)} = \boldsymbol{\sigma}^{l\omega(1)} := \frac{1}{\bar{w}} \sum_i \int_{\Gamma_i^-} \mathbf{t}(\mathbf{s}) \otimes \mathbf{s} d\mathbf{s}. \quad (2.45)$$

The absence of numerical differentiation defines an advantage of the surface average. (2.44) with respect to the volume average. The surface average of stresses (2.45) has the well-known advantage of the reduction of dimension by

one that can be crucial for the analyst. In Eqs. (2.44) and (2.45) the averages over the modified phases (e.g., the extended inclusions or truncated matrix) are used

$$\langle \mathbf{f} \rangle^{l(k)} = \{\mathbf{f}\}^{l(k)} \equiv \lim_{w \uparrow \mathbb{R}^d} |w|^{-1} \int_w \mathbf{f}(\mathbf{x})(\mathbf{x}) V^{l(k)} d\mathbf{x}, \quad (2.46)$$

instead of the averages (2.42₂) exploited in local micromechanics.

It should be mentioned that all averages(2.42)-(2.46) and the equality

$$\{\mathbf{g}\} = c^{(0)}\{\mathbf{g}\}^{(0)} + c^{(1)}\{\mathbf{g}\}^{(1)}, \quad (2.47)$$

(e.g., $\mathbf{g} = \boldsymbol{\varepsilon}, \boldsymbol{\sigma}, \boldsymbol{\tau}, \boldsymbol{\eta}$), is fulfilled only for statistically homogeneous media subjected to the homogeneous boundary conditions. For periodic structure CM, the CMI is constructed using the building blocks or cells: $w = \cup \Omega_{\mathbf{m}}$ containing the inclusions $v_{\mathbf{m}} \subset \Omega_{\mathbf{m}}$. Hereafter the notation $\mathbf{f}^\Omega(\mathbf{x})$ will be used for the average of the function \mathbf{f} over the cell $\mathbf{x} \in \Omega_i$ with the center $\mathbf{x}_i^\Omega \in \Omega_i$:

$$\mathbf{f}^\Omega(\mathbf{x}) = \mathbf{f}^\Omega(\mathbf{x}_i^\Omega) \equiv n(\mathbf{x}) \int_{\Omega_i} \mathbf{f}(\mathbf{y}) d\mathbf{y}, \quad \mathbf{x} \in \Omega_i, \quad (2.48)$$

$n(\mathbf{x}) \equiv 1/\overline{\Omega}_i$ is the number density of inclusions in the cell Ω_i .

Let $\mathcal{V}_{\mathbf{x}}$ be a ‘‘moving averaging’’ cell (or moving-window [79], [195]) with the center \mathbf{x} and characteristic size $a_{\mathcal{V}} = (\overline{\mathcal{V}})^{1/d}$, and let for the sake of definiteness $\boldsymbol{\chi}$ be a random vector uniformly distributed on $\mathcal{V}_{\mathbf{x}}$ whose value at $\mathbf{z} \in \mathcal{V}_{\mathbf{x}}$ is $\varphi_{\boldsymbol{\chi}}(\mathbf{z}) = 1/\overline{\mathcal{V}}_{\mathbf{x}}$ and $\varphi_{\boldsymbol{\chi}}(\mathbf{z}) \equiv 0$ otherwise. Then we can define the average of the function \mathbf{f} with respect to translations of the vector $\boldsymbol{\chi}$:

$$\langle \mathbf{f} \rangle_{\mathbf{x}}(\mathbf{x} - \mathbf{y}) = \frac{1}{\overline{\mathcal{V}}_{\mathbf{x}}} \int_{\mathcal{V}_{\mathbf{x}}} \mathbf{f}(\mathbf{z} - \mathbf{y}) d\mathbf{z}, \quad \mathbf{x} \in \Omega_i. \quad (2.49)$$

Among other things, ‘‘moving averaging’’ cell $\mathcal{V}_{\mathbf{x}}$ can be obtained by translation of a cell Ω_i and can vary in size and shape during motion from point to point. To make the exposition clear we will assume that $\mathcal{V}_{\mathbf{x}}$ results from Ω_i by translation of the vector $\mathbf{x} - \mathbf{x}_i^\Omega$; it can be seen, however, that this assumption is not mandatory.

3 Decomposition of the material and field parameters

3.1 Decomposition of the material parameters

The operators $\widehat{\mathcal{L}}(\mathbf{C}, \mathbf{u})$ (2.24) (and $\mathcal{L}^\sigma(\mathbf{C}, \mathbf{u}, \boldsymbol{\beta})$ (2.16), are linear ones with respect to the arguments, e.g.,

$$\begin{aligned} \widehat{\mathcal{L}}(\mathbf{C}_1 + \mathbf{C}_2, \mathbf{u}) &= \widehat{\mathcal{L}}(\mathbf{C}_1, \mathbf{u}) + \widehat{\mathcal{L}}(\mathbf{C}_2, \mathbf{u}), \\ \widehat{\mathcal{L}}(\mathbf{C}, \mathbf{u}_1 + \mathbf{u}_2) &= \widehat{\mathcal{L}}(\mathbf{C}, \mathbf{u}_1) + \widehat{\mathcal{L}}(\mathbf{C}, \mathbf{u}_2). \end{aligned} \quad (3.1)$$

For the matrix CMs with a homogeneous matrix, we decompose the material parameters as

$$\begin{aligned}\mathbf{L}(\mathbf{x}) &= \mathbf{L}^{(0)} + \mathbf{L}_1(\mathbf{x}), \\ \mathbf{C}(\mathbf{x}, \hat{\mathbf{x}}) &= \mathbf{C}^{(0)}(\mathbf{x}, \hat{\mathbf{x}}) + \mathbf{C}_1(\mathbf{x}, \hat{\mathbf{x}}),\end{aligned}\quad (3.2)$$

where $\mathbf{L}_1(\mathbf{x}) := \mathbf{L}(\mathbf{x}) - \mathbf{L}^{(0)}$ and $\mathbf{C}_1(\mathbf{x}, \hat{\mathbf{x}}) := \mathbf{C}(\mathbf{x}, \hat{\mathbf{x}}) - \mathbf{C}^{(0)}(\mathbf{x}, \hat{\mathbf{x}})$ are the jumps of material properties with respect to the of the matrix. Obviously, $\mathbf{L}_1(\mathbf{x}) \equiv \mathbf{0}$ vanishes outside the inclusion phase $\mathbf{x} \notin v$ whereas $\mathbf{C}_1(\mathbf{x}, \hat{\mathbf{x}}) \equiv \mathbf{0}$ outside the extended inclusion phase $v^l := v \oplus \mathcal{H}_0$ (obtained by a Minkovski sum of v when either $\mathbf{x} \notin v^l$ or $\hat{\mathbf{x}} \notin v^l$).

In a similar manner, the peristatic operators $\widehat{\mathcal{L}}(\mathbf{C}, \mathbf{u})$ (2.24), and the stress operator $\widehat{\mathcal{L}}^\sigma(\mathbf{C}, \mathbf{u})$ (2.27) can be decomposed as

$$\begin{aligned}\widehat{\mathcal{L}}(\mathbf{C}, \mathbf{u}) &= \widehat{\mathcal{L}}^{(0)}(\mathbf{C}, \mathbf{u}) + \widehat{\mathcal{L}}_1(\mathbf{C}, \mathbf{u}), \\ \widehat{\mathcal{L}}^\sigma(\mathbf{C}, \mathbf{u}) &= \widehat{\mathcal{L}}^{\sigma(0)}(\mathbf{C}, \mathbf{u}) + \widehat{\mathcal{L}}_1^\sigma(\mathbf{C}, \mathbf{u}),\end{aligned}\quad (3.3)$$

where $\widehat{\mathcal{L}}^{(0)}(\mathbf{C}, \mathbf{u})$ (2.24) and $\widehat{\mathcal{L}}^{\sigma(0)}(\mathbf{C}, \mathbf{u})$ (2.27) are estimated at $\mathbf{C}(\mathbf{x}, \hat{\mathbf{x}}) = \mathbf{C}^{(0)}(\mathbf{x}, \hat{\mathbf{x}})$. In so doing, $\widehat{\mathcal{L}}_1(\mathbf{C}, \mathbf{u})$ (2.24) and $\widehat{\mathcal{L}}_1^\sigma(\mathbf{C}, \mathbf{u})$ (2.27) vanish inside the truncated matrix $\mathbf{x} \in v^{(0)l} := w \setminus v^l$.

Peridynamic counterpart of the tensorial decomposition for local elasticity

$$\boldsymbol{\sigma}(\mathbf{x}) = {}^L\mathbf{L}^{(0)}\boldsymbol{\varepsilon}(\mathbf{x}) + {}^L\boldsymbol{\tau}(\mathbf{x}), \quad {}^L\boldsymbol{\tau}(\mathbf{x}) := \boldsymbol{\sigma}(\mathbf{x}) - {}^L\mathbf{L}^{(0)}(\mathbf{x})\boldsymbol{\varepsilon}(\mathbf{x}) \quad (3.4)$$

can be presented in the next form for the operator (2.17)

$$\boldsymbol{\mathcal{L}}^\sigma(\mathbf{u})(\mathbf{x}) = \boldsymbol{\mathcal{L}}^{\sigma(0)}(\mathbf{u})(\mathbf{x}) + \boldsymbol{\mathcal{L}}_1^\sigma(\mathbf{u})(\mathbf{x}), \quad (3.5)$$

where $\boldsymbol{\mathcal{L}}^{\sigma(0)}$ denotes an action of the operator $\boldsymbol{\mathcal{L}}^\sigma$ on the medium with the material properties of the matrix defined by the bond force $\mathbf{f}^{(0)}$ [for example, for the bond force (2.8), we have $\mathbf{C}(\boldsymbol{\xi}, \mathbf{x}) \equiv \mathbf{C}^{(0)}(\boldsymbol{\xi})$] and the displacement fields $\mathbf{u}(\mathbf{y})$ of the real CM. The jump operator $\boldsymbol{\mathcal{L}}_1^\sigma(\mathbf{u})(\mathbf{x})$ defined by Eq. (3.5) is called the *local stress polarization tensor* [compare with Eq. (3.5)] and represented as

$$\boldsymbol{\tau}(\mathbf{x}) = \boldsymbol{\mathcal{L}}_1^\sigma(\mathbf{u})(\mathbf{x}) = \frac{1}{2} \int_S \int_0^\infty \int_0^\infty (y+z)^{d-1} \hat{\mathbf{f}}_1(\mathbf{x} + y\mathbf{m}, \mathbf{x} - z\mathbf{m}) \otimes \mathbf{m} dz dy d\Omega_{\mathbf{m}}, \quad (3.6)$$

where

$$\hat{\mathbf{f}}_1(\mathbf{p}, \mathbf{q}) := \hat{\mathbf{f}}(\mathbf{p}, \mathbf{q}) - \hat{\mathbf{f}}^{(0)}(\mathbf{p}, \mathbf{q}).$$

In particular, for the linear bond force (2.8), the bond forces $\hat{\mathbf{f}}_1(\mathbf{p}, \mathbf{q})$ and $\hat{\mathbf{f}}_0(\mathbf{p}, \mathbf{q})$ called also the *micropolarization tensors*

$$\begin{aligned}\tilde{\boldsymbol{\tau}}(\mathbf{x}, \hat{\mathbf{x}}) &:= \hat{\mathbf{f}}_1(\mathbf{x}, \hat{\mathbf{x}}) = \mathbf{C}_1(\mathbf{x}, \hat{\mathbf{x}})\boldsymbol{\eta}(\hat{\mathbf{x}}, \mathbf{x}), \\ \tilde{\boldsymbol{\tau}}^{(0)}(\mathbf{x}, \hat{\mathbf{x}}) &:= \hat{\mathbf{f}}^{(0)}(\mathbf{x}, \hat{\mathbf{x}}) = \mathbf{C}^{(0)}(\mathbf{x}, \hat{\mathbf{x}})\boldsymbol{\eta}(\hat{\mathbf{x}}, \mathbf{x})\end{aligned}\quad (3.7)$$

are expressed through the material parameters (3.2).

3.2 Analytica and Computational Micromechanics in LM

The effective field hypothesis (EFH) dates back to Poisson, Faraday, Mossotti, Clausius, Lorenz, and Maxwell (1824-1879, see [79]) who proposed EFH **H1a** as a local homogeneous field acting on the inclusions ($\mathbf{x} \in v_i$)

$$\bar{\varepsilon}_i(\mathbf{x}) = \text{const} \quad (3.8)$$

and differing from the applied macroscopic one (at infinity). This concept of EFH (forming the first background of analytical micromechanics, see for details [53]) has directed the development of micromechanics (even if the term EFH was not used) over the last 150 years (daily and globally) and contributed to their progress incomparable with any other concept of analytical micromechanics.

Buryachenko [94] and [95] presented general classifications of Analytical Micromechanics (AMic) and Computational Micromechanics (CMic) methods. So, the concept of the EFH (even if this term is not mentioned) in combination with subsequent assumptions totally predominates (and creates the fundamental limitations) in all four groups of *Analytical Micromechanics* (AMic, classification by Willis [465]) of *random* random structure matrix CMs in physics and mechanics of heterogeneous media:

$$\begin{array}{ll} \underline{\text{Gr1}}) \text{ model methods,} & \underline{\text{Gr2}}) \text{ perturbation methods,} \\ \underline{\text{Gr3}}) \text{ variational methods,} & \underline{\text{Gr4}}) \text{ self – consistent methods,} \end{array} \quad (3.9)$$

see for references and details [53], [79], [142], [246], [442]. The ultimate goal of AMic is to develop more cheap, fast, robust, and more flexible methods (for making \mathbf{L}^* estimations) than direct numerical simulation (DNS), although it takes additional intellectual complexity to the implementations.

In contrast, *Computational Micromechanics* (CMic) for CM of *deterministic* structures is based on DNS which can be found by different numerical methods. Computational micromechanics can be classified into three broad categories (blocks):

$$\begin{array}{lll} \underline{\text{Block 1)}} \text{ Asymptotic} & \underline{\text{Block 2)}} \text{ Computational,} & \underline{\text{Block 3)}} \text{ Finite set of} \\ \text{homogenization,} & \text{homogenization,} & \text{inclusions.} \end{array} \quad (3.10)$$

Blocks 1 and 2 are applied to periodic structure composites (see Introduction). Block 3 corresponds to one and the finite set of inclusions for either the finite-size sample or the infinite matrix with a finite set of inclusions (in such a case, the problem can be solved by either the volume integral equation methods or boundary integral equation one, see for references, e.g. [79]). The key distinction between CMic and AMic lies in the reliance on DNS, which sets computational methods apart from analytical ones. This differentiation is not based on the conventional definitions of “analytical” and “computational” but instead arises from the specific techniques employed to model and estimate material properties. It should be mentioned that the classification of AMic (3.9) and CMic (3.10) hold also for PM (see for details [95]).

A key concept in analytical micromechanics is the GIE, which precisely relates random fields at a given point to those in its surroundings. Derivation of the GIE begins with the static governing equation for displacement, which follows a Navier-like form

$$\nabla^L \mathbf{L}^{(0)}(\mathbf{x}) \nabla \mathbf{u}(\mathbf{x}) = -\nabla^L \mathbf{L}_1(\mathbf{x}) \nabla \mathbf{u}(\mathbf{x}). \quad (3.11)$$

Various forms of GIEs, ranked by increasing generality, are detailed in [63] and reproduced in [79] ($\mathbf{x} \in w$):

$$\boldsymbol{\varepsilon}(\mathbf{x}) = \boldsymbol{\varepsilon}^{w\Gamma} + \int \mathbf{U}(\mathbf{x} - \mathbf{y})^L \boldsymbol{\tau}(\mathbf{y}) \, d\mathbf{y}, \quad (3.12)$$

$$\boldsymbol{\varepsilon}(\mathbf{x}) = \langle \boldsymbol{\varepsilon} \rangle(\mathbf{x}) + \int \mathbf{U}(\mathbf{x} - \mathbf{y}) [{}^L \boldsymbol{\tau}(\mathbf{y}) - \overline{{}^L \boldsymbol{\tau}}(\mathbf{y})] \, d\mathbf{y}, \quad (3.13)$$

$$\boldsymbol{\varepsilon}(\mathbf{x}) = \langle \boldsymbol{\varepsilon} \rangle(\mathbf{x}) + \int [\mathbf{U}(\mathbf{x} - \mathbf{y})^L \boldsymbol{\tau}(\mathbf{y}) - \underline{\langle \mathbf{U}(\mathbf{x} - \mathbf{y})^L \boldsymbol{\tau} \rangle}(\mathbf{y})] \, d\mathbf{y}, \quad (3.14)$$

$\langle (\cdot) \rangle$ and $\langle (\cdot) \rangle(\mathbf{x})$ are the statistical averages introduced in Subsection 2.4. Hereafter, one introduces the infinite body Green's function $\mathbf{G}^{(0)}$ of the Navier equation with homogeneous elastic moduli ${}^L \mathbf{L}^{(0)}$: $\nabla \left\{ {}^L \mathbf{L}^{(0)} [\nabla \otimes \mathbf{G}^{(0)}(\mathbf{x})] \right\} = -\boldsymbol{\delta} \boldsymbol{\delta}(\mathbf{x})$, of order $O(\int |\mathbf{x}|^{1-d} d|\mathbf{x}|)$ as $|\mathbf{x}| \rightarrow \infty$ and vanishing at infinity ($|\mathbf{x}| \rightarrow \infty$). The Green's tensors for the strains is used $\mathbf{U}(\mathbf{x}) = \nabla \nabla \mathbf{G}^{(0)}(\mathbf{x})$.

Comment 3.1. The historical development of the GIE from Eq. (3.12) to Eq. (3.14), with key milestones ([383], [411], [253], [360]), is outlined in [79]. So, the integral in Eq. (3.12) has no absolute convergence whereas in Eq. (3.13) (proposed in [383] at $\langle \boldsymbol{\varepsilon} \rangle(\mathbf{x}) \equiv \text{const.}$) there are no difficulties connected with the asymptotic behavior of the generalized functions \mathbf{U} at infinity (as $|\mathbf{x} - \mathbf{y}|^{1-d}$) and there is no need to postulate either the shape or the size of the integration domain w [219], [172], [244], [245] (see also [427]) or to resort to either regularization [248], [250], [268], [269], [276] or renormalization [105], [341], or to consider an auxiliary problem with mixed boundary conditions [48], [49] of integrals (3.12) that are divergent at infinity [465]. The shift of the statistical average bracket from $\overline{\cdot}$ (3.13) to $\underline{\langle \cdot \rangle}$ (3.14) marks the emergence the second background of micromechanics (called also Computational Analytical Micromechanics, CAM) [79], a pivotal advancement in micromechanics since Rayleigh's first intuitive formulation of GIE (3.13) [383] (at $\langle \boldsymbol{\varepsilon} \rangle(\mathbf{x}) \equiv \text{const.}$).

3.3 Modeling of one inclusion inside the infinite matrix

We consider the equilibrium equation for an infinite R^d ($d = 1, 2, 3$) homogeneous peridynamic medium (2.16) subjected to the body force with compact support $\mathbf{b}(\mathbf{x})$ (2.4).

$$\widehat{\mathcal{L}}^{(0)}(\mathbf{C}^{(0)}, \overline{\mathbf{u}})(\mathbf{x}) + \mathbf{b}(\mathbf{x}) = \mathbf{0}. \quad (3.15)$$

A prescribed displacement $\overline{\mathbf{u}}(\mathbf{x})$ (called the *effective displacement field*) corresponds to the self-equilibrated body-force density $\mathbf{b}(\mathbf{x})$. In particular, a case

$\bar{\mathbf{u}}(\mathbf{x})$ corresponding to the homogeneous effective strain is $\bar{\mathbf{u}}(\mathbf{x}) = \bar{\boldsymbol{\varepsilon}} \cdot \mathbf{x}$, $\bar{\boldsymbol{\varepsilon}} = \text{const}$. Let us consider a wacrodomain w with one inclusion v_i subjected to the prescribed effective field loading $\bar{\boldsymbol{\varepsilon}}(\mathbf{x})$ corresponding to the body force with compact support $\mathbf{b}(\mathbf{x})$ (2.4). Then, Eq. (2.6) for a general peridynamic operator $\tilde{\mathcal{L}}$ can be presented as

$$\tilde{\mathcal{L}}(\mathbf{u})(\mathbf{x}) = \tilde{\mathcal{L}}^{(0)}(\bar{\boldsymbol{\varepsilon}})(\mathbf{x}) = -\mathbf{b}(\mathbf{x}). \quad (3.16)$$

The main advantage of the representation (3.16) (see also p. 774 in [79]) is that it avoids the challenges associated with the fuzzy boundaries that are characteristic of nonlocal theories (see, e.g., [145], [256], [322], [413]). Equation (3.16) simplifies these challenges by eliminating the need for volumetric boundary conditions and sidestepping the difficulties of properly imposing surface effects (see for references and details, e.g. [393], [459], [493], and [41], Chapter 14) in nonlocal models. This approach contributes to a more tractable and efficient formulation for analyzing materials under nonlocal influences.

Hereafter for the contraction a solution of Eq. (3.16) for nonlinear elastic case, the *perturbators* and field concentrations are defined in the reduced form ($\mathbf{x} \in R^d$)

$$\boldsymbol{\vartheta}(\mathbf{z}) - \bar{\boldsymbol{\vartheta}}(\mathbf{z}) = \mathcal{L}_i^{\theta\zeta}(\mathbf{z}, \bar{\boldsymbol{\zeta}}), \quad (3.17)$$

where we introduce the substitutions

$$(\mathbf{u}, \boldsymbol{\eta}) \leftrightarrow \boldsymbol{\vartheta}, \quad (\mathbf{u}, \boldsymbol{\varepsilon}) \leftrightarrow \boldsymbol{\zeta}, \quad [\mathbf{x}, (\hat{\mathbf{x}}, \mathbf{x})] \leftrightarrow \mathbf{z}. \quad (3.18)$$

The elements of the doublet $\boldsymbol{\vartheta}$ correspond to the variables on the left-hand side of Eq. (3.18), the elements of the doublet $\boldsymbol{\zeta}$ correspond to the effective fields on the right-hand sides of the definitions, whereas the arguments \mathbf{x} and $(\hat{\mathbf{x}}, \mathbf{x})$ of the doublet \mathbf{z} correspond to the parameters \mathbf{u} and $\boldsymbol{\eta}$, respectively. The superindeces $\theta\zeta$ of the perturbators $\mathcal{L}^{\theta\zeta}$ correspond to the variables in the left-hand side $\boldsymbol{\vartheta}$ and right-hand side $\boldsymbol{\zeta}$, respectively. In particular, the operators $\mathcal{L}_k^{uu}(\mathbf{x} - \mathbf{x}_k, \bar{\boldsymbol{\mu}})$ and $\mathcal{L}_k^{u\varepsilon}(\mathbf{x} - \mathbf{x}_k, \bar{\boldsymbol{\varepsilon}})$ (called the *perturbators* of the displacement) have the physical interpretation of perturbations introduced by a single heterogeneity v_k in the infinite matrix subjected to the effective fields $\bar{\boldsymbol{\mu}}_i(\mathbf{x})$ and $\bar{\boldsymbol{\varepsilon}}_i(\mathbf{x})$, respectively, where at first no restrictions are imposed on the inhomogeneities of the effective fields $\bar{\boldsymbol{\mu}}_i(\mathbf{x})$ and $\bar{\boldsymbol{\varepsilon}}_i(\mathbf{x})$.

Let us consider two inclusions v_i and v_j placed in an infinite homogeneous matrix and subjected to the inhomogeneous field $\tilde{\boldsymbol{\zeta}}_{i,j}(\mathbf{x})$ ($\mathbf{u}, \boldsymbol{\eta} = \boldsymbol{\vartheta}$; $\mathbf{u}, \boldsymbol{\varepsilon} = \boldsymbol{\zeta}$; $[\mathbf{x}, (\hat{\mathbf{x}}, \mathbf{x})] = \mathbf{z}$; $\mathbf{x} \in \mathbb{R}^d$). We can transform Eq. (3.5) into the following ones ($\mathbf{z} \in v_i^l$)

$$\boldsymbol{\vartheta}(\mathbf{z}) - \tilde{\boldsymbol{\vartheta}}_{i,j}(\mathbf{z}) - \mathcal{L}_i^{\theta\zeta}(\mathbf{z} - \mathbf{x}_i, \tilde{\boldsymbol{\zeta}}_{i,j}) := \mathcal{L}_{i,j}^{\theta\zeta}(\mathbf{z}, \tilde{\boldsymbol{\zeta}}_{i,j}) \quad (3.19)$$

defining the perturbator $\mathcal{L}_{i,j}^{\theta\zeta}(\mathbf{z}, \tilde{\boldsymbol{\zeta}}_{i,j})$ which can be found by any numerical method analogously to the operator $\mathcal{L}_i^{\theta\zeta}(\mathbf{z} - \mathbf{x}_i, \bar{\boldsymbol{\zeta}}_i)$ (3.17). It should be mentioned that the operators $\mathcal{L}_i^{\theta\zeta}(\mathbf{z} - \mathbf{x}_i, \tilde{\boldsymbol{\zeta}}_{i,j})$ and $\mathcal{L}_{i,j}^{\theta\zeta}(\mathbf{z}, \tilde{\boldsymbol{\zeta}}_{i,j})$ (3.19) act on the

effective fields $\tilde{\boldsymbol{\zeta}}_{i,j}(\mathbf{x})$ at $\mathbf{x} \in v_i$ and $\mathbf{x} \in v_i, v_j$, respectively, and the kernel of the operator $\mathcal{L}_{i,j}^{\theta\zeta}$ can be decomposed ($K = I, J$):

$$\mathcal{L}_{i,j}^{\theta\zeta}(\mathbf{z}, \mathbf{y}) = \mathcal{L}_{i,j}^{I\theta\zeta}(\mathbf{z}, \mathbf{y}) + \mathcal{L}_{i,j}^{J\theta\zeta}(\mathbf{z}, \mathbf{y}), \quad \mathcal{L}_{i,j}^{K\theta\zeta}(\mathbf{z}, \mathbf{y}) = \mathcal{L}_{i,j}^{\theta\zeta}(\mathbf{z}, \mathbf{y})V_k(\mathbf{y}), \quad (3.20)$$

where one follows Mura's tensor indicial notation (see for details [79]). The double superindices $^{\theta\zeta}$ is used analogously to the double superindices uu and $^{u\varepsilon}$ in Eqs. (3.17).

Similarly, the effective field perturbators $\mathcal{J}_{i,j}^{\theta\zeta}$ and $\mathcal{J}_{i,j}^{\theta\zeta\infty}$ can be defined; they describe the perturbation of the effective field $\bar{\boldsymbol{\vartheta}}_i(\mathbf{z}) - \tilde{\boldsymbol{\vartheta}}_{i,j}(\mathbf{z})$ introduced by both the heterogeneity v_j (interacting with v_i) and the fictitious inclusion with the response operator $\mathcal{L}^{(0)}$ and eigenfield $\boldsymbol{\beta}_1^{\text{fict}}(\mathbf{y})$ corresponding to the field in the remote inclusion v_j (without interaction with v_i) ($\mathbf{y} \in v_j$, $\mathbf{x} \in v_i$, $\mathbf{z} \in \mathbb{R}^d$)

$$\bar{\boldsymbol{\vartheta}}_i(\mathbf{z}) - \tilde{\boldsymbol{\vartheta}}_{i,j}(\mathbf{z}) = \mathcal{J}_{i,j}^{\theta\zeta}(\tilde{\boldsymbol{\zeta}}_{i,j})(\mathbf{z}) \quad (3.21)$$

$$\bar{\boldsymbol{\vartheta}}_i(\mathbf{z}) - \tilde{\boldsymbol{\vartheta}}_{i,j}(\mathbf{z}) = \mathcal{J}_{i,j}^{\theta\zeta\infty}(\tilde{\boldsymbol{\zeta}}_{i,j})(\mathbf{z}), \quad (3.22)$$

(see for details [79]).

Comment 3.2. Estimation of the perturbator $\mathcal{L}_i^{\theta\zeta}(\mathbf{z}, \bar{\boldsymbol{\zeta}})$ (3.17) is, in fact, a basic problem of micromechanics (see Introduction) for one inclusion inside the infinite homogeneous matrix. In the PM, estimation of the perturbator $\mathcal{L}_i^{\theta\zeta}(\mathbf{z}, \bar{\boldsymbol{\zeta}})$ (3.17) was considered by four different methods (see [79], [75]) for the linear bond-based medium with the same horizon l_δ in both the inclusion and matrix. The generalization to the linear state-based model as well as to the multiphysics coupled problem (see the LM applications in [63]) are straightforward. The popular discretization methods for the solution of PD equations (see for references [120], [121], [309]) are the meshfree method with one-point Gaussian quadrature referring to it as "meshfree PD" [418] (see also the solutions for 1D case [43], [155], [156], [158], [419], [457], [459] and 2D case [42], [225], [291], [391]), finite element methods (FEM, [110], [322], [386], [432], [433], [441]), [462]), quadrature and collocation approaches [398], [502], [503], and the boundary element method [307]. Adaptive algorithm (see, e.g., [42], [43], [76]) using a multi-grid approach with fine grid spacing only in critical regions is designed in multi-adaptive approach ([363]) to dynamically switch both the discretization scheme and the grid spacing of the regions.

Comment 3.3. The significantly less trivial phenomenon is another limiting case of CCM-PD coupling, usually small areas of a domain \mathbb{R}^d , which might be affected by the presence of discontinuities is described with a PD model, whereas the remaining parts of the system are described through a more efficient CCM model. The goal of Local-to-Nonlocal (LtN) coupling (see [40], [122], [362], [495], [496], [499], [508]) is to alleviate the computational burden by combining the computational efficiency of PDEs with the accuracy of nonlocal models under the assumption that the location of nonlocal effects can be preliminary prescribed (it looks like a localized plasticity model in the vicinity of inclusions in the LM of CMs, see pp. 556-565 [79]). It would be interesting to estimate $\mathcal{L}_i^{\theta\zeta}(\mathbf{z}, \bar{\boldsymbol{\zeta}})$ for the different

nonlocal models in the phases (up to the vanishing length scale $l_\delta/a \rightarrow 0$ in some areas).

3.4 General integral equations (GIEs)

In this subsection, at first, we consider peridynamic statistically homogeneous CMs occupying the space R^d ($d = 1, 2, 3$). We consider so-called the *general integral equation* (GIE) connecting the random fields at the point being considered and all surrounding points. At first, the loading by the body force with a compact support $\mathbf{b}(\mathbf{x})$ (2.4), the direct summations of all surrounding perturbators $\mathcal{L}_j^{\theta\zeta}(\mathbf{z}, \bar{\zeta})$ (3.5) exerting on the fixed inclusion v_i is described by the GIE (called the Additive GIE, AGIE, see for details [93]) ($\mathbf{z} \in v_i$)

$$\langle \vartheta \rangle_i(\mathbf{z}) = \vartheta^{b(0)}(\mathbf{z}) + \int \mathcal{L}_j^{\theta\zeta}(\mathbf{z} - \mathbf{x}_j, \bar{\zeta}) \varphi(v_j, \mathbf{x}_j | v_i, \mathbf{x}_i) d\mathbf{x}_j \quad (3.23)$$

with the deterministic fields $\vartheta^{b(0)}(\mathbf{z})$ produced by the body force $\mathbf{b}(\mathbf{x})$ in the infinite homogeneous matrix. The term *Additive* GIE is used similarly to *Additive* Manufacturing because the perturbations in Eq. (3.23) are directly added without any renormalization terms, such as those in Eq. (3.24). A centering of Eqs. (3.16) is considered which performs a subtraction from both sides of Eq. (3.23) of their statistical averages. It leads to the GIE

$$\begin{aligned} \langle \vartheta \rangle_i(\mathbf{z}) &= \langle \vartheta \rangle(\mathbf{z}) + \int [\mathcal{L}_j^{\theta\zeta}(\mathbf{z} - \mathbf{x}_j, \bar{\zeta}) \varphi(v_j, \mathbf{x}_j | v_i, \mathbf{x}_i) \\ &\quad - \langle \mathcal{L}_j^{\theta\zeta}(\mathbf{z} - \mathbf{x}_j, \bar{\zeta}) \rangle(\mathbf{x}_j)] d\mathbf{x}_j, \end{aligned} \quad (3.24)$$

which is more general and valid for any inhomogeneous $\langle \vartheta \rangle(\mathbf{z})$ while Eqs. (3.23) are only correct for the the body force $\mathbf{b}(\mathbf{x})$ with a compact support. Owing to the centering of Eq. (3.16), Eq. (3.24) contains the renormalizing term $\langle \mathcal{L}_j^{\theta\zeta}(\mathbf{z} - \mathbf{x}_j, \bar{\zeta}) \rangle(\mathbf{x}_j)$ providing an absolute convergence of the integrals involved in Eqs. (3.24). The derivation of the exact form of the GIE (3.24) has a long and intricate history, particularly in the context of LM of CMs (see [61], [63] for references and details). The first GIE was heuristically proposed by Lord Rayleigh [383] and was later rigorously established in 1977 (see [79]). A second GIE in the framework of LM, along with its generalizations to strongly and weakly nonlocal linear heterogeneous materials, was introduced between 2010 and 2022 (see for references and details [79]). However, in all prior developments, specific instances of GIE (3.24) were obtained through intricate multistep procedures, constrained by particular linear constitutive relations governing the phases of the material. In contrast, a more general form of GIE (3.24), applicable to CMs with strongly and weakly nonlocal as well as nonlinear phase properties, was derived directly from the newly formulated AGIE (3.23) via a single-step centering operation. This advancement eliminates the need for case-specific formulations and significantly broadens the applicability of the GIE and AGIE framework.

After a statistical average of Eqs. (3.23) and (3.24), the conditional perturbator $\langle \mathcal{L}_j^{\theta\zeta}(\mathbf{z}, \bar{\zeta}) | v_i, \mathbf{x}_i \rangle_j$ can be expressed through the explicit perturbator for two interacting heterogeneities subjected to the field $\tilde{\zeta}_{i,j}$

$$\langle \bar{\vartheta}_i \rangle(\mathbf{z}) = \vartheta^{b(0)}(\mathbf{z}) + \int \mathcal{J}_{i,j}^{\theta\zeta}(\langle \tilde{\zeta}_{i,j} \rangle)(\mathbf{z}) \varphi(v_j, \mathbf{x}_j | v_i, \mathbf{x}_i) d\mathbf{x}_j, \quad (3.25)$$

$$\begin{aligned} \langle \bar{\vartheta}_i \rangle(\mathbf{z}) &= \langle \vartheta \rangle(\mathbf{z}) + \int \{ \mathcal{J}_{i,j}^{\theta\zeta}(\langle \tilde{\zeta}_{i,j} \rangle)(\mathbf{z}) \varphi(v_j, \mathbf{x}_j | v_i, \mathbf{x}_i) \\ &- \mathcal{J}_{i,j}^{\theta\zeta\infty}(\langle \tilde{\zeta}_{i,j} \rangle)(\mathbf{z}) \} d\mathbf{x}_j, \end{aligned} \quad (3.26)$$

where the conditional probability density $\varphi(v_j, \mathbf{x}_j | v_1, \mathbf{x}_1)$ for one fixed inclusion was used (see for details [79]); $\mathcal{L}_j^{\theta\zeta}(\mathbf{z} - \mathbf{x}_j, \bar{\zeta})$ stands a perturbation $\mathcal{L}_j^{\theta\zeta}(\mathbf{z} - \mathbf{x}_j, \bar{\zeta})$ at the fixed inclusion $v_1 \neq v_j$. The deterministic field $\vartheta^{b(0)}(\mathbf{z})$ (3.25) produced by the forcing term $\mathbf{b}(\mathbf{x})$ in the infinite homogeneous matrix. Equations (3.25) and (3.26) are central to the overall formulation, capturing the material's response under the applied effective field loading. These equations are constructed based on numerical solutions for one or two inclusions, and they incorporate statistically averaged fields $\langle \bar{\zeta}_i \rangle(\mathbf{x})$ and $\langle \tilde{\zeta}_{i,j} \rangle(\mathbf{x})$ to represent the overall macroscopic behavior of the composite or heterogeneous material. There are a couple of fundamental advantages of Eqs. (3.25) and (3.26). So, these equations have no Green functions and, moreover, the most intriguing feature of Eqs. (3.25) and (3.26) is the absence of a constitutive law in these equations. As we can see, Eqs. (3.25) and (3.26) for the peridynamic micromechanics coincides with the corresponding equation for the LM CMs (see [63]). It means that the same equation can be used for both the peridynamic CMs and locally elastic CMs. The GIEs (3.25) and (3.26) proposed are adapted to the straightforward generalizations of corresponding methods of local thermoelastic micromechanics (see, e.g., [53], [61], [63]) to their peridynamic counterparts.

Comment 3.4. The analytical micromechanics (Amic) formulation (3.9) is generally derived from the solutions to Eqs. (3.25) and (3.26), along with their specific cases. In particular, within the LM framework, the perturbations $\mathcal{L}_j^{\theta\zeta}(\mathbf{z} - \mathbf{x}_j, \bar{\zeta})$ are determined using various methods like FEA ([98], [99], [100], [101]), VIE method ([54], [55]), BIE approach ([59], [66], [69], [71]). These solutions are then substituted into Eq. (3.14) to estimate the effective moduli $L^*_{\mathbf{L}}$ and stress concentration factors. The classical hypotheses for the LM, such as the Effective Field Hypothesis (EFH) (3.1) and its extension, closing assumptions along with the assumption of ellipsoidal symmetry, have been analyzed in detail ([79]). These hypotheses are fundamental to the classical LM methods, including the Effective Field Method (EFM), the Mori-Tanaka Method (MTM), and the Multiparticle Effective Field Method (MEFM). The GIE (3.14) enhances the accuracy of local field estimations, even correcting the sign of predictions within inclusions ([79]). Equation (3.14) has been extended to address a variety of other problems within the LM framework: thermoelasticity ([68], [69], [99], [100], [101]), coupled problems ([61], [63]), and wave propagation ([61], [63]), and infiltration in porous media [65]. It has also been adapted for CMs with both strongly nonlocal (e.g., strain-type, displacement-type, and peridynamics) and weakly nonlocal (e.g., strain-gradient, stress-gradient, and

higher-order models) phase properties, as discussed in Chapter 14 of [79]. However, a key limitation of all these GIEs and their extensions (considered in the papers referred to in Subsection 3.4) is that they remain linear in relation to the primary unknown variable. To the author's knowledge, there are no existing nonlinear versions of the GIE (3.24) and the AGIE (3.23)—whether for LM or PM—that directly or implicitly account for nonlinear constitutive phase properties. In the following section, the author proposes a solution to the nonlinear AGIEs (3.23), offering a potential way to address this gap.

4 Solution of nonlinear AGIEs for random structure CMs

4.1 Iterative solution of AGIE

The effective field hypothesis, which serves as the fundamental approximation in numerous micromechanical methods, is mathematically formulated by Eq. (3.8) (for details, see [53]). To achieve closure of the AGIE (3.25), the following additional hypothesis is introduced:

Hypothesis H2a). *Each pair of inclusions v_i and v_j is subjected to the inhomogeneous field $\tilde{\zeta}_{i,j}(\mathbf{x})$, and statistical average $\langle \tilde{\zeta}_{i,j} \rangle(\mathbf{x})$ is defined by the formula ($\zeta = \mathbf{u}, \varepsilon$)*

$$\langle \tilde{\zeta}_{i,j} \rangle(\mathbf{x}) = \langle \bar{\zeta}_k \rangle(\mathbf{x}) \quad (4.1)$$

at $\mathbf{x} \in v_k$, $k = i, j$.

The hypothesis **H2a**, when reformulated in terms of the strain fields $\varepsilon(\mathbf{x})$ for $\mathbf{x} \in v_i$, represents a conventional closure assumption (for further details, see [53], [246], [465]). This assumption reduces to the "quasicrystalline" approximation introduced by Lax [287], which neglects the pairwise interactions between heterogeneities and assumes spatial uniformity of the effective fields.

Hypothesis H2b, "quasi-crystalline" approximation. *It is supposed that the mean value of the effective field at a point $\mathbf{x} \in v_i$ does not depend on the field inside other heterogeneities $v_j \neq v_i$, $\mathbf{x} \in v_k$, ($k = i, j$):*

$$\langle \bar{\zeta} | v_i, \mathbf{x}_i; v_j, \rangle(\mathbf{x}) = \langle \bar{\zeta}_k \rangle(\mathbf{x}) \quad (4.2)$$

$$\langle \bar{\zeta}_k \rangle(\mathbf{x}) \equiv \text{const.} \quad (4.3)$$

Acceptance of hypothesis **H2a** closes the system (3.25) in the following forms,

$$\langle \bar{\vartheta}_i \rangle(\mathbf{z}) = \vartheta^{b(0)}(\mathbf{z}) + \int [\mathcal{J}_{i,j}^{I\theta\zeta}(\mathbf{z}, \langle \bar{\zeta}_i \rangle) + \mathcal{J}_{i,j}^{J\theta\zeta}(\mathbf{z}, \langle \bar{\zeta}_j \rangle)] \varphi(v_j, \mathbf{x}_j; v_i, \mathbf{x}_i) d\mathbf{x}_j \quad (4.4)$$

were a decomposition $\mathcal{J}_{i,j}^{\theta\zeta} = \mathcal{J}_{i,j}^{I\theta\zeta} + \mathcal{J}_{i,j}^{J\theta\zeta}$ was introduced analogously to Eq. (3.20). The integral equation (4.4) can be solved using an iterative approach

based on a recursive formula

$$\begin{aligned} \langle \bar{\boldsymbol{\vartheta}}_i^{[n+1]} \rangle(\mathbf{z}) &= \boldsymbol{\vartheta}^{b(0)}(\mathbf{z}) + \int [\mathcal{J}_{i,j}^{I\theta\zeta}(\langle \bar{\boldsymbol{\zeta}}_i^{[n]} \rangle)(\mathbf{z}) + \mathcal{J}_{i,j}^{J\theta\zeta}(\langle \bar{\boldsymbol{\zeta}}_j^{[n]} \rangle)(\mathbf{z})] \\ &\quad \times \varphi(v_j, \mathbf{x}_j |; v_i, \mathbf{x}_i) d\mathbf{x}_j, \end{aligned} \quad (4.5)$$

$$\langle \boldsymbol{\vartheta}^{[n+1]} \rangle_i(\mathbf{z}) = \mathcal{A}_i^{\theta\zeta}(\langle \bar{\boldsymbol{\zeta}}_i^{[n+1]} \rangle)(\mathbf{z}), \quad (4.6)$$

$$\bar{v}_i \langle \boldsymbol{\tau}^{[n+1]} \rangle_i(\mathbf{x}) = \mathcal{R}_i(\langle \bar{\boldsymbol{\zeta}}_i^{[n+1]} \rangle)(\mathbf{x}). \quad (4.7)$$

The iterative solution is constructed with an initial approximation derived as an explicit solution from Equations (4.3), within the framework of the effective field hypothesis **H1a** (3.8) (see for details [79]).

Equation (4.3) admits a simplified form under Hypothesis Hb2, as shown in Equations (4.2), which are also utilized in the LM method (see [53]). However, a direct generalization of Lax's "quasicrystalline" approximation is possible (see Equation (4.2)) when the assumptions in (4.2) are relaxed, allowing the statistical average of the perturbed strain field, $\langle \bar{\boldsymbol{\zeta}}_k \rangle(\mathbf{z})$, to vary spatially rather than remain constant, i.e., $\langle \bar{\boldsymbol{\zeta}}_k \rangle(\mathbf{z}) \neq \text{const}$ for $\mathbf{z} \in v_k^l$, ($k = i, j$)

$$\langle \mathcal{L}_j^{\theta\zeta}(\mathbf{z}, \bar{\boldsymbol{\zeta}}_j) |; v_i, \mathbf{x}_i \rangle = \langle \mathcal{L}_j^{\theta\zeta}(\mathbf{z}, \bar{\boldsymbol{\zeta}}_j) \rangle. \quad (4.8)$$

This significantly simplifies the problem formulated in Eq. (4.3), where, under these conditions, the equation takes a more tractable form $\mathcal{J}_{i,j}^{\theta\zeta} = \mathcal{J}_{i,j}^{\theta\zeta\infty}$ ($\mathbf{x} \in v_i$) that reduces Eq. (4.3) to

$$\langle \bar{\boldsymbol{\vartheta}}_i^{[n+1]} \rangle(\mathbf{z}) = \boldsymbol{\vartheta}^{b(0)}(\mathbf{z}) + \int \mathcal{J}_{i,j}^{\theta\zeta\infty}(\langle \bar{\boldsymbol{\zeta}}_j^{[n]} \rangle)(\mathbf{z}) \varphi(v_j, \mathbf{x}_j |; v_i, \mathbf{x}_i) d\mathbf{x}_j. \quad (4.9)$$

The second background of LM, introduced in [54], [55] and mathematically formulated in Eq. (4.9), enables the relaxation of fundamental micromechanical assumptions, including the ellipsoidal symmetry hypothesis and the EFH **H1a**. As a result, novel physical effects have been identified that could not be captured within the classical (first) theoretical framework of micromechanics.

Equations (4.4) and (4.9) are derived for general nonlinear cases, incorporating both state-based (2.8) and bond-based (2.15) peridynamic models (PM). In the special case of a linear bond-based PM (2.24), these equations simplify previously established results (see [83]).

4.2 Effective constitutive law and dataset

Equation (4.9) is reformulated in terms of displacement fields ($\mathbf{x} \in v_i$)

$$\bar{\mathbf{u}}^{[n+1]}(\mathbf{x}) = \mathbf{u}^{b(0)}(\mathbf{x}) + \int \mathcal{L}_q^{uu}(\mathbf{x} - \mathbf{x}_q, \bar{\mathbf{u}}^{[n]} |; v_i, \mathbf{x}_i) \varphi(v_q, \mathbf{x}_q |; v_i, \mathbf{x}_i) d\mathbf{x}_q. \quad (4.10)$$

The initial approximation is defined by the driving term, corresponding to the zero-order approximation, given as $\bar{\mathbf{u}}^{[0]}(\mathbf{x}) = \mathbf{u}^{b(0)}(\mathbf{x})$, which itself is expressed

by Equation (3.15). The iterative scheme in Eq. (4.10) constructs a Neumann series representation for the solution ($\mathbf{x} \in v_i^l$)

$$\langle \bar{\mathbf{u}} \rangle_i(\mathbf{x}) := \lim_{n \rightarrow \infty} \langle \bar{\mathbf{u}}^{[n+1]} \rangle_i(\mathbf{x}) = \widehat{\mathcal{D}}_i^{ub}(\mathbf{b}, \mathbf{x}). \quad (4.11)$$

This leads to the formulation of the statistical averages of the field within the fixed extended inclusion, specifically the conditional averages for $\mathbf{x} \in v_i^l$

$$\langle \mathbf{u} \rangle_i(\mathbf{x}) = \widehat{\mathcal{D}}_i^{ub}(\mathbf{b}, \mathbf{x}) + \mathcal{L}_i^{uu}(\mathbf{x} - \mathbf{x}_i, \widehat{\mathcal{D}}_i^{ub}(\mathbf{b}, \mathbf{x})), \quad (4.12)$$

$$\langle \boldsymbol{\sigma} \rangle_i(\mathbf{x}) = \mathcal{L}^\sigma(\langle \mathbf{u} \rangle_i(\mathbf{x})). \quad (4.13)$$

The tensor $\widehat{\mathcal{D}}_q^{ub}(\mathbf{b}, \mathbf{y})$ (4.11) is an inhomogeneous function of coordinates of the fixed inclusion $\mathbf{x} \in v_i^l$ depending on all intersecting inclusions (at least at $|\mathbf{x}_q| \leq a^\delta + l_\delta$) whereas in the dilute approximation the corresponding tensor is $\mathbf{Ib}(\mathbf{y})$.

Equation (4.12) provides a means to compute the expected value of the displacement field over the macroscopic region \mathbf{X}

$$\langle \mathbf{u} \rangle(\mathbf{X}) := c^{l(0)} \langle \mathbf{u} \rangle^{l(0)}(\mathbf{X}) + c^{l(1)} \langle \mathbf{u} \rangle^{l(1)}(\mathbf{X}) \quad (4.14)$$

The statistical averages of the displacement field in the macropoint are expressed through the ensemble averages of displacements at the point \mathbf{X} within the matrix, denoted as $\langle \mathbf{u} \rangle^{l(0)}(\mathbf{X})$, and within the inclusions, represented as $\langle \mathbf{u} \rangle^{l(1)}(\mathbf{X})$. To establish this framework, we introduce an auxiliary domain $v_i^1(\mathbf{X})$, which is characterized by the indicator function $V_i^1(\mathbf{X})$ and is bounded by $\partial v_i^1(\mathbf{X})$, the locus of the centers of translated ellipsoidal regions $v_q(\mathbf{0})$ around the fixed macroscopic point point \mathbf{X} . The domain $v_i^1(\mathbf{X})$ is then obtained as the limiting form of a sequence $v_{ki}^0 \rightarrow v_q^1(\mathbf{X})$, where $v_{ki}^0 \rightarrow v_q^1(\mathbf{X})$ as a given ellipsoid v_k contracts to the point \mathbf{X} . Then $\langle \mathbf{u} \rangle^{l(1)}(\mathbf{X})$ can be estimated as ($\mathbf{y} \in v_q^l$)

$$c^{l(1)} \langle \mathbf{u} \rangle^{l(1)}(\mathbf{X}) = c^{l(1)} \mathbf{u}^{b(0)}(\mathbf{X}) + \int_{v_i^1(\mathbf{X})} n^{(1)}(\mathbf{x}_q) \mathcal{L}_q^{uu}(\mathbf{X} - \mathbf{x}_q, \mathcal{D}_q^u(\mathbf{b}, \mathbf{y})) d\mathbf{x}_q \quad (4.15)$$

Consequently, the statistical expectation of the displacement field, given by Eq. (4.14), can be represented in terms of the volume force density distribution within the region v_q^l , where $\mathbf{y} \in v_q^l$

$$\begin{aligned} \langle \mathbf{u} \rangle(\mathbf{X}) &= \mathbf{u}^{b(0)}(\mathbf{X}) + c^{(0)} \int \mathcal{L}_q^{uu}(\mathbf{X} - \mathbf{x}_q, \mathcal{D}_q^{ub}(\mathbf{b}, \mathbf{y})) \varphi(v_q, \mathbf{x}_q |; \mathbf{X}) d\mathbf{x}_q \\ &+ \int_{v_i^1(\mathbf{X})} n^{(1)}(\mathbf{x}_q) \mathcal{L}_q^{uu}(\mathbf{X} - \mathbf{x}_q, \mathcal{D}_q^{ub}(\mathbf{b}, \mathbf{y})) d\mathbf{x}_q, \end{aligned} \quad (4.16)$$

In Eq. (4.16), the first and second integrals correspond respectively to the first and second terms on the right-hand side of Eq. (4.14). Additionally, the function

$\varphi(v_q, \mathbf{x}_q |; \mathbf{X})$ vanishes, i.e., $\varphi(v_q, \mathbf{x}_q |; \mathbf{X}) = 0$, whenever the point \mathbf{x}_q belongs to the domain $v_i^1(\mathbf{X})$.

The macroscopic stress field in the effective constitutive law is expressed as

$$\langle \boldsymbol{\sigma} \rangle(\mathbf{x}) = \langle \mathcal{L}^{\sigma(0)}(\mathbf{u}) \rangle(\mathbf{x}) + \langle \boldsymbol{\tau} \rangle(\mathbf{x}) \quad (4.17)$$

where the first term on the right-hand side simplifies for the linear matrix and depends on the statistical averages $\langle \mathbf{u} \rangle(\mathbf{x})$: $\langle \mathcal{L}^{\sigma(0)}(\mathbf{u}) \rangle(\mathbf{x}) = \mathcal{L}^{\sigma(0)}(\langle \mathbf{u} \rangle(\mathbf{x}))$ ($\mathbf{x} \in \mathbb{R}^d$) (4.16). To estimate the average $\langle \boldsymbol{\tau} \rangle(\mathbf{x})$, we first consider the fixed inclusion v_q centered at \mathbf{x}_q , which is estimated using Eq. (2.17) with the substitution This inclusion yields the value $\mathcal{L}_1^\sigma(\mathbf{x} - \mathbf{x}_q, \mathbf{u}) = \mathcal{L}^\sigma(\tilde{\boldsymbol{\tau}})$ which is estimated using Equation (2.17) with the substitution $\tilde{\mathbf{f}}^{(0)} \rightarrow \tilde{\mathbf{f}}_1$ as indicated in Eq. (3.21). The statistical average of the local polarization tensor $\langle \boldsymbol{\tau} \rangle(\mathbf{X})$ is then obtained by averaging over the domain v_i^1

$$\langle \boldsymbol{\tau} \rangle(\mathbf{X}) = \int_{v_i^1(\mathbf{X})} n^{(1)} \mathcal{L}^\sigma(\mathbf{C}_1 \boldsymbol{\eta}^D)(\mathbf{y} - \mathbf{X}) d\mathbf{y}, \quad (4.18)$$

$$\begin{aligned} \boldsymbol{\eta}^D(\mathbf{x}, \mathbf{y}) &= \left[\mathcal{D}_i^{ub}(\mathbf{b}, \mathbf{x}) + \mathcal{L}_i^{uu}(\mathbf{x} - \mathbf{x}_i, \mathcal{D}_i^{ub}(\mathbf{b}, \mathbf{x}) \right. \\ &\quad \left. - \mathcal{D}_i^{ub}(\mathbf{b}, \mathbf{y}) - \mathcal{L}_i^{uu}(\mathbf{y} - \mathbf{x}_i, \mathcal{D}_i^{ub}(\mathbf{b}, \mathbf{y})) \right], \end{aligned} \quad (4.19)$$

Here, $v_q^1(\mathbf{x})$ is defined by Equation (2.41), and the statistical average of the displacement field within the inclusion $\mathbf{x} \in v_q$ is represented by $\langle \mathbf{u} \rangle_q(\mathbf{x})$, as shown in Equation (4.15). The estimation of the effective micromodulus [480], which involves averaging the strain energy of the peridynamic material model under homogeneous boundary conditions, raises certain concerns regarding its validity.

The new nonlocal effective constitutive law, expressed in Equation (4.17), bears a strong resemblance to the previously established nonlocal effective constitutive law

$$\langle \boldsymbol{\sigma} \rangle(\mathbf{x}) = {}^L \mathbf{L}^{(0)} \langle \boldsymbol{\varepsilon} \rangle(\mathbf{x}) + \langle {}^L \boldsymbol{\tau} \rangle(\mathbf{y}), \quad {}^L \boldsymbol{\tau}(\mathbf{y}) := {}^L \mathbf{L}_1(\mathbf{y}) \boldsymbol{\varepsilon}(\mathbf{y}). \quad (4.20)$$

This is analogous to the locally elastic constitutive law (2.2) at the microlevel. However, the first term ${}^L \mathbf{L}^{(0)} \langle \boldsymbol{\varepsilon} \rangle(\mathbf{x})$ on the right-hand side of Eq. (4.20) corresponds to a general inhomogeneous strain field, where $\langle \boldsymbol{\varepsilon} \rangle(\mathbf{x}) \neq \mathbf{0}$. On the other hand, the term $\langle \mathcal{L}^{\sigma(0)}(\mathbf{u}) \rangle(\mathbf{x})$ from Eq. (4.17) simplifies to $\mathbf{L}^{(0)} \langle \boldsymbol{\varepsilon} \rangle(\mathbf{x})$ only when the strain field $\langle \boldsymbol{\varepsilon} \rangle(\mathbf{x})$ is homogeneous, i.e., $\langle \boldsymbol{\varepsilon} \rangle(\mathbf{x}) \equiv \text{cons}$.

Numerical analysis was conducted for a 1D statistically homogeneous random structure bar [82], [83] under a self-equilibrated body force condition (2.3), where $\mathbf{b}(\mathbf{x}) = 0$ for $|\mathbf{x}| > B^b$ and $\mathbf{b}(\mathbf{x}) = -\mathbf{b}(-\mathbf{x})$ for $|\mathbf{x}| \leq B^b$; $c^b = 0$. The engineering approach, utilizing the scale separation hypothesis (2.38₂), follows this scheme: first, estimate \mathbf{L}^* by CAM (see Comment 3.4 and a generalized EFM, [79]) under homogeneous boundary conditions (2.40), and then evaluate $\langle \mathbf{u}^{\text{EA}} \rangle(\mathbf{x})$ using Eqs. (2.1)–(2.3) with the substitution $\mathbf{L} \rightarrow \mathbf{L}^*$. This leads to a monotonically increasing displacement field $\langle \mathbf{u}^{\text{EA}} \rangle(\mathbf{x})$ (represented by the solid

curve 4 in Fig. 1). In Fig. 1, the parameters $l_\delta/a = 1$ and $c^{(1)} = 0.5$ are fixed, while B^b/a takes values of 0.25, 0.375, 0.5 (shown in curves 1, 2, and 3, respectively). As observed in Fig. 1, the simultaneous inclusion of the peridynamic constitutive equation (2.5) and the inhomogeneity of the body force $\mathbf{b}(\mathbf{x})$ results in strongly nonmonotonic distributions of the displacement field $\langle \mathbf{u} \rangle(\mathbf{x})$, which differ from $\langle \mathbf{u}^{\text{EA}} \rangle(\mathbf{x})$ by a factor of 9 for curve 1. Due to nonlocal effects, the range of long-range action is restricted not only by $|\mathbf{x}| \leq B^b$, but by a domain $|\mathbf{x}| \leq a^{1-r}$ ($a^{1-r} \approx 3B^b$), meaning that the problem domain $\mathbf{x} \in R^1$ is effectively reduced to a finite domain, avoiding the inconsistencies previously mentioned in [81]. This implies that the domain size $|\mathbf{x}| \leq a^{1-r} \approx 3B^b$ (at the considered scale ratios $a/a^b/l_\delta$) requires stabilization of the displacement fields $\langle \mathbf{u} \rangle(\mathbf{x}) \approx \text{const.}$ (for $|\mathbf{x}| > a^{1-r}$), which significantly exceeds the combined scale of the body force B^b and the horizon l_δ (a synergistic effect). The parameter a^{1-r} should be further learned. Although the term ‘‘RVE’’ (see for details Subsection 8.3) was not directly employed, the domain $|\mathbf{x}| \leq a^{1-r}$ in fact represents the RVE for $\langle \mathbf{u} \rangle(\mathbf{x})$ and this RVE depends on the scale ratios $a/a^b/l_\delta$. In generalizing this phenomenon for an arbitrary body force $\mathbf{b}(\mathbf{x})$ as given in Eq. (2.4), we can define the RVE as the region for which there exists a characteristic size B^{RVE} such that

$$\langle \mathbf{u} \rangle(\mathbf{x}) = \mathbf{u}^\infty \equiv \text{const.}, \quad \text{for } \forall \mathbf{x} \geq B^{\text{RVE}}, \quad (4.21)$$

where this equality holds within a prescribed tolerance.

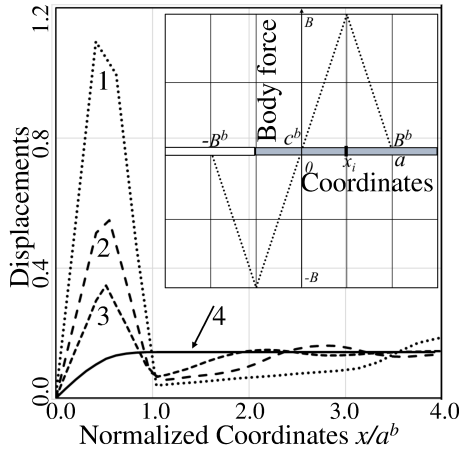


Fig. 1 Average displacement $\langle \mathbf{u} \rangle(\mathbf{x})$ vs x/a^b

For the linear bond-based model of constituents, the governing equations (4.14)–(4.17) reduce to the corresponding relations derived in [82], [83]. For statistically homogeneous composite materials with locally elastic constituent phases, the nonlocal effective operator derived in [320] incorporates microstructural information via the Green’s function of the reference matrix medium (2.5), allowing for a rigorous treatment of the effective response under arbitrary body force distributions. However, the extension of this methodology to PM, where

nonlocal interactions play a fundamental role, is not straightforward due to the absence of classical differential operators. Potential applications of micromechanical modeling of composites subjected to body forces with compact support—such as those induced by localized thermal loading (e.g., laser heating, as discussed in [479], [233], and [483])—were analyzed in [95]. These studies emphasize the necessity of incorporating spatially varying internal forces within a nonlocal framework to accurately capture the mechanical response under external stimuli.

For an arbitrary body force $\mathbf{b}(\mathbf{x})$ with compact support, we have derived formal representations for the effective macroscopic and microscopic fields in a composite material (CM) with a random microstructure. Specifically, we consider the macroscopic displacement $\langle \mathbf{u} \rangle(\mathbf{x})$ and stress $\langle \boldsymbol{\sigma} \rangle(\mathbf{x})$, as well as their corresponding microscopic counterparts $\langle \mathbf{u} \rangle_i(\mathbf{z}, \mathbf{x})$, $\langle \boldsymbol{\sigma} \rangle_i(\mathbf{z}, \mathbf{x})$ and $\langle \boldsymbol{\sigma} \rangle_i(\mathbf{z}, \mathbf{x})$, where the subscript i denotes quantities evaluated within a representative inclusion v_i . For computational implementation and subsequent applications, we construct a dataset of effective parameters for various realizations of the applied body force $\mathbf{b}_k(\mathbf{x})$, expressed as $(\mathbf{x} \in R^d)$

$$\begin{aligned} \mathcal{D}^r &= \{\mathcal{D}_k^r\}_{k=1}^N, \\ \mathcal{D}_k^r &= \{\langle \mathbf{u}_k \rangle(\mathbf{b}_k, \mathbf{x}), \langle \boldsymbol{\sigma}_k \rangle(\mathbf{b}_k, \mathbf{x}), \langle \mathbf{u}_{ik} \rangle(\mathbf{b}_k, \mathbf{z}, \mathbf{x}), \langle \boldsymbol{\sigma}_{ik} \rangle(\mathbf{b}_k, \mathbf{z}, \mathbf{x}), \mathbf{b}_k(\mathbf{x})\}. \end{aligned} \quad (4.22)$$

Here, each realization k th corresponds to a specific body force \mathbf{b}_k , for which the macroscopic displacement $\langle \mathbf{u}_k \rangle(\mathbf{x})$ and stress $\langle \boldsymbol{\sigma}_k \rangle(\mathbf{x})$ fields are computed, along with the local inclusion-scale displacement $\langle \mathbf{u}_{ik} \rangle(\mathbf{z}, \mathbf{x}) := \langle \mathbf{u}_k \rangle_i(\mathbf{z})$ and stress $\langle \boldsymbol{\sigma}_{ik} \rangle(\mathbf{b}_k, \mathbf{z}, \mathbf{x}) := \langle \boldsymbol{\sigma}_k \rangle_i(\mathbf{z})$. The macroscopic coordinate $\mathbf{x} \in R^d$ spans the domain of the homogenized CM, while the local coordinate $\mathbf{z} \in v_i$ resides within the representative inclusion v_i . This dataset \mathcal{D}^r forms a basis for data-driven modeling, enabling efficient retrieval and interpolation of effective response functions for new realizations of \mathbf{b}_k in a computationally efficient manner.

5 Periodic structure CMs

Equations (3.23) and (3.25) were derived under the general assumption of arbitrary probability densities $\varphi(v_j, \mathbf{x}_j)$ and the conditional probability density $\varphi(v_j, \mathbf{x}_j | v_1, \mathbf{x}_1)$, which characterize the statistical distribution of the microstructural inclusions within the CM. However, in subsequent developments, we specialize these representations to periodic structure CMs, where the probability densities $\varphi(v_j, \mathbf{x}_j)$ and $\varphi(v_j, \mathbf{x}_j | v_1, \mathbf{x}_1)$ take deterministic forms, given explicitly as sums of Dirac delta functions (2.36) localized at the periodic grid points $\mathbf{x}_\alpha \in \mathbf{\Lambda}$, corresponding to the structured arrangement of inclusions.

Consequently, the integral relations expressed in Eqs. (4.11)–(4.13) undergo a transformation to a discrete summation form reflecting the periodic

nature of the material structure

$$\bar{\mathbf{u}}(\mathbf{x}) := \lim_{n \rightarrow \infty} \bar{\mathbf{u}}^{[n+1]}(\mathbf{x}) = \widehat{\mathcal{D}}_i^{ub}(\mathbf{b}, \mathbf{x}), \quad (5.1)$$

$$\mathbf{u}(\mathbf{x}) = \widehat{\mathcal{D}}_i^{ub}(\mathbf{b}, \mathbf{x}) + \mathcal{L}_i^{uu}(\mathbf{x} - \mathbf{x}_i, \widehat{\mathcal{D}}_i^{ub}(\mathbf{b}, \mathbf{x})), \quad (5.2)$$

$$\boldsymbol{\sigma}(\mathbf{x}) = \mathcal{L}^\sigma(\mathbf{u})(\mathbf{x}). \quad (5.3)$$

Despite their formal similarity in appearance, these transformed equations (5.1)–(5.3) and the corresponding set of equations (4.11)–(4.13) are conceptually distinct. Equations (4.11)–(4.13) inherently involve ensemble-averaged effective parameters. Equations (5.1)–(5.3), though similar in structure, pertain specifically to periodic composites and thus rely on a deterministic framework where the microstructure $\mathbf{x}_\alpha \in \boldsymbol{\Lambda}$ is predefined.

To perform the statistical averaging of Eqs. (5.1)–(5.3), we employ the translated averaging technique (see [83], [94], [96] for details), which is based on shifting the periodic grid $\boldsymbol{\Lambda}_0$ with corresponding inclusion centers by a translation vector $\boldsymbol{\chi}$, generating a new grid $\boldsymbol{\Lambda}_\chi$. The body force field $\mathbf{b}(\mathbf{x})$ remains fixed throughout this transformation. Mathematically, we consider a $\boldsymbol{\chi}$, leading to a corresponding transformation in the material properties, the characteristic functions of inclusions, and the displacement field:

$$\mathbf{C}(\mathbf{x}, \mathbf{q}, \boldsymbol{\chi}) = \mathbf{C}_0(\mathbf{x} - \boldsymbol{\chi}, \mathbf{q} - \boldsymbol{\chi}), \quad V_i(\mathbf{x}, \boldsymbol{\chi}) = V_{i0}(\mathbf{x} - \boldsymbol{\chi}), \quad (5.4)$$

$$\mathbf{b}(\mathbf{x}, \boldsymbol{\chi}) = \mathbf{b}_0(\mathbf{x}), \quad \mathbf{u}(\mathbf{x}, \boldsymbol{\chi}) \neq \mathbf{u}_0(\mathbf{x} - \boldsymbol{\chi}), \quad (5.5)$$

where the inequality (5.5₂) holds because $\mathbf{b}(\mathbf{x})$ is fixed. For each translation $\boldsymbol{\chi} \in \mathcal{V}_\mathbf{x}$, the corresponding displacement field $\mathbf{u}(\mathbf{x}, \boldsymbol{\chi})$ is determined by solving the governing equations (2.5) or (2.6). This ensemble of solutions allows us to define the macroscopic (or effective) displacement field by averaging over all possible translations $\boldsymbol{\chi}$, ensuring a statistical homogenization of the material response across different realizations of the periodic microstructure. The macroscopic displacement field is thus given by:

$$\langle \{\cdot\} \rangle(\mathbf{x}) = \frac{1}{\bar{\mathcal{V}}_\mathbf{x}} \int_{\mathcal{V}_\mathbf{x}} \{\cdot, \boldsymbol{\chi}\} d\boldsymbol{\chi}, \quad \langle \{\cdot\} \rangle^{(1)}(\mathbf{x}) = \frac{1}{\bar{\mathcal{V}}_\mathbf{x}} \int_{\mathcal{V}_\mathbf{x}} \{\cdot, \boldsymbol{\chi}\} V_i(\mathbf{x}, \boldsymbol{\chi}) d\boldsymbol{\chi}. \quad (5.6)$$

The averages in Eqs. (5.6) represent ensemble averaging over all possible translated realizations of a periodic microstructure, where translations $\boldsymbol{\chi}$ are uniformly distributed over the periodicity cell. This translated averaging applies to periodic CMs with any phase constitutive laws and any inhomogeneous loading. A special case, similar to (5.6₁), was introduced in asymptotic homogenization by [425] and [13] for periodic media under periodic loading. Interestingly, the statistical formulations in Eq. (5.6₂) resemble a student probability problem: inclusion v_i is randomly "dropped" onto a fixed point $\mathbf{x} \in R^d$. However, in (5.6₂), the inclusion belongs to a randomly translated periodic grid $\boldsymbol{\Lambda}_\chi$.

Applying the translated averaging operation (5.6) to Eq. (5.2) and Eq.

(4.11) yields the following expressions ($\mathbf{y} \in v_q^l$)

$$\langle \mathbf{u} \rangle^{l(1)}(\mathbf{X}) = \mathbf{u}^{b(0)}(\mathbf{X}) + \frac{1}{\overline{V}_{\mathbf{x}}} \int_{\mathcal{V}_{\mathbf{x}}} V(\mathbf{x}_q) \mathcal{L}_q^{uu}(\mathbf{X} - \mathbf{x}_q, \widehat{\mathcal{D}}_q^{ub}(\mathbf{b}, \mathbf{x}_q)) d\mathbf{x}_q, \quad (5.7)$$

$$\begin{aligned} \langle \mathbf{u} \rangle(\mathbf{X}) &= \mathbf{u}^{b(0)}(\mathbf{X}) + \frac{c^{l(0)}}{\overline{V}_{\mathbf{x}}} \int_{\mathcal{V}_{\mathbf{x}}} V^{l(0)}(\mathbf{x}_q) \mathcal{L}_q^{uu}(\mathbf{X} - \mathbf{x}_q, \widehat{\mathcal{D}}_q^{ub}(\mathbf{b}, \mathbf{x}_q)) d\mathbf{x}_q, \\ &+ \frac{c^{l(1)}}{\overline{V}_{\mathbf{x}}} \int_{\mathcal{V}_{\mathbf{x}}} V^{l(1)}(\mathbf{x}_q) \mathcal{L}_q^{uu}(\mathbf{X} - \mathbf{x}_q, \widehat{\mathcal{D}}_q^{ub}(\mathbf{b}, \mathbf{x}_q)) d\mathbf{x}_q, \end{aligned} \quad (5.8)$$

which correspond to Eqs. (4.15) and (4.16), respectively, for the general case of the conditional probability density $\varphi(v_q, \mathbf{x}_q; \mathbf{X})$.

The averages $\langle \mathbf{u} \rangle^{l(1)}(\mathbf{X})$ (5.7) and $\langle \mathbf{u} \rangle(\mathbf{X})$ (5.8) depend on the macrocoordinates \mathbf{X} and are not tied to a specific periodic grid $\mathbf{\Lambda}$. In a similar manner, the effective fields $\langle \boldsymbol{\sigma} \rangle^{l(1)}(\mathbf{X})$ and $\langle \boldsymbol{\sigma} \rangle(\mathbf{X})$ can be found. Translation averaging of constitutive law (3.5) with linear matrix (3.1) will lead to formally identical Eq. (4.17)

$$\langle \boldsymbol{\sigma} \rangle(\mathbf{x}) = \mathcal{L}^{\sigma(0)}(\langle \mathbf{u} \rangle)(\mathbf{x}) + \langle \boldsymbol{\tau} \rangle(\mathbf{x}) \quad (5.9)$$

with $\langle \mathcal{L}^{\sigma(0)}(\mathbf{u}) \rangle(\mathbf{x}) = \mathcal{L}^{\sigma(0)}(\langle \mathbf{u} \rangle)(\mathbf{x})$ ($\mathbf{x} \in \mathbb{R}^d$) (5.8). I.e., the term $\langle \mathcal{L}^{\sigma}(\widehat{\boldsymbol{\tau}}^{(0)}) \rangle(\mathbf{x})$ (4.13) is equivalent to the stresses in a pure matrix $\mathbf{C}^{(0)}(\mathbf{x}, \hat{\mathbf{x}})$ produced by the total displacement $\langle \mathbf{u} \rangle(\mathbf{x})$ (5.8).

For estimation of an average $\langle \boldsymbol{\tau} \rangle(\mathbf{x}) = \langle \mathcal{L}^{\sigma}(\mathbf{C}_1, \mathbf{u}) \rangle(\mathbf{x})$ (3.6), we consider, at first, the fixed inclusion v_q with the center \mathbf{x}_q . This inclusion produces value $\mathcal{L}^{\sigma}(\mathbf{C}_1, \mathbf{u})(\mathbf{x} - \mathbf{x}_q)$. Then a statistical average of the local polarization tensor $\langle \boldsymbol{\tau} \rangle(\mathbf{X})$ is also obtained by averaging over the domain v_i^1

$$\langle \boldsymbol{\tau} \rangle(\mathbf{X}) = \frac{1}{\overline{V}_{\mathbf{x}}} \int_{\mathcal{V}_{\mathbf{x}}} V^{l(1)}(\mathbf{y}) \mathcal{L}^{\sigma}(\mathbf{C}_1 \boldsymbol{\eta}^D)(\mathbf{X} - \mathbf{y}) d\mathbf{y}, \quad (5.10)$$

$$\begin{aligned} \boldsymbol{\eta}^D(\mathbf{x}, \mathbf{y}) &= \left[\widehat{\mathcal{D}}_i^{ub}(\mathbf{b}, \mathbf{x}) + \mathcal{L}_i^{uu}(\mathbf{x} - \mathbf{x}_i, \widehat{\mathcal{D}}_i^{ub}(\mathbf{b}, \mathbf{x})) \right. \\ &\quad \left. \widehat{\mathcal{D}}_i^{ub}(\mathbf{b}, \mathbf{y}) - \mathcal{L}_i^{uu}(\mathbf{y} - \mathbf{x}_i, \widehat{\mathcal{D}}_i^{ub}(\mathbf{b}, \mathbf{y})) \right], \end{aligned} \quad (5.11)$$

where one used the representation for the displacement field in the inclusion $\mathbf{x} \in v_q$: $\mathbf{u}(\mathbf{x})$ (5.2).

Analogously to the dataset \mathcal{D}^r (4.22) for random structure CMs, we can define a dataset \mathcal{D}^p for periodic structure CMs

$$\begin{aligned} \mathcal{D}^p &= \{\mathcal{D}_k^p\}_{k=1}^N, \\ \mathcal{D}_k^p &= \{\langle \mathbf{u}_k \rangle(\mathbf{b}_k, \mathbf{x}), \langle \boldsymbol{\sigma}_k \rangle(\mathbf{b}_k, \mathbf{x}), \langle \mathbf{u}_k \rangle^{l(1)}(\mathbf{b}_k, \mathbf{x}), \langle \boldsymbol{\sigma}_k \rangle^{l(1)}(\mathbf{b}_k, \mathbf{x}), \mathbf{b}_k(\mathbf{x})\}, \end{aligned} \quad (5.12)$$

where each effective parameter is computed for a given \mathbf{b}_k using Eqs. (5.6) during the offline stage for the k -th realization. The macrocoordinates $\mathbf{x} \in R^d$ define a coarser dataset \mathcal{D}^p (5.12), which contains less detailed information than \mathcal{D}^r (4.22). The latter depends not only on the macrocoordinates $\mathbf{x} \in R^d$

but also on the local coordinates $\mathbf{z} \in v_i$ within the representative inclusion v_i , providing finer-scale resolution.

Thus, the macroscopic stresses in the effective constitutive law (5.9) depends on the statistical average $\langle \mathbf{u} \rangle(\mathbf{x})$ ($\mathbf{x} \in R^d$) (5.8) and $\mathbf{u}(\mathbf{y})$ ($\mathbf{y} \in v_q^l$) (5.2), respectively. However, these displacement fields $\langle \mathbf{u} \rangle(\mathbf{x})$ (5.8) and $\mathbf{u}(\mathbf{y})$ ($\mathbf{y} \in v_q^l$) (5.2) are not the prime variables and depend on the body force $\mathbf{b}(\mathbf{x})$. The estimation of effective constitutive law in the next subsection is based on the solution of the GIE (3.25) rather than (3.26).

Comment 5.1. To the best of the author's knowledge, the method of reducing DNS to smoothed (effective) parameters (5.12) is novel. Furthermore, a critical aspect in the analysis of periodic structure CMs is the appropriate selection of periodic boundary conditions (PBC) (2.39), (2.40) and volumetric periodic boundary conditions (VPBC) (2.37), (2.38) at the interface of unit cells (UCs), which link the field distributions between adjacent UCs. The established PBC (2.39) and VPBC (2.37) definitively correspond to both homogeneous remote loading (2.28) or (2.29) and the zero body force condition $\mathbf{b}(\mathbf{x}) \equiv \mathbf{0}$ (??). However, for a general body force case (2.4), both PBC (2.39) and VPBC (2.37) become incorrect (see Subsection 2.3). Nevertheless, enforcing any PBC (2.39) and VPBC (2.37) is unnecessary if DNS is utilized to estimate Eqs. (5.6) on a representative volume element (RVE, see Section 7) (possibly consisting of multiple UCs) rather than on a single UC. The size of the RVE (see Comment 4.13) acts as a controlled parameter that must be determined with a prescribed tolerance. Although the integrands in Eqs. (5.6) are computed through DNS within CMic, the combination of Eqs. (5.6) with the RVE concept facilitates the construction of the dataset \mathcal{D}^P . Consequently, the method (5.6) is referred to as CAM's version for periodic structure CMs.

Comment 5.2. In Sections 3 and 4, we analyzed matrix random structure composites (CMs) with GIE (3.24) and AGIE (3.23), which apply to the first group, where a continuous matrix phase contains isolated inhomogeneities. For periodic structure CMs, translation averaging (5.6) is used without microtopology restrictions. The second group [191] includes skeletal, percolated, or laminated composites, where at least two phases form a monolithic frame, such as metallic foams or cellulose-reinforced polymers. Cellulose-reinforced polymers [192], metallic wool, and glass wool have both a network connecting them to the penetrated structure, and also an incomplete network with only one connection to the network tree. The third group involves composites where the phases are contiguous but not interconnected, like polycrystalline metals with different crystallographic orientations, forming heterogeneous materials. Adjusting the constituent concentration can move a composite from one group to another. All periodic structure CMs discussed enable the creation of the dataset \mathcal{D}^P (5.12).

Comment 5.3. The effective macroscopic parameter datasets, \mathcal{D}^f and \mathcal{D}^P , corresponding to the scales B^b (2.3) and $|\Omega_{00}|$, respectively, are functionally independent of the microstructural details of the composite material. Specifically, they do not encode explicit dependencies on the two-point probability distribution $\varphi(v_q, \mathbf{x}_q; v_i, \mathbf{x}_i)$ or the grid $\mathbf{\Lambda}$, nor do they retain information regarding the methods used to evaluate the reference fields in Eqs. (4.11)–(4.19) and (5.1)–(5.11).

Furthermore, Eq. (3.24) is obtained from Eq. (3.23) via a centering transformation, thereby making it a particularized form of the latter. However, Eq. (3.23) holds a significant computational advantage over Eq. (3.24) as it provides the foundation for constructing the dataset \mathcal{D}^f , which is instrumental in the development of machine learning (ML) and neural network (NN) methodologies—particularly surrogate operators (see Subsection 7). These ML-based techniques facilitate the generation of surrogate operators for arbitrary macroscopic loading conditions, whether specified in terms of the macroscopic displacement field $\langle \mathbf{u} \rangle(\mathbf{x})$ or the body force distribution $\mathbf{b}(\mathbf{x})$. Importantly, this approach circumvents the need to explicitly solve the micro-scale problem dictated by Eq. (3.24), thereby significantly reducing computational complexity.

6 Estimation of field fluctuations and effective energy-based criteria

In nonlinear LM problems, a key challenge is estimating the second moment of phase fields ($\boldsymbol{\pi} = \boldsymbol{\varepsilon}, \boldsymbol{\sigma}; \mathbf{x} \in v^{(i)}$):

$$\langle \boldsymbol{\pi} \otimes \boldsymbol{\pi} \rangle_i(\mathbf{x}) = \langle \boldsymbol{\pi} \rangle_i(\mathbf{x}) \otimes \langle \boldsymbol{\pi} \rangle_i(\mathbf{x}) + \Delta_i^{\pi^2}(\mathbf{x}), \quad (6.1)$$

where $\Delta_i^{\pi^2}(\mathbf{x})$ is called the dispersion (or the fluctuation field). Two methods—exact differential analysis and integral equations—yield similar numerical results ([53], [79]). However, using the simplified engineering assumption $\langle \langle \boldsymbol{\pi} \otimes \boldsymbol{\pi} \rangle_i(\mathbf{x}) = \langle \boldsymbol{\pi} \rangle_i(\mathbf{x}) \otimes \langle \boldsymbol{\pi} \rangle_i(\mathbf{x})$ can result in infinite errors under hydrostatic loading of porous isotropic media.

The integral equation method in LM allows for its extension to PM. Specifically, by considering only binary inclusion interactions, new approximations for the second moment can be derived:

$$\begin{aligned} \langle \boldsymbol{\vartheta} \otimes \boldsymbol{\vartheta} \rangle_i(\mathbf{x}) &= \langle \boldsymbol{\vartheta} \rangle_i(\mathbf{x}) \otimes \langle \boldsymbol{\vartheta} \rangle_i(\mathbf{x}) + \int \mathcal{A}_i^{\theta\theta} * \langle \mathcal{L}_p^{\theta\zeta}(\mathbf{x}, \bar{\boldsymbol{\zeta}}) |; v_i, \mathbf{x}_i \rangle \\ &\otimes \mathcal{A}_i^{\theta\theta} * \langle \mathcal{L}_p^{\theta\zeta}(\mathbf{x}, \bar{\boldsymbol{\zeta}}) |; v_i, \mathbf{x}_i \rangle \varphi(v_p, \mathbf{x}_p |; v_i, \mathbf{x}_i) d\mathbf{x}_p. \end{aligned} \quad (6.2)$$

Comment 6.1. The new equation (6.3) is derived for nonlinear PM problems involving the operators $\mathcal{A}_i^{\theta\theta}$ (3.10₂) and $\mathcal{L}_p^{\theta\zeta}(\mathbf{x}, \bar{\boldsymbol{\zeta}})$ (3.10₁). Notably, it exactly matches the equation for a medium with remote BCs (6.3), (3.24) rather than body force loading (2.4), (3.25). These equations extend previous results from linear bond-based and state-based models [89], [85] and unify them with existing LM formulations [53], [79]. This marks a rare instance where PM methods for second-moment fields (nonlinear problems) inspire new LM techniques for nonlinear analysis. Furthermore, the formulations can be extended, as in [85], to include triple-point probability densities $\varphi(v_p, \mathbf{x}_p, v_q, \mathbf{x}_q |; v_i, \mathbf{x}_i)$ for greater accuracy.

Equation (6.3) can be simplified for linear operators $\mathcal{A}_i^{\theta\theta}$ (3.10₂) and $\mathcal{L}_p^{\theta\zeta}(\mathbf{x}, \bar{\boldsymbol{\zeta}})$ (3.10₁) within the EFH framework **H1a** (3.8), enabling its application to derive effective energy-based criteria:

$$\langle \boldsymbol{\eta} \otimes \boldsymbol{\eta} \rangle_i(\mathbf{z}) = \langle \boldsymbol{\eta} \rangle_i(\mathbf{z}) \otimes \langle \boldsymbol{\eta} \rangle_i(\mathbf{z}) + \Delta_i^{\eta^2}(\mathbf{z}), \quad (6.3)$$

where

$$\Delta_i^{\eta^2}(\mathbf{z}) = \int [\mathbb{A}_{i,j}(\mathbf{z})\langle \varepsilon \rangle] \otimes [\mathbb{A}_{i,j}(\mathbf{z})\langle \varepsilon \rangle] \varphi(v_j, \mathbf{x}_j |; v_i, \mathbf{x}_i) d\mathbf{x}_j, \quad (6.4)$$

$$\mathbb{A}_{i,j}(\mathbf{z}) = \mathbf{A}_i^{\eta^\varepsilon}(\mathbf{z})[\mathbf{J}_{i,j}^{I\varepsilon\varepsilon}\mathbf{D}_i^0 + \mathbf{J}_{i,j}^{J\varepsilon\varepsilon}(\mathbf{y})\mathbf{D}_j^0]. \quad (6.5)$$

Here $\mathbf{A}_i^{\eta^\varepsilon}(\mathbf{z}) = \underline{\mathbf{A}}_i^{u\varepsilon}[\mathbf{x}]\langle \xi \rangle$ ($\xi = \hat{\mathbf{x}} - \mathbf{x}$) whereas \mathbf{D}_i^0 is the effective field concentration factor $\langle \bar{\varepsilon} \rangle_i = \mathbf{D}_i^0\langle \varepsilon \rangle$ (see for details [85]).

Equation (6.3) serves as a “elementary block” for developing various effective energy-based criteria. For instance, in the peridynamic approach to fatigue cracking, [358] estimated the energy release rate by analyzing the micropotentials governing interactions between material points. The state-based formulation of this effective energy-based criterion is as follows. ($\xi, \zeta \in \mathcal{H}_{\mathbf{x}} \subset v_i$)

$$\langle \underline{\mathbf{U}}^\top \underline{\mathbb{K}} \underline{\mathbf{U}} \rangle_i(\xi, \zeta) = \langle \underline{\mathbf{U}}^\top \rangle_i \underline{\mathbb{K}} \langle \underline{\mathbf{U}} \rangle_i(\xi, \zeta) + \Delta^{\text{UKU}}(\xi, \zeta), \quad (6.6)$$

$$\Delta^{\text{UKU}}(\xi, \zeta) = \int [\mathbb{A}_{i,j}(\xi)\langle \varepsilon \rangle]^\top \underline{\mathbb{K}}(\xi, \zeta) [\mathbb{A}_{i,j}(\zeta)\langle \varepsilon \rangle] \varphi(v_j, \mathbf{x}_j |; v_i, \mathbf{x}_i) d\mathbf{x}_j \quad (6.7)$$

where the statistical average of the displacement state is defined as $\langle \underline{\mathbf{U}} \rangle_i[\mathbf{x}]\langle \xi \rangle = \underline{\mathbf{A}}_i^{u\varepsilon*}[\mathbf{x}]\langle \xi \rangle\langle \varepsilon \rangle = \mathbf{A}_i^{\eta\varepsilon*}(\mathbf{z})\langle \xi \rangle\langle \varepsilon \rangle$ (4.17); $\underline{\mathbb{K}}$ is the modulus state (2.13) [419]. The energy-based failure model [236] evaluates the local strain energy density in bond-based peridynamics. From this, an effective criterion for the state-based model can be derived

$$4\langle \mathcal{W} \rangle_i(\mathbf{x}) = \langle \underline{\mathbf{U}}^\top \bullet \underline{\mathbb{K}} \bullet \underline{\mathbf{U}} \rangle_i(\mathbf{x}) = \langle \underline{\mathbf{U}}^\top \rangle_i \bullet \underline{\mathbb{K}} \bullet \langle \underline{\mathbf{U}} \rangle_i(\mathbf{x}) + \Delta^{\text{UKU}}(\mathbf{x}), \quad (6.8)$$

$$\begin{aligned} \Delta^{\text{UKU}}(\mathbf{x}) &= \int \left\langle [\mathbb{A}_{i,j}(\xi)\langle \varepsilon \rangle]^\top \underline{\mathbb{K}}(\xi, \zeta) [\mathbb{A}_{i,j}(\zeta)\langle \varepsilon \rangle] \right\rangle^{\mathcal{H}_{\mathbf{x}}}(\mathbf{x}) \\ &\times \varphi(v_j, \mathbf{x}_j |; v_i, \mathbf{x}_i) d\mathbf{x}_j \end{aligned} \quad (6.9)$$

averaging over the horizon region, $\mathcal{H}_{\mathbf{x}} \subset v_i$ ($\mathbf{y} \in v_j$).

Seemingly, a second moment of the force vector state $\underline{\mathbf{T}} = \underline{\mathbb{K}} \bullet \underline{\mathbf{U}}$ (2.19) can be obtained ($\xi, \zeta \in \mathcal{H}_{\mathbf{x}} \subset v_i$)

$$\langle \underline{\mathbf{T}} \otimes \underline{\mathbf{T}} \rangle_i^{\mathcal{H}_{\mathbf{x}}}(\mathbf{x}) = \left\langle (\underline{\mathbb{K}} \bullet \langle \underline{\mathbf{U}} \rangle_i) \otimes (\underline{\mathbb{K}} \bullet \langle \underline{\mathbf{U}} \rangle_i) \right\rangle^{\mathcal{H}_{\mathbf{x}}}(\mathbf{x}) + \Delta^{\text{T}^2}(\mathbf{x}), \quad (6.10)$$

$$\begin{aligned} \Delta^{\text{T}^2}(\mathbf{x}) &= \int \left\langle \underline{\mathbb{K}}(\xi, \zeta) [\mathbb{A}_{i,j}(\zeta)\langle \varepsilon \rangle] \right\rangle^{\mathcal{H}_{\mathbf{x}}} \otimes \left\langle \underline{\mathbb{K}}(\xi, \zeta) \right. \\ &\times \left. [\mathbb{A}_{i,j}(\zeta)\langle \varepsilon \rangle] \right\rangle^{\mathcal{H}_{\mathbf{x}}}(\mathbf{x}) \varphi(v_j, \mathbf{x}_j |; v_i, \mathbf{x}_i) d\mathbf{x}_j. \end{aligned} \quad (6.11)$$

From Eq. (6.10), we can determine $\langle \underline{\mathbf{T}} \cdot \underline{\mathbf{T}} \rangle_i^{\mathcal{H}_{\mathbf{x}}}(\mathbf{x})$ ($\mathbf{x} \in \mathcal{H}_{\mathbf{x}} \subset v_i$), providing an estimate for the yield function. Specifically, the criterion based on the co-deviatoric force state is given by: $\psi(\mathbf{x}) = \langle \underline{\mathbf{t}}^{\text{d}}[x]\langle \xi \rangle \times \underline{\mathbf{t}}^{\text{d}}[x]\langle \xi \rangle \rangle^{\mathcal{H}_{\mathbf{x}}}(\mathbf{x})/2$. This corresponds to the second invariant of the deviatoric stress tensor in classical local theory, where $\underline{\mathbf{t}}^{\text{d}}[x]\langle \xi \rangle$ represents the co-deviatoric component of the scalar force state $\underline{\mathbf{t}}$ (see [348], [419] for details).

A failure criterion for bond breakage between material points is based on energy dissipation, $\mathcal{W}_\xi(\mathbf{x})$ (see [176], [432], [433], [455]). It depends on the stress state $\mathbf{T} = \mathbb{K} \bullet \mathbf{U}$ (2.19) and the displacement state \mathbf{U} between two points ($\xi \in \mathcal{H}_x \subset v_i$)

$$\mathcal{W}_\xi(\mathbf{x}) = \langle (\mathbb{K} \bullet \mathbf{U})_i \langle \mathbf{U} \rangle_i \rangle(\mathbf{x}) = (\mathbb{K}^{(i)} \bullet \langle \mathbf{U} \rangle_i) \langle \mathbf{U} \rangle_i(\mathbf{x}) + \Delta^{\text{TU}^2}(\xi, \mathbf{x}), \quad (6.12)$$

$$\Delta^{\text{TU}^2}(\xi, \mathbf{x}) = \int \langle \mathbb{K}(\xi, \zeta) [A_{ij}(\zeta) \langle \varepsilon \rangle] \rangle^{\mathcal{H}_x} [A_{ij}(\xi) \langle \varepsilon \rangle](\mathbf{x}) \varphi(v_j, \mathbf{x}_j | v_i, \mathbf{x}_i) d\mathbf{x}_j \quad (6.13)$$

Equations (6.6)-(6.13) for the linear operators $\mathcal{A}_i^{\theta\theta}$ (3.10₂) and $\mathcal{L}_p^{\theta\zeta}(\mathbf{x}, \bar{\zeta})$ (3.10₁) simplify to the corresponding equations for both the linear state-based [85] and bond-based [89] models.

Comment 6.2. All effective energy-based criteria in (6.6)-(6.13) are derived from a single fundamental component: the second moment of relative displacement $\langle \eta \otimes \eta \rangle_i(\mathbf{z})$ (6.3) (or, that is the same, $\langle \mathbf{U}[\mathbf{x}](\xi) \otimes \mathbf{U}[\mathbf{x}](\xi) \rangle_i(\mathbf{x})$ ($\mathbf{x} \in v_i$, $\xi \in \mathcal{H}_x \subset v_i$)). These criteria are defined on either one bond $\xi \in \mathcal{H}_x \subset v_i$, or two bonds $\xi, \zeta \in \mathcal{H}_x \subset v_i$ with the field fluctuations, either $\Delta^{\text{UKU}}(\xi, \zeta)$, $\Delta^{\text{UKU}}(\mathbf{x})$, $\Delta^{\text{T}^2}(\mathbf{x})$, or $\Delta^{\text{TU}^2}(\xi, \mathbf{x})$. All the field fluctuations can be incorporated into the dataset \mathcal{D}^r (4.22).

Comment 6.3. Effective energy-based criteria using field second moments were developed for the linear bond-based [85] and state-based [89] models, while Eq. (6.3) applies to nonlinear constitutive laws [93]. A promising approach would be to estimate effective strain energy directly, as in [377], without preliminary computing field second moments.

7 CMs with other constitutive laws of phases

7.1 Locally elastic

We will consider the local basic equations of thermoelastostatics (2.1)-(2.3) of composites. Locally elastic counterpart of Eqs. (3.17) and (4.6) are

$${}^L\zeta(\mathbf{x}) - {}^L\bar{\zeta}(\mathbf{x}) = {}^L\mathcal{L}_i^{\zeta\zeta}(\mathbf{x}, {}^L\bar{\zeta}), \quad {}^L\zeta(\mathbf{x}) = {}^L\mathcal{A}^{\zeta\zeta}({}^L\bar{\zeta})(\mathbf{x}), \quad (7.1)$$

where we introduce the substitutions $(\varepsilon, \sigma) \leftrightarrow {}^L\zeta$. The most straightforward method is reduced to the solution of the integral Eq. (3.12) using the Green function $\mathbf{G}^{(0)}$ and replacing $\varepsilon^{w\Gamma} \rightarrow {}^L\bar{\zeta}(\mathbf{x})$. For a homogeneous ellipsoidal inclusion under a uniform effective field, this yields Eshelby's solution [164]. When the effective field is inhomogeneous, the multipole expansion method [279] is effective. For an infinite medium, the volume integral equation (VIE) [79], [292] applies, allowing discretization of inclusions only, unlike FEA (which is effectively used at ${}^L\bar{\zeta}(\mathbf{x}) \equiv \text{const.}$). The boundary integral equation (BIE) methods [24], [220], [353], [431] are widely used for homogeneous elasticity but face challenges like 3D meshing and singular integral computation. Alternative meshless methods [171], such as local boundary integral equation, boundary

knot method, boundary collocation method, non-dimensional dynamic influence functions method, and the method of fundamental solutions (MFS) [280] (see also [106]), offer advantages. In Amic (3.9), MFS [69] adapted to CAM is most effective. Each method has its strengths and limitations, requiring careful selection based on application.

We also consider a case of an imperfect interface

$$[[\mathbf{u}(\mathbf{x})]] \neq \mathbf{0}, \quad [[\boldsymbol{\sigma}(\mathbf{x})]] \cdot \mathbf{n}(\mathbf{x}) \neq \mathbf{0}, \quad (7.2)$$

with the jumps (7.2₁) and (7.2₂) at the $\mathbf{x} \in \Gamma_i^u$ and $\mathbf{x} \in \Gamma_i^\sigma$ ($\Gamma_i^u, \Gamma_i^\sigma \subset \Gamma_i$), respectively, described by the different models of interface imperfections. As such, in the right-hand side of Eq. (3.12) with the volume integral, we need to add the surface integrals with some Green functions kernels and integrands (7.2₁) and (7.2₂) (see for details [69]). The first kind of model can be referred to as interface models in which the traction is continuous across the interface $\mathbf{x} \in \Gamma_i^u$ while the displacement is in general discontinuities (7.2₁) at $\mathbf{x} \in \Gamma_i^u$ such as, e.g., in *linear spring model* (LSM, see, e.g., [211], [212], [213], [143], [229], [509]). The LSM was generalized to a *cohesive zone model* (CZM), where the traction vector assumed to be continuous is a non-linear function of the displacement jump (bilinear, trapezoidal, exponential, and polynomial cohesive laws). The cohesive model originated by Barenblatt [25] in fracture mechanics (see also [356], [364]) has received wide development in micromechanics of CM (see, e.g., [367], [435], [436]).

The second kind of interface model, the Gurtin–Murdoch interface stress model (ISM) [201], [202] (see also [232], [333], [378], [450]), also known as the coherent interface model, is dual to the linear spring-layer model. It enforces displacement continuity across $\mathbf{s} \in \Gamma_i^\sigma \subset \Gamma_i$ while allowing discontinuities in stress and strain. Steigmann and Ogden [430] extended ISM to account for surface resistance to stretching and bending by incorporating surface membrane strain and curvature tensors. ISM has been applied to nanoscale structures [345], [410] and adapted for Eshelby-type inclusion problems [108], [109], [150], [215], [408], [409], see also [179], [180]. All imperfect interface models can be incorporated into the perturbator ${}^L\mathcal{L}_i^{\zeta\zeta}(\mathbf{x}, {}^L\bar{\boldsymbol{\zeta}})$ (7.1) [69].

Replacing the PM perturbator (3.17) with the LM perturbator (7.1) transforms AGIE (3.23) into the LM-based AGIE:

$$\langle {}^L\boldsymbol{\zeta} \rangle_i(\mathbf{x}) = \boldsymbol{\zeta}^{b(0)}(\mathbf{x}) + \int {}^L\mathcal{L}_j^{\zeta\zeta}(\mathbf{x} - \mathbf{x}_j, {}^L\bar{\boldsymbol{\zeta}}) \varphi(v_j, \mathbf{x}_j | v_1, \mathbf{x}_1) d\mathbf{x}_j \quad (7.3)$$

where $\boldsymbol{\zeta}^{b(0)}(\mathbf{x})$ represents the deterministic field induced by the body force $\mathbf{b}(\mathbf{x})$ in an infinite homogeneous matrix. When the perturbator ${}^L\mathcal{L}_j^{\zeta\zeta}$ is expressed via the Green function (as in Eq. (3.12)), the left-hand side and integral terms in Eqs. (3.12) and (7.3) match. However, Eq. (7.3)—derived for body forces (2.4)—is exact, whereas Eq. (3.12), formulated for remote boundary conditions (2.30), is incorrect.

Similarly to Eq. (7.3), the second field moment within an inclusion $\mathbf{x} \in v_i$ is given by

$$\begin{aligned} \langle {}^L\boldsymbol{\zeta} \otimes {}^L\boldsymbol{\zeta} \rangle_i(\mathbf{x}) &= \langle {}^L\boldsymbol{\zeta} \rangle_i(\mathbf{x}) \otimes \langle {}^L\boldsymbol{\zeta} \rangle_i(\mathbf{x}) + \int {}^L\mathcal{A}_i^{\zeta\zeta} * \langle {}^L\boldsymbol{\zeta}_p^{\zeta\zeta}(\mathbf{x}, {}^L\bar{\boldsymbol{\zeta}}) |; v_i, \mathbf{x}_i \rangle \\ &\otimes {}^L\mathcal{A}_i^{\theta\theta} * \langle {}^L\boldsymbol{\zeta}_p^{\zeta\zeta}(\mathbf{x}, {}^L\bar{\boldsymbol{\zeta}}) |; v_i, \mathbf{x}_i \rangle \varphi(v_p, \mathbf{x}_p |; v_i, \mathbf{x}_i) d\mathbf{x}_p. \end{aligned} \quad (7.4)$$

As expected, this equation coincides with its counterpart in LM under remote boundary conditions (2.30), as derived in [79].

Solution of Eq. (7.3) is performed by repeating step-by-step of solution of Eq. (3.23), see Eqs. (4.5)-(4.22). Finally, we obtain a dataset ($\mathbf{x} \in R^d$)

$$\begin{aligned} {}^L\mathcal{D}^r &= \{ {}^L\mathcal{D}_k^r \}_{k=1}^N, \\ {}^L\mathcal{D}_k^r &= \{ \langle \boldsymbol{\varepsilon}_k \rangle(\mathbf{b}_k, \mathbf{x}), \langle \boldsymbol{\sigma}_k \rangle(\mathbf{b}_k, \mathbf{x}), \langle \boldsymbol{\varepsilon}_{ik} \rangle(\mathbf{b}_k, \mathbf{z}, \mathbf{x}), \langle \boldsymbol{\sigma}_{ik} \rangle(\mathbf{b}_k, \mathbf{z}, \mathbf{x}), \mathbf{b}_k(\mathbf{x}) \}, \end{aligned} \quad (7.5)$$

which looks as the dataset \mathcal{D}^r (4.22). Analysis of periodic structure CM is reduced to replacement of probability densities $\varphi(v_i, \mathbf{x}_i)$ and $\varphi(v_i, \mathbf{x}_i |; v_j, \mathbf{x}_j)$ by their δ function representations (2.36) that leads to a dataset ${}^L\mathcal{D}^p$ similar to \mathcal{D}^p (5.12).

7.2 Strongly nonlocal (strain type) model

Following Rogula [388] and Eringen [163], the stress-strain relationship in nonlocal linear thermoelasticity is governed by the integral equation:

$$\boldsymbol{\sigma}(\mathbf{x}) = \boldsymbol{\mathcal{L}} * \boldsymbol{\varepsilon}(\mathbf{x}) + \boldsymbol{\alpha}(\mathbf{x}), \quad \boldsymbol{\varepsilon}(\mathbf{x}) = \boldsymbol{\mathcal{M}} * \boldsymbol{\sigma}(\mathbf{x}) + \boldsymbol{\beta}(\mathbf{x}) \quad (7.6)$$

where the integral response operators $\boldsymbol{\mathcal{K}} = \boldsymbol{\mathcal{L}}, \boldsymbol{\mathcal{M}}; \boldsymbol{\gamma} = \boldsymbol{\alpha}, \boldsymbol{\beta}$ and transformation field $\boldsymbol{\gamma} = \boldsymbol{\alpha}, \boldsymbol{\beta}$ are defined as

$$\boldsymbol{\mathcal{K}} * (\cdot) = \int \boldsymbol{\mathcal{K}}(\mathbf{x}, \mathbf{y})(\cdot)(\mathbf{y}) d\mathbf{y}, \quad \boldsymbol{\gamma}(\mathbf{x}) = \int \mathbf{m}^\gamma(\mathbf{x}, \mathbf{y}) \Delta T(\mathbf{y}) d\mathbf{y}. \quad (7.7)$$

Here, $\boldsymbol{\mathcal{K}}(\mathbf{x}, \mathbf{y})$ is the kernel governing nonlocal interactions, while $\boldsymbol{\gamma}(\mathbf{x})$ represents the transformation field, assuming a uniform temperature difference $\Delta T(\mathbf{y}) \equiv (T - T^0)$. This formulation modifies only the stress-strain relation, keeping equilibrium and compatibility equations unchanged, as in linear isotropic elasticity [30], [153], [162], [163], [265].

The response and inverse response parameters in Eq. (7.6) satisfy the relationships:

$$\boldsymbol{\mathcal{L}} * \boldsymbol{\mathcal{M}} = \boldsymbol{\mathcal{M}} * \boldsymbol{\mathcal{L}} = \mathbf{I}, \quad \boldsymbol{\mathcal{M}} * \boldsymbol{\alpha} = -\boldsymbol{\beta}, \quad \boldsymbol{\mathcal{L}} * \boldsymbol{\beta} = -\boldsymbol{\alpha}, \quad (7.8)$$

with material parameters subjected to the following symmetry regulations: $\boldsymbol{\mathcal{K}} = \boldsymbol{\mathcal{L}}, \boldsymbol{\mathcal{M}}; \boldsymbol{\gamma} = \boldsymbol{\alpha}, \boldsymbol{\beta}$: $\mathcal{K}_{ijkl} = \mathcal{K}_{ijlk} = \mathcal{K}_{jikl}$, $\mathcal{K}_{ijkl}(\mathbf{x}, \mathbf{y}) = \mathcal{K}_{klij}(\mathbf{y}, \mathbf{x})$, $\gamma_{ij} = \gamma_{ji}$ [275], [267]. The kernel $\boldsymbol{\mathcal{K}}(\mathbf{x}, \mathbf{y})$ is given by:

$$\boldsymbol{\mathcal{K}}(\mathbf{x}, \mathbf{y}) = \mathbf{K}(\mathbf{x}) \lambda(\mathbf{x}, \mathbf{y}), \quad (7.9)$$

where $\lambda(\mathbf{x}, \mathbf{y})$ is a nonlocal weight function, often distance-dependent $\lambda(\mathbf{x}, \mathbf{y}) = \lambda_\infty(|\mathbf{x} - \mathbf{y}|)$ [375], and normalized as:

$$\int_w \lambda(\mathbf{x}, \mathbf{y}) d\mathbf{y} = 1, \quad \forall \mathbf{x} \in w = R^d \quad (7.10)$$

This ensures \mathcal{K} represents stiffness or compliance in uniform straining and stressing. In the limit $\lambda_\infty(\mathbf{x}) \rightarrow \delta(\mathbf{x})$, the nonlocal operator reduces to the local case $\mathcal{K}(\mathbf{x}, \mathbf{y}) \rightarrow \mathbf{K}(\mathbf{x})\delta(\mathbf{x} - \mathbf{y})$, recovering the classical formulation (2.2).

Micromechanical models begin with analyzing a single heterogeneity in an infinite matrix under remote loading [273] (see comprehensive reviews in [58], [200], and [333]). For various nonlocal models, involving spatial integrals or field gradients, the internal field within a homogeneous ellipsoidal inclusion remains non-uniform even under homogeneous remote loading. The strongly nonlocal strain-based counterparts of Eqs. (3.17) and (4.6) are:

$${}^S\zeta(\mathbf{x}) - {}^S\bar{\zeta}(\mathbf{x}) = {}^S\mathcal{L}_i^{\zeta\zeta}(\mathbf{x}, {}^S\bar{\zeta}), \quad {}^S\zeta(\mathbf{x}) = {}^S\mathcal{A}^{\zeta\zeta}({}^S\bar{\zeta})(\mathbf{x}), \quad (7.11)$$

where $(\varepsilon, \sigma) \leftrightarrow {}^S\zeta$. Unlike MEF and MTM (see Comment 3.4), which focus on perturbators inside the inclusion [see e.g. [407], [476], [504]], CAM requires evaluating ${}^S\mathcal{L}_i^{\zeta\zeta}$ outside $\mathbf{x} \notin v_i$ (see [95]). This was addressed in [58] using an iterative solution of the volume integral equation.

Substituting the PM perturbator (3.17) with the strongly nonlocal strain-based perturbator (7.11) modifies AGIE (3.23) into the following nonlocal AGIE formulation:

$$\langle {}^S\zeta \rangle_i(\mathbf{x}) = \zeta^{b(0)}(\mathbf{x}) + \int {}^S\mathcal{L}_j^{\zeta\zeta}(\mathbf{x} - \mathbf{x}_j, {}^S\bar{\zeta}) \varphi(v_j, \mathbf{x}_j | v_1, \mathbf{x}_1) d\mathbf{x}_j \quad (7.12)$$

where $\zeta^{b(0)}(\mathbf{x})$ denotes the deterministic field generated by the body force $\mathbf{b}(\mathbf{x})$ in an infinite homogeneous matrix. By centering Eq. (7.12), we obtain a GIE analogous to (3.24), which was applied in [58] to study CMs reinforced with circular inclusions. It was shown that the local statistical average stress $\langle \sigma \rangle_i(\mathbf{x})$ ($\mathbf{x} \in v_i$) depends on both the radial distribution functions (RDFs) and the excluded volume v_i^0 , potentially leading to stress values that differ in sign from those predicted by classical methods such as the MEF and MTM. However, the differences in the effective moduli \mathbf{L}^* estimated using GIEs—nonlocal counterparts to Eqs. (3.13) and (3.14)—were found to be relatively minor.

To estimate the second field moment $\langle {}^S\zeta \otimes {}^S\zeta \rangle_i(\mathbf{x})$ within an inclusion $\mathbf{x} \in v_i$, one simply needs to replace the superscript L with S in Eq. (7.3). Likewise, the dataset ${}^D\mathcal{D}$ can be derived from Eq. (7.5) by substituting the superscript L with S .

7.3 Coupled problems of composites

We formulate the Additive GIEs for coupled problems using thermoelectroelasticity as an example. To maintain consistency, elastic and electric variables

are treated equivalently. Following the notation from [27] and referencing works like [335], [372], and [250], the local linear constitutive relations are recast in a unified form, leading to a basic equation analogous to Eqs. (2.1)–(2.3).

$$\mathcal{D}\Sigma = \mathbf{0}, \quad \mathcal{E} = \mathcal{D}\mathcal{U}, \quad (7.13)$$

$$\mathcal{E} = \mathbb{M}\Sigma + \Lambda, \quad \Sigma = \mathbb{L}(\mathcal{E} - \Lambda), \quad (7.14)$$

where

$$\mathcal{E} = \left\| \begin{array}{c} \varepsilon \\ \mathbf{E} \end{array} \right\|, \quad \Sigma = \left\| \begin{array}{c} \sigma \\ \mathbf{D} \end{array} \right\|, \quad \mathcal{U} = \left\| \begin{array}{c} \mathbf{u} \\ \phi \end{array} \right\|, \quad \mathcal{D} = \left\| \begin{array}{cc} \text{def} & 0 \\ 0 & \text{grad} \end{array} \right\|, \quad (7.15)$$

$$\mathbb{M} = \left\| \begin{array}{cc} \mathbf{M} & \mathbf{d}^\top \\ \mathbf{d} & -\mathbf{b} \end{array} \right\|, \quad \mathbb{L} = \left\| \begin{array}{cc} \mathbf{L} & \mathbf{e}^\top \\ \mathbf{e} & -\mathbf{k} \end{array} \right\|, \quad \Lambda = \left\| \begin{array}{c} \beta \\ \mathbf{q}\theta \end{array} \right\|, \quad (7.16)$$

here \mathbf{D} and \mathbf{E} are the vectors of induction and electric field intensity, θ is a deviation of a stationary temperature field from a given value, \mathbf{k} and \mathbf{b} are the tensors of dielectric permeability and impermeability, \mathbf{q} is the pyroelectric coefficient, \mathbf{e} and \mathbf{d} are the piezoelectric moduli, and ϕ is the electric potential. To obtain a symmetric matrix of coefficients we replaced the electric field \mathbf{E} by $-\mathbf{E}$, and the tensors \mathbf{k} and \mathbf{b} by $-\mathbf{k}$ and $-\mathbf{b}$ on the right-hand sides of (7.14). It is assumed that the properties of both the comparison medium and the matrix coincide. Some background representations for micromechanics of thermoelectroelasticity such as generalized Hill's conditions, effective energy functions, and phase-averaged first and second moments are considered in [53] (see also [380]).

These and other methods with the classical background defined by both the hypothesis **H1** and GIEs counterpart of (3.13) (see, e.g. Dinzart and Sabar, 2011; Levin *et al.*, 2011; Lu *et al.*, 2011; and referenced in Buryachenko, 2013b) are based on the estimation of the average field and polarization tensors inside the heterogeneities rather than outside ones. Exploiting of the new background (3.25) and (3.26) is accomplished by a straightforward generalization of the approaches of Subsections 4.1 and 4.2 taking the unified notations (7.13)–(7.16) into account.

The coupled electroelasticity counterparts of Eqs. (3.17) and (4.6) are given by ($\mathbf{x} \in R^d$):

$$\mathcal{E}(\mathbf{x}) - \bar{\mathcal{E}}(\mathbf{x}) = {}^{EE}\mathcal{L}_i^{EE}(\mathbf{x}, \bar{\mathcal{E}}), \quad \mathcal{E}(\mathbf{x}) = {}^{EE}\mathcal{A}^{EE}(\bar{\mathcal{E}})(\mathbf{x}), \quad (7.17)$$

Unlike classical methods such as MEF and MTM, which rely on hypothesis **H1a** (3.8) and the GIE counterpart of (3.13) (see [130], [131], [148], [149], [151], [199], [300], [301], [302], [255], [412]), the CAM approach (both Eqs. (3.23) and (3.24)) requires evaluating ${}^{EE}\mathcal{L}_i^{EE}$ (7.17) outside the inclusion region ($\mathbf{x} \notin v_i$), rather than just inside ($\mathbf{x} \in v_i$). For inclusions of arbitrary shape and non-uniform effective fields ($\bar{\mathcal{E}}(\mathbf{x}) \neq \text{const.}$), numerical methods mentioned in Subsections 4.1 and 4.2 must also be adapted accordingly.

Replacing the PM perturbator (3.17) with the coupled electroelasticity perturbator (7.17) transforms AGIE (3.23) into:

$$\langle \mathcal{E} \rangle_i(\mathbf{x}) = \mathcal{E}^{b(0)}(\mathbf{x}) + \int {}^{EE}\mathcal{L}_j^{EE}(\mathbf{x} - \mathbf{x}_j, \bar{\mathcal{E}}) \varphi(v_j, \mathbf{x}_j | v_1, \mathbf{x}_1) d\mathbf{x}_j. \quad (7.18)$$

Here, $\mathcal{E}^{b(0)}(\mathbf{x})$ represents the deterministic field produced by the coupled body force $\mathbf{b}(\mathbf{x})$ in an infinite homogeneous matrix. By centering Eq. (7.18), we derive a GIE analogous to (3.24), which was introduced in [79] for analyzing random-structured piezoelectric composite materials.

To estimate the second field moment $\langle \mathcal{E} \otimes \mathcal{E} \rangle_i(\mathbf{x})$ within an inclusion $\mathbf{x} \in v_i$, one only needs to replace the superscript L with EE in Eq. (7.3). Similarly, the dataset $^{EE}\mathcal{D}^r$ can be obtained in the same way as \mathcal{D}^r (7.5).

7.4 First Strain Gradient Medium

Subsections 6.3 and 6.4 provide an excerpt from [79].

In the linearized theory of Mindlin's form-II first strain gradient elasticity ([346], [347], see also [288], [374], [428]), the strain energy density of a homogeneous centrosymmetric material depends quadratically on both the strain $\boldsymbol{\varepsilon}$ and its gradient $\boldsymbol{\kappa} = \nabla \boldsymbol{\varepsilon}$:

$$W(\boldsymbol{\varepsilon}, \nabla \boldsymbol{\varepsilon}) = \frac{1}{2} \boldsymbol{\varepsilon} : \mathbf{L} : \boldsymbol{\varepsilon} + \frac{1}{2} \boldsymbol{\kappa} \cdot \mathbf{C} \cdot \boldsymbol{\kappa} = \frac{1}{2} L_{ijkl} \varepsilon_{ij} \varepsilon_{kl} + \frac{1}{2} C_{ijmkl n} \partial_m \varepsilon_{ij} \partial_n \varepsilon_{kl}, \quad (7.19)$$

where \mathbf{L} is the rank-four elasticity tensor, and \mathbf{C} is the rank-six strain gradient elasticity tensor, both possessing specific symmetries ([79]). The operator \cdot denotes contraction over the last three indices of the left operand and the first three of the right.

Using the Euler–Lagrange equations, the corresponding static governing equation for displacement takes the Navier-like form:

$$\mathbb{L}^M \mathbf{u} = -\mathbf{b}, \quad \mathbb{L}^M = \mathbb{L} - \mathbb{C}, \quad \mathbb{L}_{ik} = L_{ijkl} \partial_j \partial_l, \quad \mathbb{C}_{ik} = C_{ijmkl n} \partial_j \partial_l \partial_m \partial_n. \quad (7.20)$$

Thus, the Mindlin operator \mathbb{L}^M incorporates both standard elasticity and strain gradient effects, ensuring a symmetric total stress tensor in the first strain-gradient model [20]. Some well-known simplified strain gradient theories, such as couple stress theory, Aifantis, Kleinert, Mindlin, and Wei & Hutchinson's models ([6], [12], [20], [261], [284], [346], [511]) have similar forms of governing equations as that of the general isotropic second gradient theory (see their connection in [79]).

Consider an inhomogeneity v_i centered at \mathbf{x}_i with material parameters $\mathbf{L}^{(1)}(\mathbf{x})$ and $\mathbf{C}^{(1)}(\mathbf{x})$ (7.18) embedded in an infinite homogeneous matrix w characterized by $\mathbf{L}^{(0)}$ and $\mathbf{C}^{(0)}$. Under generalized traction-free remote boundary conditions and body force $\mathbf{b}(\mathbf{x})$ (2.4), the resulting fields in the homogeneous matrix (without v_i) are $\bar{\boldsymbol{\varepsilon}}^b(\mathbf{x})$ and $\bar{\boldsymbol{\kappa}}^b(\mathbf{x})$ ($\mathbf{x} \in w$). The equilibrium equation takes the form:

$$\mathbb{L}^{M(0)} \mathbf{u} = -\mathbb{L}_1^M \mathbf{u} - \mathbf{b}, \quad (7.21)$$

where $\mathbf{L}_1(\mathbf{x}) := \mathbf{L}(\mathbf{x}) - \mathbf{L}^{(0)}$ and $\mathbf{C}_1(\mathbf{x}) := \mathbf{C}(\mathbf{x}) - \mathbf{C}^{(0)}$ vanish outside v_i .

Following [426], we define the stress and double-stress polarization tensors:

$$\boldsymbol{\tau}(\mathbf{x}) = \boldsymbol{\sigma}(\mathbf{x}) - \mathbf{L}^{(0)} : \boldsymbol{\varepsilon}(\mathbf{x}), \quad \boldsymbol{\pi}(\mathbf{x}) = \boldsymbol{\mu}(\mathbf{x}) - \mathbf{C}^{(0)} \cdot \boldsymbol{\kappa}(\mathbf{x}), \quad (7.22)$$

which are zero outside v_i . Substituting these into the equilibrium equation (7.21) results in:

$$\mathbb{L}^{\text{M}(0)} \mathbf{u} = -\nabla[\boldsymbol{\tau} - \nabla\boldsymbol{\pi}]. \quad (7.23)$$

For convenience, we introduce the notation:

$$\hat{\boldsymbol{\tau}} = \begin{pmatrix} \boldsymbol{\tau} \\ \boldsymbol{\pi} \end{pmatrix}, \quad \hat{\boldsymbol{\varepsilon}} = \begin{pmatrix} \boldsymbol{\varepsilon} \\ \boldsymbol{\kappa} \end{pmatrix}, \quad \hat{\boldsymbol{\varepsilon}} = \begin{pmatrix} \bar{\boldsymbol{\varepsilon}} \\ \bar{\boldsymbol{\kappa}} \end{pmatrix}, \quad \hat{\mathbf{U}} = \begin{pmatrix} \mathbf{U}^{\varepsilon\tau} & \mathbf{U}^{\varepsilon\pi} \\ \mathbf{U}^{\kappa\tau} & \mathbf{U}^{\kappa\pi} \end{pmatrix}, \quad (7.24)$$

Here, $\hat{\boldsymbol{\varepsilon}} = (\bar{\boldsymbol{\varepsilon}}, \bar{\boldsymbol{\kappa}})$ represents the field in a homogeneous medium with $\mathbf{L}^{(0)}$, $\mathbf{C}^{(0)}$ under given BC (like (2.4)). The Green functions and their derivatives, $\mathbf{U}^{\varepsilon\tau} = \nabla\nabla\mathbf{G}^{\text{M}}$, $\mathbf{U}^{\varepsilon\pi} = -\nabla\nabla\nabla\mathbf{G}^{\text{M}}$, $\mathbf{U}^{\kappa\tau} = \nabla\nabla\nabla\mathbf{G}^{\text{M}}$, $\mathbf{U}^{\kappa\pi} = -\nabla\nabla\nabla\nabla\mathbf{G}^{\text{M}}$, relevant for both isotropic and anisotropic media, are detailed in [289] and [374].

By applying the Green function (7.24) and integrating by parts, the equilibrium equation (7.24) is transformed into the convolution form

$$\hat{\boldsymbol{\varepsilon}} = \hat{\boldsymbol{\varepsilon}} + \hat{\mathbf{U}} * \hat{\boldsymbol{\tau}}, \quad (7.25)$$

which corresponds to Eq. (3.11) up to notation differences.

The integral equation (7.25) with a nonsingular convolution kernel $\hat{\mathbf{U}}$ can be rewritten in operator form as

$$\begin{aligned} \hat{\boldsymbol{\varepsilon}}(\mathbf{x}) - \hat{\boldsymbol{\varepsilon}}(\mathbf{x}) &:= {}^\varepsilon\mathcal{L}_i(\mathbf{x} - \mathbf{x}_i, \hat{\boldsymbol{\tau}}) = {}^\varepsilon\mathcal{L}_i(\mathbf{x} - \mathbf{x}_i, \hat{\boldsymbol{\varepsilon}}), \\ \hat{\boldsymbol{\varepsilon}}(\mathbf{x}) &= {}^\varepsilon\mathcal{A}_i(\mathbf{x} - \mathbf{x}_i, \hat{\boldsymbol{\varepsilon}}), \end{aligned} \quad (7.26)$$

Particular case of homogeneous effective field $\hat{\boldsymbol{\varepsilon}}(\mathbf{x}) \equiv \text{const.}$ and homogeneous ellipsoidal inclusion corresponds to the Eshelby solution considered in [186], [321], [504], [507]. In the general case of the inclusion shape and inhomogeneity of the effective field $\hat{\boldsymbol{\varepsilon}}(\mathbf{x}) \neq \text{const.}$, the solutions ${}^\varepsilon\mathcal{L}_i(\mathbf{x} - \mathbf{x}_i, \hat{\boldsymbol{\tau}})$ and $\mathcal{A}_i(\mathbf{x} - \mathbf{x}_i, \hat{\boldsymbol{\varepsilon}})$ can be obtained via the volume integral equation method (Subsection 6.1) or finite element analysis (e.g., [20], [137], [447]).

Replacing the PM perturbator (3.17) with the strain gradient perturbator (7.26) transforms AGIE (3.23) into:

$$\langle \hat{\boldsymbol{\varepsilon}} \rangle_i(\mathbf{x}) = \hat{\boldsymbol{\varepsilon}}^{b(0)}(\mathbf{x}) + \int {}^\varepsilon\mathcal{L}_j(\mathbf{x} - \mathbf{x}_j, \hat{\boldsymbol{\varepsilon}}) \varphi(v_j, \mathbf{x}_j | v_1, \mathbf{x}_1) d\mathbf{x}_j. \quad (7.27)$$

Here, $\hat{\boldsymbol{\varepsilon}}^{b(0)}(\mathbf{x})$ represents the deterministic field produced by the body force $\mathbf{b}(\mathbf{x})$ in an infinite homogeneous matrix. By centering Eq. (7.27), we derive a GIE analogous to (3.24), which was introduced in [79] for analyzing random-structured CMs with strain gradient properties of phases.

To estimate the second field moment $\langle \hat{\boldsymbol{\varepsilon}} \otimes \hat{\boldsymbol{\varepsilon}} \rangle_i(\mathbf{x})$ within an inclusion $\mathbf{x} \in v_i$, one only needs to replace the superscript L with ε in Eq. (7.4). Similarly, the dataset ${}^\varepsilon\mathcal{D}^r$ can be obtained in the same way as \mathcal{D}^r (7.5).

7.5 Stress-Gradient Elasticity Model

In this subsection, we briefly summarize the stress-gradient elasticity framework, introduced by Forest and Sab [175] and further developed in [48], [389], [444], adapted for obtaining AGIE (as discussed in Section 3 for PM). In the strain-gradient model (7.19), the strain-energy density W depends on the strain $\boldsymbol{\varepsilon}$ and its gradient $\nabla\boldsymbol{\varepsilon}$. Similarly, in the stress-gradient model of Forest and Sab [175] (see also [79]), the complementary strain-energy density W^c of a linear homogeneous centrosymmetric material depends on the stress $\boldsymbol{\sigma}$ and its first gradient $\nabla\boldsymbol{\sigma}$

$$W^c(\boldsymbol{\sigma}, \mathbf{R}) = \frac{1}{2}\boldsymbol{\sigma} : \mathbf{M} : \boldsymbol{\sigma} + \frac{1}{2}\mathbf{R} \cdot\cdot \mathbf{S} \cdot\cdot \mathbf{R}, \quad (7.28)$$

where \mathbf{M} and \mathbf{S} are the classical and generalized compliances which are tensors with minor and major symmetries. The trace-free part \mathbf{R} of the stress-gradient $\nabla\boldsymbol{\sigma}$ is the orthogonal projection of $\nabla\boldsymbol{\sigma}$ onto the space of third-rank, trace-free tensors, and we write $\mathbf{R} = \mathbf{I}'_6 \cdot\cdot \nabla\boldsymbol{\sigma}$, where the sixth-rank tensor $I'_{6|ijklpqr} = I_{ijpq}\delta_{kr} - (I_{pq(ir}\delta_{j)k})/2$ [444] is defined as the orthogonal projection (in the sense of the $\cdot\cdot$ scalar product). Being a projector, \mathbf{I}'_p enjoys the classical property $\mathbf{I}'_p \cdot\cdot \mathbf{I}'_p = \mathbf{I}'_p$.

The strain measures, the energy-conjugate to the stress $\boldsymbol{\sigma}$ and trace-free variable \mathbf{R} , are

$$\mathbf{e} = \mathbf{M} : \boldsymbol{\sigma} = \frac{\partial W^c}{\partial \boldsymbol{\sigma}}, \quad \boldsymbol{\phi} = \mathbf{S} \cdot\cdot \mathbf{R} = \frac{\partial W^c}{\partial \mathbf{R}}, \quad (7.29)$$

where the total strain \mathbf{e} is not necessarily the symmetric gradient of the displacement \mathbf{u} .

Equations (7.28) can be considered as an inversion of Eq. (7.29)

$$\boldsymbol{\sigma} = \mathbf{L} : \mathbf{e}, \quad \mathbf{R} = \mathbf{C} \cdot\cdot \boldsymbol{\phi}, \quad (7.30)$$

where $\mathbf{L} = (\mathbf{M})^{-1}$ is a classical stiffness whereas the generalized compliance \mathbf{S} and stiffness \mathbf{C} are inverse to each other $\mathbf{C} \cdot\cdot \mathbf{S} = \mathbf{S} \cdot\cdot \mathbf{C} = \mathbf{I}'_6$.

Analogously to (7.22), we introduce the stress and stress gradient polarization tensors

$$\boldsymbol{\tau}(\mathbf{x}) = \boldsymbol{\sigma}(\mathbf{x}) - \mathbf{L}^{(0)} : \mathbf{e}(\mathbf{x}), \quad \boldsymbol{\pi}(\mathbf{x}) = \mathbf{R}(\mathbf{x}) - \mathbf{C}^{(0)} \cdot\cdot \boldsymbol{\phi}(\mathbf{x}), \quad (7.31)$$

vanishing in the matrix $\mathbf{x} \in w \setminus v_i$. Similarly to Eq. (7.25) (see also [444]), we get an equation for one inhomogeneity in the infinite matrix

$$\hat{\mathbf{e}} = \hat{\bar{\mathbf{e}}} + {}^e\hat{\mathbf{U}} * \hat{\boldsymbol{\tau}}, \quad (7.32)$$

where

$$\hat{\boldsymbol{\tau}} = \begin{pmatrix} \boldsymbol{\tau} \\ \boldsymbol{\pi} \end{pmatrix}, \quad \hat{\mathbf{e}} = \begin{pmatrix} \mathbf{e} \\ \boldsymbol{\phi} \end{pmatrix}, \quad \hat{\bar{\mathbf{e}}} = \begin{pmatrix} \bar{\mathbf{e}} \\ \bar{\boldsymbol{\phi}} \end{pmatrix}, \quad {}^e\hat{\mathbf{U}} = \begin{pmatrix} \boldsymbol{\mathfrak{U}}^{e\tau} & \boldsymbol{\mathfrak{U}}^{e\pi} \\ \boldsymbol{\mathfrak{U}}^{\phi\tau} & \boldsymbol{\mathfrak{U}}^{\phi\pi} \end{pmatrix}, \quad (7.33)$$

where $\hat{\mathbf{e}} = (\bar{\mathbf{e}}, \bar{\boldsymbol{\pi}})$ is a field that would exist in the medium with homogeneous properties $\mathbf{M}^{(0)}$, $\mathbf{S}^{(0)}$ and appropriate remote boundary condition. Green operators $\mathfrak{U}^{e\pi}$, $\mathfrak{U}^{\phi\tau}$, and $\mathfrak{U}^{\phi\pi}$ can be derived from the single operator $\mathfrak{U}^{e\tau}$, as obtained by Tran [443] for an isotropic simplified model.

The integral Eq. (7.32) with nonsingular convolution kernel $\hat{\mathbf{U}}$ and their solution can be presented in an operator form (3.17) and (4.6)

$$\begin{aligned} \hat{\mathbf{e}}(\mathbf{x}) - \hat{\bar{\mathbf{e}}}(\mathbf{x}) &:= \mathfrak{L}_i^\tau(\mathbf{x} - \mathbf{x}_i, \hat{\boldsymbol{\tau}}) = \mathfrak{L}_i^e(\mathbf{x} - \mathbf{x}_i, \hat{\mathbf{e}}), \\ \bar{v}_i \hat{\boldsymbol{\tau}}(\mathbf{x}) &= \mathfrak{R}_i^e(\mathbf{x} - \mathbf{x}_i, \hat{\mathbf{e}}), \end{aligned} \quad (7.34)$$

where the solutions $\mathfrak{L}_i^e(\mathbf{x} - \mathbf{x}_i, \hat{\mathbf{e}})$ and $\mathfrak{R}_i^e(\mathbf{x} - \mathbf{x}_i, \hat{\mathbf{e}})$ can be found, e.g. either by the volume integral equation method (see Subsection 7.1) by finite element analysis (see, e.g., [20], [137], [447]).

8 Representative volume element (EVE)

8.1 RVE for CMs subjected to remote homogeneous loading

The Representative Volume Element (RVE), introduced by Hill [216], has a complex history (see [365]). To accurately convey its definition and significance, we cite Hill [216], which provides its rigorous foundation.

Definition 8.1. *Representative volume element (RVE) (a) is structurally entirely typical of the whole mixture on average, and (b) contains a sufficient number of inclusions for the apparent overall moduli (AND STATISTICALLY AVERAGED FIELD DISTRIBUTIONS IN THE PHASES) to be effectively independent of the surface values of traction and displacement, so long as these values are ‘macroscopically uniform.... The contribution of this surface layer to any average can be negligible by taking the sample large enough.*

In Hill’s original definition [216], a SMALL CAPS font fragment was included and is explained later. We highlight key RVE concepts reflecting this definition:

1. The RVE applies to statistically homogeneous or periodic CMs under remote homogeneous boundary conditions (BCs) (2.28) or (2.29). While Hill [216] did not use terms like ”statistically homogeneous” or ”periodic structure CMs,” the concept aligns with them. Additionally, ”functionally graded structures” (a later term) do not fit within the RVE framework.

2. The RVE estimates effective moduli \mathbf{L}^* by averaging phase fields. For periodic structure, CMs, RVE is equivalent to a unit cell (RVE \equiv UC), and remote homogeneous BCs (2.28) or (2.29) reduce to periodic BCs (2.39). For statistically homogeneous CMs, no specific geometric representation is required. However, in practice, RVE sampling via computational or image-based methods is common, and verifying finite-size BC replacements is crucial to avoid distortions in property estimation.

3. Hill [216] applied his definition to linear locally elastic CMs, but Definition 8.1 omits the term “constitutive law.” It generalizes to peridynamic CMs by replacing “surface” (2.42), (2.43) with “volumetric” (2.40), (2.41).

The RVE concept, widely used in practice, often serves as a heuristic rather than a strict mathematical definition. Engineers rely on intuitive choices based on experience, especially for complex microstructures unsuitable for analytical or computational homogenization. However, such approximations can be misleading when microstructural details significantly impact material behavior. In practice, RVEs for finite samples (with BC or VBC) are generated using two main approaches: (1) random inclusion fields (synonymous with “arbitrary simulated fields”, e.g., [361], [462], [480], [481]) and (2) image-based methods like micro-CT for modeling “real” RVEs (e.g., [4], [14], [434]).

The inaccuracies of intuitive RVEs in PM have long been addressed in LM (see the Introduction for references, see also [187], [210], [251], [352], [392], [438]). In LM, a sample response is estimated from DNS of microstructural volume elements (MVEs) simulated or extracted (e.g., from micro-CT). The homogenized properties $\mathbf{L}_{\text{KUBC}}^{\text{A}}$ and $\mathbf{M}_{\text{SUBC}}^{\text{A}}$ for KUBC (2.41) and SUBC (2.42) are different. The convergence of $\mathbf{L}_{\text{KUBC}}^{\text{A}} - (\mathbf{M}_{\text{SUBC}}^{\text{A}})^{-1}$ as MVE size increases help approximate the RVE size and estimate the effective moduli \mathbf{L}^* , requiring large (theoretically infinite) material domains (see [365] and [79]). However, even with convergence in the number of realizations (e.g., [361]), boundary layer and edge scale effects may persist. The approaches used in LM for RVE investigations are based on Block 3 methods (3.2), which are well-developed for peridynamics (see Subsequent 3.4), making their use in PM straightforward.

Another well-known inconsistency in LM is the replacement of PBC by homogeneous BC (see [53], p. 508). The same issues are expected in PM when modeling infinite (e.g., periodic) media with finite domains: (see, e.g., [4], [16], [17], [18], [112], [119] [241], [482], [498], [505]). Using body force with compact support (e.g., (4.5)) as a training parameter helps eliminate sample size, boundary layer, and edge effects.

In the context of AMic, the RVE interpretation for random structure CMs avoids issues like sample size and edge effects, as well as the need for “surface values.” This is because the domain is the full space R^d , and homogeneous BCs or PBCs are not a concern. The RVE size is now fully determined by the micromechanical model used, making the concept of “taking the sample large enough” irrelevant. For both random and periodic structure CMs, the effective moduli \mathbf{L}^* and field concentration factors $\mathbf{A}^*(\mathbf{z})$ ($\mathbf{z} \in v_i$) are related by mutual coupling (see SMALL CAPS in Definition 8.1), see equation

$${}^L\mathbf{L}^* = {}^L\mathbf{L}^{(0)} + {}^L\mathbf{R}^*, \quad \langle \varepsilon \rangle_i(\mathbf{z}) = {}^L\mathbf{A}^*(\mathbf{z})\langle \varepsilon \rangle. \quad (8.1)$$

In random structure CMs, the RVE size depends on the micromechanical estimation method. For one-particle methods (like EFM, MTM, and EMM, see Comment 3.4), the RVE is defined as v_i , and the interaction size $a^{\text{int}} = a$. In the multiparticle EFM, considering binary interactions increases $a^{\text{int}} = 6a$, thus increasing the RVE size. In PM, methods for one-particle approaches yield

different \mathbf{L}^* estimations with the same RVE size. This eliminates the need for sample size control in Amic methods. For periodic structure CMs, the RVE coincides with the unit cell (UC). Therefore, under the hypothesis (2.33₂) in LM, the equality $\text{RVE}^{\mathbf{L}^*} \equiv \text{RVE}^{(\epsilon)_i(\mathbf{z})}$ holds for both random and periodic structure CMs.

8.2 RVE for CMs subjected to inhomogeneous loading

The RVE concept is rigorously valid when the field scale (inhomogeneity) vastly exceeds the material scale (microstructural variations, see (2.33₂), (2.34₂)). When these scales are comparable, nonlocal material behavior emerges requiring stress-strain descriptions via statistical averages weighted by a tensorial kernel. Nonlocal models range from strong nonlocality (strain type and displacement type, peridynamics) to weakly nonlocality (strain-gradient, stress-gradient, and higher-order models).

Definition 8.2. *RVE (a) is structurally entirely typical of the whole mixture in R^d on statistical average sense, and (b) contains a sufficient number of inclusions for the apparent effective nonlocal operator (and statistically averaged field distributions in the phases) to be effectively independent of the applied inhomogeneous field.*

Definition 8.2 omits the notion of a “large enough sample” and instead considers a heterogeneous medium (statistically homogeneous or periodic) in full space R^d . Rather than estimating effective moduli \mathbf{L}^* , it focuses on effective nonlocal operators of a given structure.

If $\langle \epsilon \rangle(\mathbf{y})$ varies slowly near \mathbf{y} , it allows for a Taylor expansion of its statistical average and the use of Fourier transforms. The most common effective nonlocal operator is a second-order differential operator

$$\langle \sigma \rangle(\mathbf{x}) = \mathbf{L}^* \langle \epsilon \rangle(\mathbf{x}) + \mathcal{L}^* \nabla \otimes \nabla \langle \epsilon \rangle(\mathbf{x}). \quad (8.2)$$

The quasi-crystalline approximation by Lax [287] (4.2) is commonly used to truncate integral equation hierarchies, enabling explicit derivations of the nonlocal differential operator via methods like the effective field method [249] or conditional moments [254]. A key advantage of the rigorous approach [138], [139], [140] is its foundation in variational principles, providing approximation bounds [140]. By combining MEFM with the Fourier transform method [140], explicit expressions for the nonlocal overall operator as a second-order differential operator (8.2) were derived [51], [102]. For MEFM, the RVE size is $B^{\text{RVE}\mathbf{L}^*} = 6a$ (see Subsection 8.1), while for the corresponding nonlocal operator, it is $B^{\text{RVE}\mathcal{L}^*} = 18a$ [51], [52]. This approach, initially developed within the first background of micromechanics in LM [53], was later extended to the second background in [80].

We analyze periodic structure CMs in LM using CMic methods. For a fixed periodic body force $\mathbf{b}(\mathbf{x})$ using variational and asymptotic expansion techniques (see Block 1 in (3.10)), the approach in [425] constructs elliptic higher-order

homogenized equations rigorously (for the particular case of translation averaging solution (5.6)). However, [425] did not address numerical examples or RVE definitions. A quantitative assessment was performed in [13] on a two-phase composite under periodic anti-plane shear. Another method, second-order computational homogenization [263], [264], incorporates macroscopic deformation gradients and higher-order stress measures, resulting in a full second gradient continuum. Analytical second-order homogenization of linear elastic CMs leads to the second gradient Mindlin continuum (see [79]), where the macroscopic length scale parameter depends on UC size. This approach highlights the impact of physical and geometrical nonlinearities on the relation between RVE size and macroscopic response.

The approach in [51], [102] was later extended to PM in [96]. Equation (3.24) was analyzed under Hypothesis **H1a** (3.8) for linear operators $\mathcal{J}_{i,j}^{\theta\zeta}$, which decompose into tensors when applied to constant effective fields (3.8). The most general method, an iterative scheme (see LM counterpart in [80]), derives a nonlocal integral operator without assuming a predefined form. However, a major drawback is that solving the micromechanical problem (3.24) must be repeated for each different external loading $\langle \boldsymbol{\vartheta} \rangle(\mathbf{z})$. If the field $\langle \zeta_j \rangle$ is smooth, it can be approximated using a Taylor expansion (see [165]), reducing the integral operator to a differential one (8.2). This method [96] can be adapted for periodic structure CMs [97] by replacing the conditional probability density $\varphi(v_q, \mathbf{x}_k | v_i, \mathbf{x}_i)$ by its δ function form (2.36) in Eq. (3.24).

In Subsection 8.2, we identified two main shortcomings in the discussed methods. The first issue is that the approaches for both random and periodic structure CMs (see [249], [254] [138], [139], [140], [51], [102], [51], [102], [425], [13], [263], [264]) are designed specifically for estimating the second-order gradient model effective operator (8.2). Their applicability to constructing a more general (e.g., integral) effective operator remains uncertain. The second issue, related to [52], [96], is that these methods rely on the EFH (3.8) and assume linear phase properties. Additionally, when evaluating the effective response $\langle \boldsymbol{\sigma} \rangle$ under changing overall strains $\langle \boldsymbol{\varepsilon} \rangle$, the entire micromechanical problem must be solved again from scratch. In the next subsection, we introduce a universal method for estimating any form of the effective (surrogate) nonlocal operator for both random and periodic structure CMs. Its computational complexity matches that of the original approach in Subsection 8.1. Thus, in terms of generality and applicability (see Subsection 8.3 and Section 7), the methods in Subsection 8.2 are a dead end.

8.3 RVE for CMs subjected to body force with compact support

Not all datasets \mathcal{D}^f and \mathcal{D}^p are suitable for ML and NN-based surrogate operators. A generalized RVE concept, extending Hill's [216] definition, serves as a threshold to filter out inappropriate sub-datasets, ensuring compatibility with PM under self-equilibrated forcing $\mathbf{b}(\mathbf{x})$ (2.4).

Definition 8.3. *RVE is structurally entirely typical of the whole CM area which is sufficient for all apparent effective parameters \mathcal{D}^I ($I = r, p$ to be effectively stabilized outside RVE (as, e.g. in Eq. (4.12)) in the infinite random or periodic structure CMs with any elastic constitutive laws of phases.*

We analyze the region $\overline{\text{RVE}} = R^d \setminus \text{RVE}$, where the dataset \mathcal{D}^r (or \mathcal{D}^p) stabilizes. Ensuring stabilization and selecting the correct $\overline{\text{RVE}} = R^d \setminus \text{RVE}$ guarantees that all effective parameters between $|\mathbf{x}| = B^{\text{RVE}}$ and $|\mathbf{x}| = B^{\text{RVE}} + B^b/2$ remain consistent within a given tolerance. When this holds, the region $|\mathbf{x}| > B^{\text{RVE}} + B^b/2$ can be disregarded, allowing an infinite medium to be approximated by a finite sample. A properly chosen RVE eliminates edge effects, typically confined to a boundary layer of thickness $6|\Omega|$ if $\langle \boldsymbol{\varepsilon} \rangle^\Omega(\mathbf{x})$ (though this is not the case here; refer to p. 129 in [53]). Conversely, an undersized B^{RVE} leads to numerical errors due to sample size limitations and edge effects (see Subsection 8.1). In this framework, datasets \mathcal{D}^r and \mathcal{D}^p are computed via micromechanical methods like CAM. Under the scale separation hypothesis (2.33₂) in LM, Definition 8.3 reduces to Hill’s classical definition [216] for apparent effective moduli ${}^L\mathbf{L}^*$.

The RVE concept is even more critical in PM, where three types of nonlocal effects emerge: inhomogeneous applied fields B^b , Eq. (2.4), material nonlocality l_δ , and inclusion interactions a^{int} , all of which interact synergistically. In contrast, in LM [216], under the scale separation hypothesis (2.33₂), the nonlocal effects of a^{int} and a reduce to a constant. For a self-equilibrated forcing term (2.4), statistical displacements $\langle \mathbf{u} \rangle(\mathbf{x})$ in a random heterogeneous bar ($\mathbf{x} \in R^1$) were analyzed in [82] using the AMic framework (see Fig. 1). Results showed that for $|\mathbf{x}| \geq a^{1-r}$, the solution $\langle \mathbf{u} \rangle(\mathbf{x}) \approx \text{const.}$; i.e. the domain $|\mathbf{x}| \leq a^{1-r}$ is $\text{RVE}^{\langle \mathbf{u} \rangle(\mathbf{x})}$ for $\langle \mathbf{u} \rangle(\mathbf{x})$, depending on scale ratios $a/B^b/l_\delta$. These studies, though not explicitly naming RVE, pioneered its estimation in PM for random composites. Additionally, RVEs must be assessed for other effective parameters, such as \mathcal{D}^r (4.22) and \mathcal{D}^p (5.12), across different scale ratios $a/B^b/l_\delta^{(1)}/l_\delta^{(0)}$. Unlike LM (8.1), where $\text{RVE}^{\mathbf{L}^*} \equiv \text{RVE}^{\langle \boldsymbol{\varepsilon} \rangle_i(\mathbf{x})}$, these RVEs may differ for each scale ratio.

In peridynamic CMic, the term RVE is commonly used in both Block 3 (finite inclusion samples) and Block 2 (periodic structure CMs), as referenced in (3.9). The general limitations of Block 3 were discussed in Subsection 8.1. For infinite periodic media, RVE has primarily been used in Block 2 as a shorthand for “unit cell (UC) of CM under remote homogeneous loading (2.28)” at extreme scale separations $\Lambda/L = \infty$, $\Lambda/|\Omega_{00}| = \infty$, and $L/|\Omega_{00}| = \infty$, as seen in studies like [324], [325], [134], [135], [182], [183], [184], [185], [227], [305], [379], [469], [468], [470], [471], and [453]. While this shortcut is valid in LM under the scale separation hypothesis (2.33₂) and has been widely accepted for decades, its direct application in PM requires caution. In particular, using periodic boundary conditions (PBC, (2.39))—which are correct in LM—can be problematic in PM (see Subsection 2.3 and Comment 5.1). Instead, the variable periodic boundary conditions (VPBC) originally proposed in [82] should be further generalized to accommodate arbitrary scale ratios $|\Omega_{00}|/a/l_\delta^{(1)}/l_\delta^{(0)}$

and unit cell geometries (see also Subsection 2.4).

This implies that the RVE for the k -th implementation serves as a crucial parameter (or prerequisite) for building the dataset required for the surrogate operator (refer to Subsection 8.2). Specifically, if $\text{RVE} \subset w$, then \mathcal{D}_k^r is incorporated into \mathcal{D}^r . Otherwise, these elements are excluded from further analysis of the surrogate operator. The dimensions B_k^{RVE} of the RVE may vary across different implementations indexed by k -th. The primary role of the RVE is to ensure the stabilization of the field variables within the domain $\overline{\text{RVE}}_k$, rather than merely serving as a mechanism to determine the size of a subdomain for modeling the medium. In this context, the RVE is not strictly a tool for selecting a characteristic size of subdomain (see, e.g., [216]) of the micro inhomogeneous medium but is instead a means of achieving convergence in the statistical or spatial distribution of field quantities. This does not imply that the final size of the RVE, $B_{\text{final}}^{\text{RVE}}$, is equal to $\max_k B_k^{\text{RVE}}$. Once the contribution \mathcal{D}_k^r has been accepted into the overall dataset \mathcal{D}^r , the specific value of B_k^{RVE} associated with that particular k -th implementation may no longer be retained or considered. Furthermore, it is well-established in LM that increasing the sample size effectively mitigates the sample size effect (see, e.g., [251], [439]). However, even resolving the sample size effect does not address boundary layer and edge effects associated with nonlocal phenomena. The primary advantage of the new RVE concept (as defined) lies in its ability to completely eliminate boundary layer and edge effects for random and periodic structured composite materials, irrespective of the phases' elastic properties—whether local or nonlocal, linear or nonlinear.

For estimating any effective nonlocal operator, including surrogate models in ML or NN (see Section 9), analyzing field distributions and determining the appropriate RVE size for a finite scale ratio $B^b/|\Omega_{00}| \neq \infty$ is crucial. To the author's knowledge, the term RVE has not been explicitly used in LM or PM concerning the forcing term (2.4). The RVE depends on scale ratios $a/B^{\text{RVE}}/l_\delta^{(1)}/l_\delta^{(0)}$ and varies with the gradient $\nabla \mathbf{b}(\mathbf{x})$. This means two functions $\mathbf{b}(\mathbf{x})$ and $\mathbf{b}'(\mathbf{x})$ with identical scale ratios may yield different RVEs. Additionally, satisfying $b(\mathbf{0}, B^b) \subset \Omega_{00}$ does not guarantee $\text{RVE} \subset \Omega_{00}$; in fact, the RVE may span multiple unit cells. Despite this complexity, the RVE remains a key benchmark: if the solution domain w of Eqs. (4.10)-(4.20) fully contains the RVE ($\text{RVE} \subset w$), the computed elements \mathcal{D}_k^I ($I = r, p$, $k = 1, \dots, N$) contribute to the surrogate operator dataset (Subsection 8.2). Otherwise, w must be expanded or $|\nabla \mathbf{b}(\mathbf{x})|$ reduced. If the RVE size $\text{RVE} \subset w$, then \mathcal{D}_k^I varies across implementations, ensuring field stabilization rather than merely defining a subdomain for modeling. Unlike traditional LM approaches, where increasing the sample size mitigates finite-size effects [251], [439], this novel RVE concept eliminates boundary layer and edge effects in random or periodic composites, regardless of phase properties—local or nonlocal, linear or nonlinear.

Comment 8.1. Special attention is given to statistically inhomogeneous (or functionally graded, FG) composites, where the arrangement of elements (such as concentration and orientation, see [79]) depends on position, as described in Eq. (2.35). FG composites were studied using the multiparticle effective field method

(MEFM) within the framework of the EFH (3.1), where the exact GIE (3.14) is simplified to Eq. (3.13). The area where Eq. (3.14) should be solved is defined as $w^{\text{FG}} = B(\varepsilon) \oplus b(0, a^{\text{int}})$; here, $B(\varepsilon)$ represents a domain where $\langle \varepsilon \rangle(\mathbf{x}) \neq \text{const}$, and a^{int} is the scale of long-range interactions between inclusions (2.33). However, a new rigorous Definition 8.3 is immediately beneficial for FG composites with random structures (2.35). In statistically homogeneous media, the RVE is invariant to parallel translation, meaning that if $\mathbf{x} \rightarrow \mathbf{y}$ ($\mathbf{y} = \mathbf{x} + \mathbf{z}$), then $\text{RVE}(\mathbf{x}) = \text{RVE}(\mathbf{y})$ for any \mathbf{z} . However, in statistically inhomogeneous (functionally graded) media (2.35), this invariance is lost, so $\text{RVE}(\mathbf{x}) \neq \text{RVE}(\mathbf{y})$. As a result, the AGIE (3.23) should be solved for a set of uncoupled solutions of $\text{RVE}(\mathbf{x})$ instead of a less effective coupled solution over the domain w^{FG} . The resulting datasets $\mathcal{D}^{\text{r}}(\mathbf{x})$, depending on body force \mathbf{b} , are not invariant (in contrast to \mathcal{D}^{r} (4.22)) under parallel translation along the cross-section of FG composites.

8.4 RVE for deterministic structure CMs

Random or periodic structure CMs are characterized by general probability densities ($\varphi(v_i, \mathbf{x}_i)$ and $\varphi(v_i, \mathbf{x}_i; v_j, \mathbf{x}_j)$, see Subsection 2.3) or specific cases (2.36) with a periodic grid \mathbf{A} . In contrast, deterministic structure CMs do not exhibit randomness or periodicity. For example, from microcomputer tomography (micro-CT) or scanning electron microscopy (SEM) images of composite samples and typically consist of several hundreds or thousands of inclusions [152]. Notably, CM images obtained through CT techniques can be viewed as observational snapshots (“window of observation”) of deterministic structure CMs. The observation window w with boundary conditions (either (2.28) or (2.29)) is shown in Fig. 2.

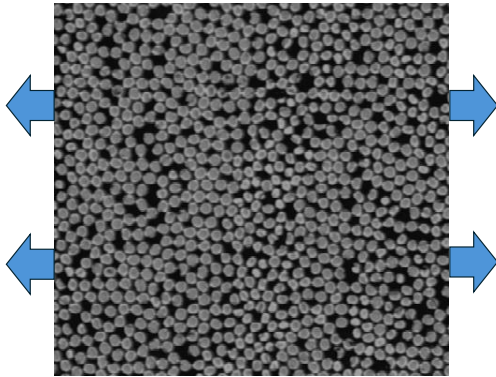


Fig. 2: CT image with BC

As discussed in Subsection 8.2, even with a sufficiently large window w for estimating \mathbf{L}^* and the application of highly precise numerical methods in DNS, the boundary layer effect persists and cannot be fully eliminated. The difficulties in using finite-size samples to approximate effective behavior are well recognized in LM (see, e.g., [79], p. 593; [53], pp. 226-229). It is known

that determining the overall behavior of a sample w using DNS, such as, e.g., in Eq. (4.22),

$$\mathcal{D}^{\text{DNS}} = \{\mathcal{D}_k^{\text{DNS}}\}_{k=1}^N, \quad \mathcal{D}_k^{\text{DNS}} = \{\mathbf{u}(\mathbf{b}_k, \mathbf{x}), \mathbf{b}_k(\mathbf{x})\}, \quad \mathbf{x} \in w, \quad (8.3)$$

results in the complete loss of information related to boundary layer effects; Here, the applied body force $\mathbf{b}(\mathbf{x})$ does not necessarily conform to Eq. (2.4). For example, Fig. 3a (Fig. 3 is reproduced from in [490]) presents an experimental counterpart of Fig. 2, showing a biological tissue specimen under biaxial stretching, with the digital image correlation (DIC) displacement tracking grid marked in green. A schematic of a specimen subjected to Dirichlet-type boundary conditions is illustrated in Fig. 3b. Additionally, a neural network-based learning model was utilized to develop a surrogate operator capable of predicting overall displacement fields for previously unseen loading conditions in finite samples of soft biological tissue (see Fig. 3c). Figures 3a-3c from [490] have been reproduced in several key studies on physics-informed neural operators (e.g., [194], [238], [242], [491], see also [239]). However, how the sample size and boundary layer effects influence these estimations remains an unresolved issue.

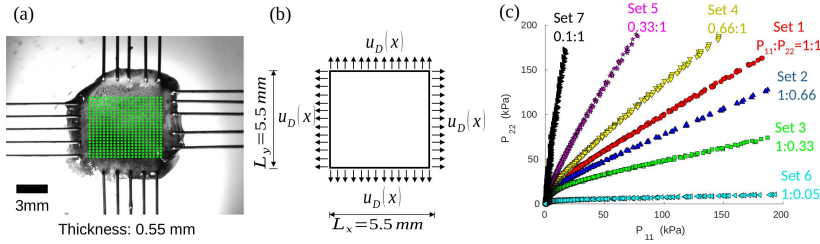


Fig. 3: Biological tissue specimen

A refined version of Maxwell’s approach [338], often referred to as its “second birth,” represents an infinite statistically homogeneous (or periodic) CM as an inclusion cloud embedded within an infinite matrix [404]. Unlike the classical Maxwell model [338], these generalized approaches account for the interactions between inclusions within the cloud. However, Buryachenko [81] demonstrated that 23 key papers in this field [404] are fundamentally flawed when using homogeneous remote BC (2.28). To address this, BC (2.28) can be replaced with freeloading at infinity, supplemented by a body force (2.4). This allows the inclusion cloud (of learnable size) to estimate the RVE per Definition 8.3. Through Monte Carlo simulations of “random” inclusion sets, we can determine \mathcal{D}^{P} similarly to (5.6), replacing uniform χ in (5.6) with random inclusion sets. At this stage, the microstructure of the cloud and its computation method (e.g., multipole expansion [404]) become irrelevant. The final step involves using ML or NN techniques (see Section 9) to derive a surrogate nonlocal operator for modeling infinite statistically homogeneous media. This marks the “third birth” of Maxwell’s approach, proving highly effective.

The concept of the ‘‘inclusion cloud’’ in Maxwell’s approach [338] can be reformulated by replacing the remote BC (2.28) (or (2.29)), with a body force $\mathbf{b}(\mathbf{x})$ (2.4) that has compact support. Under this modification, the domain of interest $\mathbf{x} \in w$ (8.3), effectively reduces to the $\mathbf{x} \in \text{RVE}$ in the sense of Definition 8.3. The DNS data can then be represented as

$$\mathcal{D}^{\text{DNSd}} = \{\mathcal{D}_k^{\text{DNSd}}\}_{k=1}^N, \quad \mathcal{D}_k^{\text{DNSd}} = \{\mathbf{u}(\mathbf{b}_k, \mathbf{x}), \mathbf{b}_k(\mathbf{x})\}, \quad \mathbf{x} \in \text{RVE}. \quad (8.4)$$

The loading configuration of a deterministic structure within the domain $\mathbf{x} \in w$ (as depicted in Fig. 2) by a body force $\mathbf{b}(\mathbf{x})$ (2.4) is illustrated in Fig. 4. In this figure, the localized force application region $b(\mathbf{x}_i, B^b) \subset \text{RVE}$ is explicitly shown. This highlights that the applied force is confined within a subset of the RVE, ensuring the stabilization of effective parameters $\mathcal{D}^{\text{DNSd}}$ outside RVE. In this approach, the dataset $\mathcal{D}^{\text{DNSd}}$ is constructed from various realizations of the body force $\mathbf{b}(\mathbf{x})$ and the microstructural configurations (e.g., derived from distinct CT images). Generations of deterministic structures at the fixed $\mathbf{b}_k(\mathbf{x})$ allow the analog of dataset (5.12). The generation of deterministic structures while keeping the body force $\mathbf{b}_k(\mathbf{x})$ fixed enables the construction of an analogous dataset to Eq. (5.12)

$$\begin{aligned} \mathcal{D}^{\text{d}} &= \{\mathcal{D}_k^{\text{d}}\}_{k=1}^N, \\ \mathcal{D}_k^{\text{d}} &= \{\langle \mathbf{u}_k \rangle(\mathbf{b}_k, \mathbf{x}), \langle \boldsymbol{\sigma}_k \rangle(\mathbf{b}_k, \mathbf{x}), \langle \mathbf{u}_k \rangle^{(1)}(\mathbf{b}_k, \mathbf{x}), \langle \boldsymbol{\sigma}_k \rangle^{(1)}(\mathbf{b}_k, \mathbf{x}), \mathbf{b}_k(\mathbf{x})\}, \end{aligned} \quad (8.5)$$

where the statistical averages $\langle \cdot \rangle$ are computed by averaging over the ensemble of configurations, ensuring a statistical representation of the mechanical response for the given loading conditions.

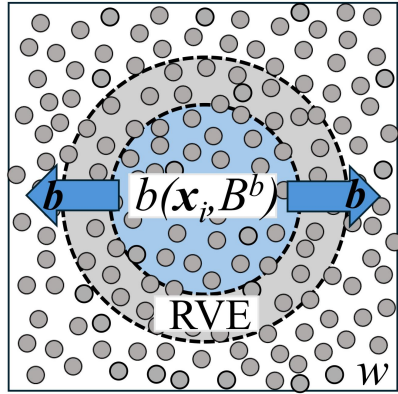


Fig. 4: Scheme of CT image with $b(\mathbf{x}_i, B^b) \subset \text{RVE} \subset w$

In the context of computational micromechanics for 2D particular realizations of statistically homogeneous random structures (i.e., deterministic structures), Silling *et al.* [421] proposed a coarse-graining model for the upscaling of mechanical properties of composite materials (CMs). This model is based on Monte Carlo-simulated inclusion placements (≈ 900 inclusions) within a finite-sized square domain w , which is subjected to a self-equilibrated body force with

compact support $\mathbf{b}(\mathbf{x})$ (2.4). The body force $\mathbf{b}(\mathbf{x})$ corresponds to the region of long-range interaction, as described in [82]. The geometric scale separation is characterized by the ratio $\text{dist}(\partial\text{RVE}, \partial w) \approx 10a = 100\lambda$, where a represents the lattice spacing. This scale separation satisfies the conditions of an RVE according to Definition 8.3. The validity of this RVE assumption is supported by the numerical observation that the effective strain field $\langle \boldsymbol{\varepsilon} \rangle(\mathbf{x})$ vanishes in the vicinity of ∂w , as illustrated in colored Fig. 12 of [421], which is consistent with Fig. 4. Notably, the term ‘‘RVE’’ was not explicitly used in [421]. The purple regions, where $\langle \boldsymbol{\varepsilon} \rangle(\mathbf{x}) \approx \mathbf{0}$, and the blue regions in Fig. 5 correspond to the areas outside $w \setminus \text{RVE}$ and inside RVE, respectively, as shown in Fig. 4. The proposed upscaled peridynamic model allows for a significantly coarser discretization compared to the original fine-scale model, which relies on DNS. This coarse-graining approach enables large-scale simulations to be conducted efficiently, through the estimation of quantities such as $\langle \mathbf{u} \rangle_i(\mathbf{z}, \mathbf{x})$, $\langle \boldsymbol{\sigma} \rangle_i(\mathbf{z}, \mathbf{x})$, $\mathbf{z} \in v_i$, $\mathbf{x} \in R^d$ remains outside the scope of the study.

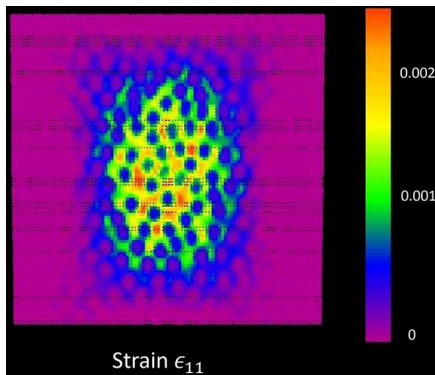


Fig. 5: Strain $\langle \boldsymbol{\varepsilon} \rangle(\mathbf{x})$ in a sample w

8.5 Classification and schematic representation of CAM

We begin by classifying PM in relation to the homogeneous volume boundary condition (VBC) (2.28), starting with the Amic branch. The classification of the LM method (3.9) also applies to PM. Model methods (Gr1) include simplified approaches like mixture theory [16], [17], [18], [112], [223], [224], [339], [466], [467], which have been widely used for laminated structures [29], [133], [189], [226], [328], [330], [331], [385], [472]). The CAM of peridynamic CM, a part of *Analytical Micromechanics* (Amic), does not rely on DNS, although nothing in Eq. (3.24) and their solution (see [94]) is analytical. The effective medium method (EFM), a Gr1 approach in LM, extends naturally to PM as a peridynamic inclusion in a local effective medium. Perturbation methods (Gr2) relate to the dilute approximation in PM [77], while variational methods (Gr3) are discussed in [78]. The original CAM formulation in PM (Gr4) was introduced in [76] for linear bond-based properties and later generalized to nonlocal elastic

properties [93], [79]. Additionally, the classification of *Computational Mechanics* using DNS (Eq. (3.10)) in LM applies to PM as well. Asymptotic homogenization methods (Block 1 in (3.10)) for PM are explored in [11], [146], [144]). The generalization of classical computational homogenization approaches (Block 2 in (3.10)) has been explored in studies such as [70], [72],[134], [135], [182], [183], [420] [379], [469], [474] [475] [491] [489]. Additionally, numerous works address problems involving single or multiple inclusions (or cracks) within a sample (Block 3 in (3.10)): [3] [16], [17], [18], [21], [40] , [42], [47], [132], [203], [225], [241], [257], [258], [286], [291], [322], [327], [351], [358], [386] , [391], [456], [460], [482], [498], [512].

Amic functions like a solar system, with GIE (3.24) as its gravitational core, guiding all related methodologies Gr1)-Gr4). In contrast, the Cmic branch orbits independently, employing approaches that do not rely on GIE (3.24). Now, we turn to an entirely different centralized framework, where AGIE (3.23) becomes the new focal point, standing on its own without any dependence on GIE (3.24)

The scheme of the CAM (3.17), (3.19), (4.5)-(4.7) is represented in a block diagram in Fig. 6. To simplify notation, the scheme corresponds to the iterative solution of Eq. (4.5)-(4.7). At its core, the process revolves around Block 3

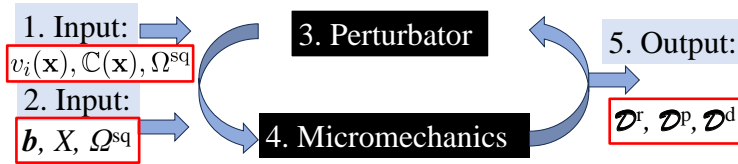


Fig. 6: The iteration scheme of the CAM (4.5)

Perturbator and Block 4 Micromechanics, which form a central feedback loop. Block 3 computes the perturbator $\mathcal{L}_i^{\theta\zeta}(\mathbf{z}, \bar{\zeta})$ (3.17). The preprocessing Block 1 Input provides Block 3 with essential data, including the microstructural geometry of an inclusion $v_i(\mathbf{x})$ within an infinite homogeneous matrix (or a large sample), material properties $\mathbb{C}(\mathbf{x})$ (such as micromodulus \mathbf{C}^{bond}), and a square mesh $\Omega^{\text{sq}} := \{(x_1, \dots, x_d)^\top | x_i = hp_i\}$ ($\mathbf{p} = (p_1, \dots, p_d) \in Z^d$). Similarly, Block 2 Input supplies Block 4 with geometrical information, specifically the same square mesh Ω^{sq} and the spatial distribution of inclusions X . For random structures, this distribution is characterized by probability densities $\varphi(v_j, \mathbf{x}_j)$ and conditional densities $\varphi(v_j, \mathbf{x}_j | v_i, \mathbf{x}_i)$. For the periodic structures $X = \mathbf{\Lambda}$ whereas X is a deterministic field for deterministic structure CMs. The use of the same mesh Ω^{sq} in Block 3 and Block 4 is primarily for ease of integration between these two components (see the case of LM on p. 428 in [79]). In the iterative cycle [Block 3]=[Block 4] (4.5), Block 3 takes as input $\langle \bar{\zeta} \rangle_i(\mathbf{x})$ and outputs $\mathcal{L}_i^{\theta\zeta}(\mathbf{z}, \langle \bar{\zeta} \rangle_i)$, where $\mathbf{x}, \mathbf{z} \in \Omega^{\text{sq}}$. However, the mesh Ω^{sq} is used solely to maintain consistency between Block 3 and Block 4 and does not determine the internal solution method within Block 3 (see Eqs. (3.17)). Importantly, the internal workings of Block 3 are irrelevant to Block 4, and vice versa. As a result, these blocks function as independent “Black Boxes” that interact solely

through their inputs and outputs, as indicated in Fig. 6 by their black shading. Output Block 5 contains the datasets either \mathcal{D}^r , \mathcal{D}^p , or \mathcal{D}^d for CMs with either random, periodic, or deterministic structures, respectively. It should be mentioned that particular cases of problems indicated in Block 3 in Eq. (3.10) can be considered as a Block 3 Perturbator (see Fig. 6) for one inclusion (or crack) in a big sample.

The AGIE (3.23) plays a fundamental role in both Amic and Cmic within the PM framework. Sections 3 and 4 focus on the formulation of AGIE (3.23) and its solution (4.1)–(4.20), establishing it as the core component of the self-consistent method Gr4) (4.1)–(4.20) in Amic (see Fig. 7). The perturbation methods Gr2) can be derived from Gr4) by taking the limit $c \rightarrow 0$. Furthermore, the model methods Gr1) corresponding to (3.10) (referenced in the first paragraph of this subsection) implicitly or explicitly rely on EFH (3.8), which is eliminated under body force loading (2.4). Consequently, the physical interpretation of Gr1) methods under such loading conditions remains unclear. Variational methods, widely used in LM (see [79] for references), have been extended to PM in [79], [78] for statistically homogeneous materials and field parameters. However, even for statistically homogeneous media subjected to body force loading (2.4), the statistical homogeneity of the field is disrupted, making the formulation of variational methods for this loading nontrivial. In the Cmic branch, for periodic structured CMs, the equations (5.1)–(5.3) derived from CAM (3.25) formally resemble the equations (4.11)–(4.13) for random structured CMs. Additionally, the translation averaging (5.6) applied to periodic structures leads to equations (5.7)–(5.11), which are structurally similar to (4.15)–(4.19) for random structures. This process generates the dataset \mathcal{D}^p (5.12), which is analogous to \mathcal{D}^r (4.22). Notably, periodic boundary conditions (2.39), (2.40) (or VPBC (2.39), (2.40)) are effectively eliminated, raising questions about the generalization of methods from Blocks 1 and 2 (see (3.10) and the first paragraph of this Subsection) for body force loading (2.4) in both LM and PM. Ultimately, CAM reduces the analysis of periodic structured CMs to the study of a finite deterministic field of inclusions, aligning it with the methods of Block 3 (see Fig. 7). This suggests that DNSs within Cmic are systematically reorganized within Amic to construct datasets \mathcal{D}^p (5.12) and \mathcal{D}^d (8.5), both structurally analogous to \mathcal{D}^r (4.22).



Fig. 7: AGIE as a central governing equation of PM

The fundamental framework and key results of this paper—embodied in Eqs. (3.17)–(3.26), (4.7)–(4.22), (5.1)–(5.12), (6.2)–(6.12), and Subsections 8.3 and 8.4—are formulated in an operator form that remains entirely independent of any specific constitutive law of elasticity. This universality ensures that these

equations hold for any constitutive model, including, e.g., those detailed in Section 7. In essence, the representation of PD using Eqs. (2.1)-(2.27) and (3.1)-(3.7) can be seamlessly substituted with the more detailed constitutive formulations presented in Section 7, without affecting the overall structure and validity of the results, see Sections 3-8. The choice of PD as the primary modeling approach in this work does not stem from an inherent superiority over other models but rather from the author's long-standing dedication to peridynamic CMs—an expertise and intellectual commitment developed over more than a decade of focused research in this field.

9 Estimation of a set of surrogate operators

Silling's pioneering work [417], [486], later expanded in [488], introduced data-driven ML techniques for modeling composite materials (CMs) by constructing surrogate nonlocal operators from DNS. These studies focused on a finite 1D heterogeneous bar under wave loading at the boundary and oscillatory forcing.

In the current (see for details [82], [83]), Silling's approach [417] is adapted by replacing the DNS dataset \mathcal{D}^{DNS} (8.3) with \mathcal{D}^{r} (4.22), \mathcal{D}^{p} (5.12) or \mathcal{D}^{d} (8.5), corresponding to random, periodic, and deterministic structures, respectively. The inhomogeneous forcing term $\mathbf{b}(\mathbf{x})$ with compact support (2.4) serves both as a loading parameter and a tool for learning surrogate nonlocal constitutive laws for CMs. The surrogate datasets $\tilde{\mathcal{D}}^{\text{r}}$, $\tilde{\mathcal{D}}^{\text{p}}$, $\tilde{\mathcal{D}}^{\text{d}}$ approximate their respective datasets while efficiently compressing micromechanical data. The field PM dataset $\tilde{\mathcal{D}}^{\text{r}}$ is constructed via a surrogate model \mathcal{S} , mapping statistical micromechanical averages to macroscopic fields: $\tilde{\mathcal{D}}^{\text{r}} = \mathcal{S}(\mathcal{D}^{\text{r}})$. This approach retains essential micromechanical features while simplifying data representation.

$$\begin{aligned} \mathcal{L}_\gamma[\langle \mathbf{u}_k \rangle](\mathbf{x}) &= \gamma(\mathbf{x}), \\ \mathcal{L}_\gamma[\langle \mathbf{u}_k \rangle](\mathbf{x}) &= \int \mathbf{K}_\gamma(|\mathbf{x} - \mathbf{y}|)(\langle \mathbf{u}_k \rangle(\mathbf{y}) - \langle \mathbf{u}_k \rangle(\mathbf{x})) d\mathbf{y}, \end{aligned} \quad (9.1)$$

where $\gamma := b, \sigma, u_i, \sigma_i$ and $\Gamma(\mathbf{x}) := -\mathbf{b}(\mathbf{x}), \langle \sigma \rangle(\mathbf{x}), \langle \mathbf{u} \rangle_i(\mathbf{z}, \mathbf{x}), \langle \sigma \rangle_i(\mathbf{z}, \mathbf{x})$, respectively, correspond to four surrogate operators \mathcal{L}_γ . Each of these fields corresponds to a surrogate operator \mathcal{L}_γ associated with the problem. The objective is to construct an optimal surrogate model for the kernel functions \mathbf{K}_γ^* , which define the surrogate dataset $\tilde{\mathcal{D}}^{\text{r}}$. This is formulated as four optimization problems, one for each γ

$$\mathbf{K}_\gamma^* = \underset{\mathbf{K}_\gamma}{\operatorname{argmin}} \sum_{k=1}^N \|\mathcal{L}_\gamma[\langle \mathbf{u}_k(\mathbf{b}_k) \rangle](\mathbf{x}) - \Gamma_k(\mathbf{x})\|_{l_2}^2 + \mathcal{R}(\mathbf{K}_\gamma). \quad (9.2)$$

The objective function quantifies the discrepancy between the surrogate model and the original dataset using an l_2 -norm over $\mathbf{x} \in R^d$, with a regularization term $\mathcal{R}(\mathbf{K}_\gamma)$ (e.g., Tikhonov regularization) to improve conditioning. To optimize \mathbf{K}_γ , the Adam optimizer [260] is employed in an iterative gradient descent

scheme, where \mathbf{K}_γ is expressed as a linear combination of Bernstein-based polynomials. Further details are available in [486], with additional insights in [166], [489], [491], and [488].

The approaches in [486] and [488] use uncompressed datasets (8.3), unlike the compressed methodology in (4.22) (or (5.12)). The DNS dataset \mathcal{D}^{DNS} (8.3) captures detailed microscale displacements $\mathbf{x} \in w$ for each applied force $\mathbf{b}_k(\mathbf{x})$, making it significantly larger than \mathcal{D}^{I} ($I = \text{r, p, d}$) (4.22) even for identical loadings. Compression in \mathcal{D}^{I} does not require full-field DNS computations but instead leverages micromechanics to estimate effective parameters more efficiently. On the other side, for homogeneous linearized peridynamic medium (2.12) and (2.13) subjected to remote homogeneous BC (2.28) (e.g. $\boldsymbol{\eta}(\boldsymbol{\xi}) = \boldsymbol{\xi}$), the corresponding local moduli can be obtained from the equation of constitutive law (see [424]). Seemingly, for surrogate homogeneous media subjected to remote homogeneous BC (2.28), we obtain

$${}^L\mathbf{L}^* = \int \mathbf{K}_\sigma(|\mathbf{x} - \mathbf{y}|)(\mathbf{y} - \mathbf{x}) \, d\mathbf{y}, \quad (9.3)$$

Comment 9.1 The method in [474] (see also [475]) and [489]) defines the averaged displacement field as $\langle \tilde{\mathbf{u}} \rangle_i^\Omega(\mathbf{x}) = |\Omega_i|^{-1} \int_{\Omega_i} \tilde{\mathbf{u}}(\boldsymbol{\chi}) \, d\boldsymbol{\chi}$ where Ω_i is the averaging domain for a fixed grid point \mathbf{x} . This approach assigns the computed field to a fixed computational grid $\boldsymbol{\Lambda}$, producing a discrete kernel \mathbf{K}_b^* . In contrast, translation-averaging methods (e.g., Eq. (5.6)) use moving averaging cells, yielding continuous kernels. For a detailed comparison of discrete vs. continuous formulations, see [79], p. 895.

The original approach in [417], [486] estimates the kernel \mathcal{D}^{DNS} by solving the optimization problem (9.2). However, it does not establish that \mathbf{K}_b^* can directly approximate statistical average stresses $\langle \boldsymbol{\sigma} \rangle(\mathbf{x})$, similar to how a micromodulus estimates the stress field $\boldsymbol{\sigma}(\mathbf{x})$ (2.17). Moreover, within \mathcal{D}^{DNS} , key displacement averages inside inclusions, $\langle \mathbf{u} \rangle_i(\mathbf{x})$ ($\mathbf{x} \in v_i$), are not retained during the online stage. Instead of relying on \mathbf{K}_b^* , kernels $\mathbf{K}_{u_i}^*$ and $\mathbf{K}_{\sigma_i}^*$ are more applicable for nonlinear problems like fracture mechanics and plasticity. To address this, we use compactly supported forcing terms to construct surrogate operators, bypassing the need for effective moduli estimation via $B^b \rightarrow \infty$.

The upscaled peridynamic model allows for a coarser spatial discretization (see [491], [485] and [420]) compared to DNS, greatly improving computational efficiency for large-scale simulations. However, estimating specific effective field parameters, such as $\langle \mathbf{u} \rangle^{l(1)}(\mathbf{x})$, $\langle \boldsymbol{\sigma} \rangle^{l(1)}(\mathbf{x})$, ($\mathbf{x} \in R^d$), is beyond the study's scope. This framework ensures scalability while preserving fidelity to micromechanical behavior within the RVE-based approach.

The surrogate operators in (9.1) and (9.2) are predefined and limited to linear response prediction. To address this, nonlocal neural operators have been introduced to learn mappings between function spaces [285] and [306]. An ordinary artificial neural network (ANN) defines a nonlinear local operator. Consider an L -layer fully connected neural network (FCNN) $\Psi(\mathbf{x}): \mathbf{R}^{d_x} \rightarrow \mathbf{R}^{d_u}$,

mapping input \mathbf{x} to output \mathbf{u} through multiple layers. Each layer processes the previous layer's output using a weight matrix \mathbf{w}^l and bias vector \mathbf{b}^l for ($1 \leq l \leq L-1$)

$$\mathbf{z}^l(\mathbf{x}) = \mathcal{A}(\mathbf{w}^l \mathbf{z}^{l-1}(\mathbf{x}) + \mathbf{b}^l), \quad \mathbf{u}(\mathbf{x}) = \mathbf{w}^L \mathbf{z}^{L-1}(\mathbf{x}) + \mathbf{b}^L, \quad (9.4)$$

where \mathcal{A} is a nonlinear activation function (e.g., tanh). The tractable parameters $\boldsymbol{\vartheta} := \{\mathbf{w}^l, \mathbf{b}^l\}_{1 \leq l \leq L}$ are optimized via a loss function. This function $\Psi(\mathbf{x})$ is local since $\Psi(\mathbf{x})$ depends only on $\mathbf{z}(\mathbf{x})$ at the same point \mathbf{x} . In contrast, nonlocal neural operators incorporate integral operators to capture long-range dependencies:

$$\mathbf{z}^l(\mathbf{x}) = \mathcal{A}(\mathbf{w}^l \mathbf{z}^{l-1}(\mathbf{x}) + \mathbf{b}^l + (\mathcal{K}^l(\mathbf{z}^{l-1}))(\mathbf{x})), \quad (9.5)$$

where \mathcal{K}^l integrates against a matrix-valued kernel \mathbf{K}^l . Various architectures—DeepONet, PCA-Net, graph neural operators, Fourier neural operator (FNO), and Laplace neural operator (LNO)—have been developed, with detailed comparisons available in [194], [228], [282], [285].

The Peridynamic Neural Operator (PNO) [238] introduces a surrogate operator $\mathcal{G}(\langle \mathbf{u} \rangle)(\mathbf{x}) \approx -\mathbf{b}(\mathbf{x})$ for predicting the behavior of highly nonlinear, anisotropic, and heterogeneous materials, offering greater accuracy and efficiency than traditional models based on predefined constitutive laws (e.g., Eq. (9.1)). An extension, Heterogeneous PNO (HeteroPNO) [239], enables data-driven constitutive modeling of fiber orientation fields in anisotropic materials. Two loading cases were analyzed for a finite square sample: (1) volumetric Dirichlet boundary conditions without body forces, and (2) body forces $\mathbf{b}(\mathbf{x})$ generated via FFT from a Gaussian white noise field rather than a compactly supported function (2.4). However, extending the surrogate operator to an infinite medium while eliminating sample size and boundary layer effects without relying on the RVE concept (see Definition 8.3 and Fig. 12 in [421]) remains a challenge.

Physics-Informed Neural Networks (PINNs) [117], [205], [209],[221], [252], [259], [382], and [387] enforce physical equations (e.g., (2.5), (2.6)) as constraints within neural networks, ensuring physically consistent training. Residuals of these equations are incorporated into the loss function. By integrating neural operators with PINNs [170], [194], [454], models can efficiently capture complex nonlinearities, heterogeneity, and nonlocal effects with high generalization. However, these methods are typically applied to finite-size samples without direct extension to infinite media. In particular, peridynamic (PD) differential operators are incorporated into PINNs for problems with sharp gradients [204], though the constraint equations are based on solid mechanics PDEs. PINNs with PD governing equations have been used to analyze displacement fields in homogeneous and heterogeneous elastic plates [357] and to predict quasi-static damage and crack propagation in brittle materials [157]. PINN approach establishes a relationship between the material parameters of a mesoscale model and the material parameters with constraints based on known physical relationships [308]. The PD-PINN framework effectively captures complex displacement patterns influenced by geometric parameters like pre-crack

position and length. The total loss function \mathcal{L}_{tot} (see [194], [252], [382]) combines governing equation loss \mathcal{L}_{gov} , boundary condition losses $\mathcal{L}_{\text{BC}}^u$, a local balance between the internal and external forces $\mathcal{L}_{\text{BC}}^f$, and data loss $\mathcal{L}_{\text{data}}$, each weighted appropriately. Model parameters $\boldsymbol{\vartheta}^*$ are optimized by minimizing \mathcal{L}_{tot} until a set accuracy or iteration limit is met [260], [373].

Instead, nonlocal energy-informed neural networks (EINN) [493], [494], [513] define the total loss function based on the system's total potential energy, combining internal strain energy loss and external work loss while enforcing boundary conditions. To solve the inverse problem of computing the peridynamic kernel, [127] proposed using radial basis functions (RBFs) as activation functions in PINNs. It was demonstrated that selecting an appropriate RBF is crucial for obtaining physically meaningful solutions consistent with the data.

The nonlinear micromechanical model of CAM (see Sections 4 and 5) can be integrated into PNO and PINN by replacing the full-field dataset \mathcal{D}^{DNS} with the compressed statistical dataset \mathcal{D}^r (4.22) (or \mathcal{D}^p , \mathcal{D}^d), forming CAMNN (CAM Neural Network approach). This approach eliminates boundary layer and size effects, and the known difficulties for generalizability to different domain shapes for neural operators (see for references [238]), a known issue in local micromechanics [53]. The proposed approach ensures generalizability since the domain of interest is the entire space R^d . Unlike previous methods ([157], [357], [493], [494], and [513]), it removes boundary condition residual losses. Boundary layer and edge effects (appearing in [238], [239], and [490]), previously addressed through inefficient minus-sampling [79], are inherently avoided. Using \mathcal{D}^r instead of \mathcal{D}^{DNS} results in four surrogate operators $\mathcal{G}_\gamma(\langle \mathbf{u} \rangle)(\mathbf{x})$ ($\gamma = b, \sigma, u_i, \sigma_i$) instead of a single operator $\mathcal{G}(\langle \mathbf{u} \rangle)(\mathbf{x})$ [238], akin to mixed PINN formulations [205], [209]. Crucially, this enables a nonlocal counterpart to the effective concentration factor (8.1₂), making it applicable to nonlinear problems like fracture and plasticity.

The key advantage of substituting $\mathcal{D}^{\text{DNS}} \rightarrow \mathcal{D}^r$ (4.22) is that \mathcal{D}^r is derived for a compact-support forcing term (2.4) and incorporates the crucial RVE concept (Subsection 8.3). This ensures the elimination of size-scale and boundary layer effects at the dataset preparation stage. Without RVE, these effects inevitably arise, compromising the accuracy of the four surrogate operators $\mathcal{G}_\gamma(\langle \mathbf{u} \rangle)(\mathbf{x})$ ($\gamma = b, \sigma, u_i, \sigma_i$, Eq. (9.1)), and cannot be reliably corrected later. Thus, RVE is essential for ensuring accurate, scale-independent ML and NN applications in computational micromechanics.

The process for generating surrogate models is illustrated in Fig. 8. Block 1 DNS \mathcal{D}^{DNS} (8.3) has been utilized in studies such as [166], [238], [486], [489], and [491]. In the proposed CAMNN approach, we analyze either \mathcal{D}^r (4.22), \mathcal{D}^p (5.12) or \mathcal{D}^d (8.5), employing AGIE (3.23) in AMic and CMic tools, respectively. These datasets are compressed in Block 2 (Field PM Data) and used as input in Block 3 (Optimization), which applies established ML and NN techniques (Section 9). By replacing the large dataset \mathcal{D}^{DNS} (8.3) with the more compact \mathcal{D}^r , \mathcal{D}^p , or \mathcal{D}^d , computational efficiency is significantly improved. Only the alignment between Blocks 2 and 3 is required, with no changes to

Block 3 itself. Solving the optimization problem in Block 3 results in either a single surrogate operator (Block 4) or a set of surrogate models (Block 5).

To the best of the author's knowledge, the analysis of composite materials (CMs) subjected to a forcing term with compact support was first explored in [82] and [83], where this issue was framed as a highly specific example of the interaction between nonlocal effects, driven by the distinct material and field scale a, i_δ, B^p . However, it has now become clear that the systematic application of a forcing term with compact support, as articulated in (2.4) [82] and [83] (and further explored in [95], [96], [421]), far exceeds its initial role as a mere specialized loading scenario for composite materials. This methodology has evolved into a formidable and highly versatile framework for probing nonlocal effects in CMs, unlocking new dimensions in the study of heterogeneous media. When integrated with the RVE, the forcing term (2.4) emerges as an indispensable element in advancing the application of LM and NN techniques, facilitating the construction of surrogate operators within the powerful context of the PM. This marks a transformative leap, pushing the boundaries of traditional micromechanics to a more sophisticated and adaptable paradigm capable of addressing complex material behaviors with unprecedented precision and scalability.

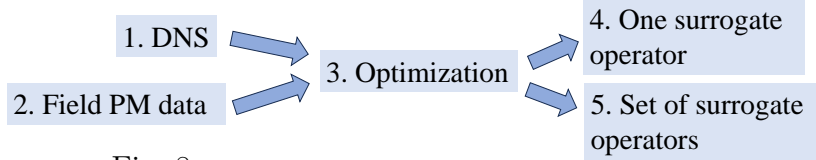


Fig. 8: The scheme of obtaining of surrogate model set

Comment 9.2. PNO was utilized in [238] to develop a continuum constitutive model for single-layer graphene at zero temperature using synthetic data from molecular dynamics (MD) simulations. Graphene, a two-dimensional carbon allotrope with a hexagonal lattice structure (with an interatomic distance of 1.46\AA), possesses remarkable mechanical properties and various applications [7]. The MD code calculates the equilibrium atomic displacements and interatomic forces under external force fields and boundary conditions, with data generation details in [420], [491]. Integrating CAMNN into the model [238] is straightforward. At each $\mathbf{b}_k(\mathbf{x})$ ($k = 1, \dots, N$) (2.4), we conducted an MD simulation $\mathcal{D}_k^{\text{DNS}}(\Lambda_j^k)$ as described in [238], for a grid Λ_j ($j = 1, \dots, M$). For the fixed $\mathbf{b}_k(\mathbf{x})$, we estimate $\mathcal{D}_k^{\text{DNS}}(\Lambda_j^k)$ ($j = 1, \dots, M$) and compute \mathcal{D}_k^p by applying a translation average to $\mathcal{D}_k^{\text{DNS}}(\Lambda_j^k)$ (with the step, e.g., $d|\chi| = 0.1\text{\AA}$ in Eq. (5.6)). This leads to the calculation of \mathcal{D}^p (5.12), which then transitions from Block 2 Field PM data to Block 3 Optimization in Fig. 8, followed by the construction of Block 4 One surrogate operator or Block 5 Set of surrogate operators. To fully align with the original PNO approach [238], $\mathcal{D}_k^{\text{DNS}}(\Lambda_j^k)$ can be estimated using a coarse-grained method [238]. The key benefit of \mathcal{D}^p (5.12) is that it eliminates size and boundary effects, and does not rely on a fixed computational grid Λ (as in [238], and see also Comment 9.1). Extending CAMNN to CMs with random or periodic distributions of inclusions from different materials, or to a two-dimensional lattice with random properties [421], is straightforward and provides the same benefits as those seen with the uniform grid Λ .

Comment 9.3. In the LM, the ML and ANNs are being increasingly utilized to model composite systems, demonstrating their power as predictive tools for data-driven multi-physical modeling. These techniques provide insights into system properties that go beyond the capabilities of traditional computational and experimental analyses. Comprehensive reviews on these advancements can be found in the works [1], [198], [317], [311], [406]. For example, in the work [198], a Convolutional NN (CNN) was applied to predict key mechanical properties such as toughness and strength of materials. Additionally, in a study [484], a combined approach of CNN and Principal Component Analysis (PCA) was proposed to efficiently predict stress-strain curves, incorporating three critical material features: tensile strength, modulus, and toughness for fiber-reinforced composites. Lefik *et al.* [293] applied ANN models to predict the nonlinear elastic-plastic behavior (e.g., the strain-stress curve) of a two-phase composite material, while Le *et al.* [290] used RVE analyses with periodic boundary conditions to generate training data for constructing a constitutive model for nonlinear elastic behavior. Finally, the PINN homogenization theory, proposed by Chen *et al.* [107], is a method for identifying homogenized moduli and local electromechanical fields in periodic piezoelectric composites. In the study of micromechanics of periodic CMs, Buryachenko [87] demonstrated that Dvorak's [141] transformation field analysis provides the foundation for the self-consistent clustering analysis (SCA), also known as clustering discretization methods (CDM), developed by Liu *et al.* [315] (see also [297], [437], [500]). CDM has been applied to a broad range of nonlinear problems, such as nonlinear elasticity [297], various nonlinear interface properties [107], elastoplasticity [230], elastic-viscoplasticity [492], and damage analysis [214]. A further step in the generalization of data-driven machine learning (ML) approaches in local micromechanics (LM) [79], [207], [208], [214], [247], [297], [316] can be easily extended to their peridynamic equivalents [90]. This includes modeling different physical phenomena, such as state-based models, diffusion, viscosity, thermoelastoplasticity, damage accumulation, debonding, plastic localization, and wave propagation, for composite materials with various periodic structures (e.g., polycrystals, fiber networks, hybrid structures, foam materials). Recently, Liu *et al.* [317] developed a deep material network for process modeling, material homogenization, machine learning, and multiscale simulation.

The main limitation of these ML and ANN techniques (referred in Comment 9.3) in CMs modeling lies in the implicit use of Definition 8.1, which implies either a finite sample size [208] or a periodic system [207], [214], [247], [297], [316], [479], [492] with corresponding boundary conditions (BC). As a result, factors like sample size, boundary layers, and edge effects are typically not considered in the analysis. For periodic structures in CMs, PBC, as shown in equations (2.39) and (2.40), are imposed. Extending the mentioned methods based on Definition 8.1 to cases corresponding to Definition 8.3, and then constructing surrogate nonlocal operators, is a challenging and uncertain task.

10 Conclusion

The term “micromechanics” traditionally brings to mind concepts such as effective moduli, linear local elasticity, rRVE by Hill [216], and remote homogeneous boundary conditions. These foundational ideas have long defined the field, providing a structured and rigorous framework for analyzing material behavior at the microscale. However, we have moved beyond these conventional constraints—breaking free from this rigid, *Procrustean bed* of assumptions. By challenging and redefining the fundamental principles of micromechanics, we have expanded its scope, introducing new methodologies and perspectives that transcend the limitations of traditional approaches. This shift allows for a more flexible and comprehensive understanding of microscale interactions, paving the way for innovative applications and deeper insights into material behavior.

In particular, a systematic analysis of composite materials (CMs) subjected to a body force (2.4) with compact support—rather than remote homogeneous boundary conditions—immediately removes all the aforementioned restrictions. More specifically, the proposed universal framework, referred to as CAM, is highly adaptable and built upon physically intuitive hypotheses. These hypotheses can be modified or refined as needed, even to the extent of being discarded, not merely for the sake of theoretical complexity but in response to practical challenges and advancements. Within a unified analytical scheme, CAM enables the study of a broad spectrum of micromechanical problems. This approach encompasses CMs with random (statistically homogeneous and inhomogeneous), periodic, and deterministic (neither random nor periodic) structures. It also addresses materials exhibiting linear and nonlinear behavior, coupled and uncoupled locally elastic responses, as well as weakly nonlocal (strain gradient and stress gradient) and strongly nonlocal (strain-type and displacement-type, peridynamics) phase properties. Although PM of both the random and periodic structure CMs was historically developed as a generalization of the corresponding methods of the LM, it does not mean that PM’s society manifests itself as a user of the LM methods; we also demonstrated that some methods developed in PM initiate the new methods of LM unknown before (i.e. the methods of both the LM and PM mutually enrich one another).

To present LM and PM within a unified theoretical framework, we introduce—for the first time—a structured, modular approach. Both LM and PM are formulated as block-based (or modular) schemes, allowing specialists in one block to contribute without requiring expertise in the underlying details of other blocks. This modular structure consists of distinct block teams, including the image technique team (see Figs. 2 and 4), the Block 3 Perturbator and Block 4 Micromechanics teams (see Fig. 5), and the machine learning (ML) and neural network (NN) technique team (see Fig. 6 and 7). Each team operates independently within its designated block while ensuring seamless integration within the larger framework. Furthermore, during the development of joint software, each block team can refine and modify its own software component at any stage without directly informing the other teams. The only necessary

coordination occurs at the level of Block 4 Micromechanics (see Fig. 6), which ensures proper integration and alignment among the different modules. This structured approach facilitates effective collaboration while maintaining flexibility and efficiency in the overall system. The development of this modular structure in PM is enabled by a critical generalization of CAM, which builds on the new AGIE (3.23). CAM is an exceptionally flexible, robust, and physics-based framework that integrates data-driven, multi-scale, and multi-physics modeling, accelerating both fundamental and applied research in random, periodic, and deterministic heterogeneous media. However, fully leveraging CAM's potential requires collaborative efforts across multiple disciplines, including image processing, computational mathematics, micromechanics, material science, physics, and data science. The proposed modular PM structure provides an ideal foundation for fostering effective interdisciplinary collaboration in this complex and multidisciplinary field. The blocked (or modular) structures, as depicted in Figures 2, 4, 6, 7, and 8, are meticulously designed to allow experts working on one block to focus on their specialized area without needing to be well-versed in the intricacies of other blocks. This modularity fosters independence among teams, enabling them to work concurrently with minimal overlap of expertise. Furthermore, when developing joint software, each block team (e.g., such as Teams 3 or 4, as shown in Fig. 6) has the autonomy to make modifications or improvements to their block at any stage of its development, without the need to inform or disrupt the partner team (Teams 4 or 3, respectively). The only necessary coordination arises between Blocks 3 and 4, where effective collaboration requires alignment on specific adjustments between the two blocks.

Broadly speaking, this review focuses on the development of Block 4 Micromechanics and its integration with Block 3 Perturbator (see Fig. 6), along with its alignment with other blocks. The specific methods for solving Block 3 Perturbator are not examined in detail; they are only briefly mentioned in the Introduction and Subsection 3.2 and are assumed to be known. The review does not include comparisons between different peridynamic models, numerical results, or discussions on the significance, applications, and limitations of peridynamic theory—these topics are beyond their scope (refer to the Introduction for relevant references). Additionally, while the blocks from Fig. 2 and 7 are only briefly referenced, their interaction with Blocks 3 and 4 in Fig. 6 is analyzed in greater depth.

One of the key advancements introduced by the new body force loading (2.4) is the creation of datasets with a unified structure— \mathcal{D}^r (4.22), \mathcal{D}^p (5.12), and \mathcal{D}^d (8.5)—using the unified AGIE (3.23). These datasets encompass CMs of various structures and phase properties, ensuring a comprehensive and consistent framework. A critical threshold for filtering out unsuitable sub-datasets \mathcal{D}_k^r , \mathcal{D}_k^p , and \mathcal{D}_k^d is established through a revolutionary RVE concept that extends Hill's classical framework [216]. Unlike conventional RVE definitions, which are constrained by the constitutive laws of material phases or the functional forms of surrogate operators, this new approach is based on intrinsic field concentration factors within the phases of both random and periodic CMs.

This makes it a universal and highly adaptable tool applicable across a broad range of material systems. By integrating this generalized RVE concept into dataset generation, the framework becomes inherently suited for ML and NN techniques in predicting nonlocal surrogate operators. This innovation effectively addresses and mitigates key challenges such as sample size dependency, boundary layer effects, and edge-related inaccuracies. As a result, the approach ensures highly accurate and reliable models for periodic structure CMs, regardless of whether their phases exhibit local or nonlocal, linear or nonlinear elastic properties. The surrogate operators derived from these datasets demonstrate exceptional robustness and reliability, maintaining consistent performance even in complex micromechanical systems. This breakthrough significantly expands the capabilities of ML and NN models, enhancing their accuracy and generalization potential in applications requiring precise micromechanical analysis of intricate material systems.

The resolution of the *Procrustean bed*—typically understood through effective moduli, linear local elasticity, the RVE) [216], and remote homogeneous BC (2.30) or (2.31)—is not the primary objective, but rather an important byproduct of the innovative AGIE-CAM formulation. While the substitution of one type of loading (2.30) or (2.31) (or (2.28) or (2.29)) with another form of loading (2.4) might appear as a mere technicality, it signifies a profound shift in the philosophy of micromechanics research. This replacement, far from being a trivial adjustment, represents a fundamental transformation that moves away from the traditional reliance on the *Procrustean bed*. The introduction of AGIE (3.23) demonstrates, by its very inception, that the attempt to adapt classical methods to fit the rigid confines of the *Procrustean bed* is misguided. The correct approach, instead of refining or generalizing the specific components of *Procrustean bed*, lies in the complete departure from this restrictive framework. This shift is rooted in the recent development of AGIE (3.23) for body forces with compact support (2.4). While preserving the generality of classical GIE-CAM based on GIE (3.24), the specific nature of the loading condition (2.4) allows AGIE (3.23) to be formulated with the same precision as GIE (3.24). This, however, is not merely a restatement; it serves as a pivotal step toward a more comprehensive generalization, enabling GIE (3.24) to handle arbitrary loading scenarios. These include (i) general body forces, which may or may not have compact support (2.4), and (ii) remote boundary conditions (VBC), which are not necessarily homogeneous (2.28). What distinguishes AGIE (3.23) is its remarkable increase in flexibility and the broader spectrum of surrogate operators it accommodates, extending far beyond the capabilities of GIE (3.24). This leap forward leads to the development of a truly universal AGIE-CAM framework for studying composites (CMs) with arbitrary microstructures and phase properties, as outlined in the paper. More significantly, this next-generation AGIE-CAM serves as a unifying framework, harmonizing various analytical approaches, as illustrated in Figures 2, 4, 6, 7, and 8. It ensures that these methodologies can operate both in synergy and independently, thus establishing a more integrated yet modular analytical paradigm. In essence, this development signifies the creation of a *Unified*

Micromechanics Theory for heterogeneous media, marking a groundbreaking advancement in the field.

Acknowledgements:

The author acknowledges Dr. Stewart A. Silling for the fruitful personal discussions, encouragements, helpful comments, and suggestions.

Declarations

Funding: The author received no financial support for the research, authorship, and/or publication of this article.

References

- [1] Agarwal M, Pasupathy P, Wu X, Recchia SS, Pelegri AA. (2024) Multiscale computational and artificial intelligence models of linear and nonlinear composites: a review. *Small Science*, **4**: 2300185
- [2] Aguiar, A.R., Fosdick, R., 2014. A constitutive model for a linearly elastic peridynamic body *Mathematics and Mechanics of Solids*, **19**: 502–523
- [3] Agwai, A., Guven, I., Madenci, E. (2011) Predicting crack propagation with peridynamics: a comparative study *Int. J. Fracture*, **171**: 65–78
- [4] Ahmadi M, Sadighi M, Hosseini-Toudeshky H. (2022) Microstructure-based deformation and fracture modeling of particulate reinforced composites with ordinary state-based peridynamic theory. *Compos Struct*, **279**:114734.
- [5] Aifantis EC (2003) Update on a class of gradient theories. *Mechanics of Materials*, **35**:259–280
- [6] Aifantis EC (2003) Fractional generalizations of gradient mechanics. In: Tarasov, V.E., Ed. De Gruyter (Eds): *Handbook of Fractional Calculus with Applications*, Berlin, Germany, **4**:241–262
- [7] Akinwande D, Brennan CJ, Bunch JS, Egberts P, Felts JR, Gao H, Huang R, Kim J-C, Li T, Li Y, et al. (2017) A review on mechanics and mechanical properties of 2d materials—graphene and beyond. *Extreme Mechanics Letters*, **13**, 42–77
- [8] Aksoylu B, Parks ML (2011) Variational theory and domain decomposition for nonlocal problems. *Applied Mathematics and Computation*, **217**: 6498–6515
- [9] Alali, B., Albin, N. (2020) Fourier spectral methods for nonlocal models. *J. Peridynamics Nonlocal Modeling*, **2**, 317–335.
- [10] Alali B, Gunzburger M (2015) Peridynamics and material interfaces *J. Elast.*, **120**: 225–248
- [11] Alali B, Lipton R, (2012) Multiscale dynamics of heterogeneous media in the peridynamic formulation. *J. Elast.*, **106**: 71–103
- [12] Altan B, Aifantis E (1997) On some aspects in the special theory of gradient elasticity”. *J. Mech.l Behavior of Materials*, **8**:231–282
- [13] Ameen MM, Peerlings RHJ, Geers MGD. (2018) quantitative assessment of the scale separation limits of classical and higher-order asymptotic homogenization *European J. Mech. A. Solids*, **71**: 89–100
- [14] Anbarlooie B, Hosseini-Toudeshky H. (2024) Damage mechanisms analyses in DP steels using SEM images, FEM, and nonlocal peridynamics methods *Mech. Adv. Materials and Structures*, <https://doi.org/10.1080/15376494.2024.2367010>
- [15] Arthur, D., Vassilvitskii, S. *k*-means++: the advantages of careful seeding. *Proc. of the 18th Annual ACM-SIAM Symposium on Discrete Algorithms*, 2007; 1027–1035.
- [16] Askari, E., Xu, J., Silling S.A., 2006. Peridynamic analysis of damage and failure in composites. *44th AIAA Aerospace Sciences Meeting and Exhibition*, **AIAA 2006–88**, Reno, NV, 1–12.

- [17] Askari E, Bobaru F, Lehoucq RB, Parks ML, Silling SA, Weckner O (2009) Peridynamics for multiscale materials modeling. *Journal of Physics: Conference Series*, 125:012078
- [18] Askari, A., Azdoud, Y., Han, F., Lubineau, G., Silling, S. 2015. Peridynamics for analysis of failure in advanced composite materials *Numerical Modelling of Failure in Advanced Composite Materials*, Woodhead Publishing Series in Composites Science and Engineering, 331–350
- [19] Askes H, Aifantis EC (2011) Gradient elasticity in statics and dynamics: An overview of formulations, length scale identification procedures, finite element implementations, and new results. *Int. J. Solids Structures* **48**:1962–1990
- [20] Askes H, Aifantis EC (2011) Gradient elasticity in statics and dynamics: An overview of formulations, length scale identification procedures, finite element implementations and new results. *Int. J. Solids Structures* **48**: 1962–1990
- [21] Azdoud Y, Han F, Lubineau G. (2013) A Morphing framework to couple non-local and local anisotropic continua *Int. J. Solids Struct.*, **50**, 1332–1341
- [22] Babuska I (1976) Homogenization and its application. Mathematical and computational problems. In: Lions, J.-L., Glowinski, R. (Eds.) *Numerical Solution of Partial Differential Equations*. III. Academic Press, New York, pp. 89–116
- [23] Bakhvalov NS, Panasenko GP (1984) *Homogenisation: Averaging Processes in Periodic Media*. Nauka, Moscow (in Russian; English translation: Kluwer, 1989)
- [24] Ballas J, Sladek J, Sladek V (1989) *Stress Analysis by Boundary Element Methods*. Elsevier, Amsterdam
- [25] Barenblatt GI (1962) The mathematical theory of equilibrium of cracks in brittle fracture. *Advances in Applied Mechanics*. **7**:55—129.
- [26] Bargmann S, Klusemann B, Markmann J, Schnabel JE, Schneider K, Soyarslan C, Wilmers J (2018) Generation of 3D representative volume elements for heterogeneous materials: A review. *Progress in Materials Science*, **96**:322–384
- [27] Barnett DM, Lothe J (1975) Dislocation and line charges in anisotropic piezoelectric insulators. *Phys Stat Solids (b)*, **67**:105–111
- [28] Barrett R, Berry M, Chan TF, Demmel J, Donato J, Dongarra J, Eijkhout V., Pozo R, Romine C, der Vorst HV. (1994) *Templates for the Solution of Linear Systems: Building Blocks for Iterative Methods*, 2nd Edition, SIAM.
- [29] Basoglu MF, Kefal A, Zerín Z, Oterkus E. (2022). Peridynamic modeling of toughening enhancement in unidirectional fiber-reinforced composites with micro-cracks. *Composite Structures*, **297**: 115950
- [30] Bazánt ZP, Jirásek M (2002) Nonlocal integral formulations of plasticity and damage Survey of progress. *J. Engineering Mechanics*, **128**:1119–1149.
- [31] Bazánt ZP, Luo W, Chau VT, Bessa MA (2016) Wave dispersion and basic concepts of peridynamics compared to classical nonlocal damage models. *J. Appl. Mech.*, **83**:111004
- [32] Bažant, Z, Nguyen N.H., Dönmez, A.A. (2022) Critical Comparison of Phase-Field, Peridynamics, and Crack Band Model M7 in Light of Gap Test and Classical Fracture Tests *J. Appl. Mech.*, **89**: 061008 (26 pages)
- [33] Beckmann R, Mella R, Wenman MR (2013) Mesh and timestep sensitivity of fracture from thermal strains using peridynamics implemented in Abaqus. *Comput. Methods Appl. Mech. Engrg.*, 263: 71–80
- [34] Benaïmeche MA, Yvonnet J, Bary B, He Q-C (2022) A k-means clustering machine learning-based multiscale method for inelastic heterogeneous structures with internal variables. *Int J Numer Methods Eng*. 123: 2012–2041
- [35] Benner P, Grivet-Talocia S., Quarteroni A, Rozza G, Schilders W, Silveira LM. (Eds) (2020) *Model Order Reduction. V.2: Snapshot-Based Methods and Algorithms*. Walter de Gruyter GmbH, Milano

- [36] Benveniste Y (1987) A new approach to application of Mori-Tanaka's theory in composite materials. *Mech. Mater.* 6: 147–157
- [37] . Bessa MA, Foster JT, Belytschko T, Liu WK. (2014) A meshfree unification: reproducing kernel peridynamics. *Comput. Mech.*, **53**, 1251–1264.
- [38] Bialecki RA, Kassab AJ, Fic A. (2005) Proper orthogonal decomposition and modal analysis for acceleration of transient FEM thermal analysis *Int. J. Numer. Meth. Engng*, **62**:774–797
- [39] Bie Y, Ren H, Rabczuk T, Bui TQ, Wei Y. (2024) The fully coupled thermo-mechanical dual-horizon peridynamic correspondence damage model for homogeneous and heterogeneous materials *Comput. Meth. Appl. Mech. Engng*, **420**: 116730
- [40] Birner M, Diehl P, Lipton R, Schweitzer MA. (2023) A fracture multiscale model for peridynamic enrichment within the partition of unity method. *Adv. Engineering Software*, **176** 103360.
- [41] Bobaru, F., Foster, J., Geubelle, P., Silling, S., (Editors) 2016. *Handbook of Peridynamic Modeling*, CRC Press, Boca Raton, FL.
- [42] Bobaru, F., Ha, Y.D., 2011. Adaptive refinement and multiscale modeling in 2D peridynamics. *Int. J. Multiscale Comput. Eng.*, **9**, 635–659
- [43] Bobaru, F., Yang, M., Alves, L.F., Silling, S.A., Askari, A., Xu, J., 2009. Convergence, adaptive refinement, and scaling in 1d peridynamics. *Int. J. Numerical Methods Engng*, **77**, 852–877
- [44] Bode T, Weißenfels C, Wriggers P. (2022) Peridynamic Galerkin method: an attractive alternative to finite elements. *Computational Mechanics*. **70**: 723–743.
- [45] Bornert M, Stolz C, Zaoui A (1996) Morphologically representative pattern-based bounding in elasticity. *J Mech Phys Solids*, **44**: 307–331
- [46] Boyaval, S. Reduced-basis approach for homogenization beyond the periodic setting, *Multiscale Modeling & Simulation* 2008; **7**: 466-494.
- [47] Breitenfeld MS, Geubelle PH, Weckner O, Silling SA. (2014) Non-ordinary state-based peridynamic analysis of stationary crack problems *Comput. Meth. Appl. Mech. Engng*, **272**, 233–250
- [48] Brisard S (2017) *Mémoire d'Habilitation à Diriger des Recherches From microstructure to macroscopic properties Some applications of the Hashin-Shtrikman principle*. Mechanics of materials [physics.class-ph]. Université Paris-Est, Paris
- [49] Brisard S, Sab K, Dormieux L (2013) New boundary conditions for the computation of the apparent stiffness of statistical volume elements. *J. Mech. Physics Solids*, **61**:2638–2658
- [50] Brunton SL, Kutz JN (2022) *Data-driven science and engineering: Machine learning, dynamical systems, and control*. Cambridge University Press, Cambridge, UK
- [51] Buryachenko VA (1998) Some nonlocal effects in graded random structure matrix composites. *Mech Res Commun*, **25**:117–122
- [52] Buryachenko VA (1999b) Effective thermoelastic properties of graded doubly periodic particulate composites in varying external stress fields. *Int J Solids Struct*, **36**:3861–3885
- [53] Buryachenko VA (2007) *Micromechanics of Heterogeneous Materials*. Springer, NY.
- [54] Buryachenko VA (2010) On the thermo-elastostatics of heterogeneous materials. I. General integral equation. *Acta Mechanica*, 213: 359-374
- [55] Buryachenko VA (2010) On the thermo-elastostatics of heterogeneous materials. II. Analyze and generalization of some basic hypotheses and propositions. *Acta Mech.*, 213: 375-398.

- [56] Buryachenko VA (2011a) Inhomogeneity of the first and second statistical moments of stresses inside the heterogeneities of random structure matrix composites. *Int. J. Solids and Structures*, **48**:1665–1687.
- [57] Buryachenko VA (2011b) On thermoelastostatics of composites with nonlocal properties of constituents. I. General representations for effective material and field parameters. *Int. J. Solids and Structures*, **48**:1818–1828.
- [58] Buryachenko VA (2011c) On thermoelastostatics of composites with nonlocal properties of constituents. II. Estimation of effective material and field parameters. *Int. J. Solids and Structures*, **48**:1829–1845.
- [59] Buryachenko VA (2013) General integral equations of micromechanics of composite materials with imperfectly bonded interfaces. *Int. J. Solids and Structures*, **50**:3190–3206.
- [60] Buryachenko V A (2014) Some general representations in thermoperidynamics of random structure composites. *Int. J. Multiscale Comput. Enging*, **12**: 331–350.
- [61] Buryachenko V (2014) Solution of general integral equations of micromechanics of heterogeneous materials. *Int. J. Solids and Structures*, **51**: 3823–3843
- [62] Buryachenko V (2014) Effective elastic modulus of heterogeneous peristatic bar of random structure. *J. Solids and Structures*, **51**: 2940-2948
- [63] Buryachenko V (2015) General integral equations of micromechanics of heterogeneous materials. *J. Multiscale Comput. Enging.*, **13**: 11–53
- [64] Buryachenko VA (2015) Effective thermoelastic properties of heterogeneous thermoperi- static bar of random structure. *Int. J. Multiscale Comput. Enging.*, **13**: 55-71
- [65] Buryachenko VA (2015c) General integral equations of Stokes flow through the random structure porous media. *Int. J. Multiscale Comput. Enging.*, **13**:375–392
- [66] Buryachenko VA (2016) Estimation of effective elastic moduli of random structure composites by the method of fundamental solutions. *Engng Anal. Boundary Elements*. **62**:13–21
- [67] Buryachenko VA (2017) Effective properties of thermoperidynamic random structure composites: some background principles. *Math. Mech. of Solids.*, **22**: 366–1386
- [68] Buryachenko V.A (2017b) Statistical average of residual stresses in elastically homogeneous medium with random field of noncanonical inclusions. *Computers and Structures*, **187**:24–34
- [69] Buryachenko V (2017c) Method of fundamental solutions in micromechanics of elastic random structure composites. *Int. J. Solids and Structures*, **124**:135-150
- [70] Buryachenko VA (2018) Computational homogenization in linear elasticity of peridynamic periodic structure composites. *Math. Mech. of Solids*, **23**: 2497–2525
- [71] Buryachenko VA (2018a) General interface integral equations in elasticity of random structure composites. Eds. S. A. Meguid, G. J. Weng. *Micromechanics and Nanomechanics of Composite Solids*, Springer, NY, 469-506
- [72] Buryachenko V (2018) Effective elastic modulus of heterogeneous peristatic bar of periodic structure. *Computers & Structures*, **202**:129-139
- [73] Buryachenko V (2018) Effective elastic modulus of damaged peristatic bar of periodic structure. *J. Multiscale Comput. Enging*, **16**:101–118
- [74] Buryachenko VA (2019) Interface integral technique for the thermoelasticity of random structure matrix composites. *Math. Mech. of Solids*, **24**: 2785–2813
- [75] Buryachenko VA (2019) Modeling of one inclusion in the infinite peridynamic matrix subjected to homogeneous remote loading *J. Peridynamics and Nonlocal Modeling*, **1**: 75–87

- [76] Buryachenko V (2020a) Generalized effective field method in peridynamic micromechanics of random structure composites. *Int. J. Solid Structure*, 202: 765-786
- [77] Buryachenko V (2020b) Generalized Mori-Tanaka approach in micromechanics of peristatic random structure composites. *J. Peridynamics and Nonlocal Modeling*, 2: 26-49
- [78] Buryachenko V. (2020c) Variational principals and generalized Hill's bounds in micromechanics of peristatic random structure composites. *Math. Mech. of Solids*, **25**: 682-704
- [79] Buryachenko VA (2022) *Local and Nonlocal Micromechanics of Heterogeneous Materials*. Springer, NY.
- [80] Buryachenko V. A. (2022) Multiscale and multiphysics modeling of advanced heterogeneous materials. *International Association of Advanced Materials Award Lecture*, see 20min Fellow of IAAM video presentation <https://lnkd.in/gYp3SJmy>; Vid. Proc. Adv. Mater., Volume 3, DOI: 10.5185/vpoam.2022.08325)
- [81] Buryachenko, V. (2022) Critical analysis of generalized Maxwell homogenization schemes and related prospective problems. *Mechanics of Materials*, **165**, 104181
- [82] Buryachenko VA (2023a) Effective nonlocal behavior of peridynamic random structure composites subjected to body forces with compact support and related prospective problems. *Math. Mech. of Solids*, **28**: 1401-1436
- [83] Buryachenko V (2023b) Effective displacements of peridynamic heterogeneous bar loaded by body force with compact support. *J. Multiscale Comput. Enging*, **21**: 27-42
- [84] Buryachenko V. A. (2023c). Linearized ordinary state-based peridynamic micromechanics of composites. *J. Materials and Structures*, **18**, 445-477
- [85] Buryachenko V. A. (2023d). Second moment of displacement state and effective energy-based criteria in peridynamic micromechanics of random structure composites *J. Peridynamics and Nonlocal Modeling* **5**, Published: 23 September 2023
- [86] Buryachenko V. A. (2024e) Generalized Mori-Tanaka approach in peridynamic micromechanics of multilayered composites of random structure. *J. Peridynamics and Nonlocal Modeling* **6**, Published: 12 February 2024
- [87] Buryachenko V. A. (2023f) Transformation field analysis as a background of clustering discretization methods in micromechanics of composites. *Math. Mech. of Solids*, **28** 2677-2703
- [88] Buryachenko V. (2023g) Effective nonlocal behavior of peridynamic random structure composites subjected to body forces with compact support. *Math. Mech. of Solids*, **28**: 1401-1436
- [89] Buryachenko VA (2024) Estimations of energy-based criteria in nonlinear phenomena in peridynamic micromechanics of random structure composites. *J. Peridynamics and Nonlocal Modeling*, **6**: 250-269
- [90] Buryachenko V. A. (2024) Transformation field analysis and clustering discretization method in pyridynamic micromechanics of composites. *J. Peridynamics and Nonlocal Modeling* **6**: Published: 22 February 2024
- [91] Buryachenko V. A. (2024) Fast Fourier transform method for peridynamic bar of periodic structure. *J. Multiscale Comput. Enging*, **22**: 1-17
- [92] Buryachenko V. A. (2024) Fast Fourier transform in peridynamic micromechanics of composites *Math. Mech. of Solids*, **29**, <https://doi.org/10.1177/10812865241236878>
- [93] Buryachenko V., (2024) Nonlinear general integral equations in micromechanics of random structure composites. *Math. Mech. of Solids*, **29**
- [94] Buryachenko V. A. (2024) Peridynamic micromechanics of composites: a review. *J. Peridynamics and Nonlocal Modeling* **6**, 531-601

- [95] Buryachenko V. A. (2024) Peridynamic micromechanics of composites: a critical review. <https://arxiv.org/abs/2402.13908v4> (109pp., 466 refs., extended version of JPER, 2024, 6, 531–601)
- [96] Buryachenko V. A. (2024) Critical analyses of RVE concepts in local and peridynamic micromechanics of composites. <https://arxiv.org/abs/2402.13908v5> (71pp., 336 refs., submitted to JPER)
- [97] Buryachenko V. A. (2025) Thermoperidynamic periodic structure composites subjected to body force with compact support. (submitted)
- [98] Buryachenko VA, Brun M (2011) FEA in elasticity of random structure composites reinforced by heterogeneities of noncanonical shape. *Int. J. Solid Struct.* **48**:719–728.
- [99] Buryachenko VA, Brun M (2012a) Random residual stresses in elasticity homogeneous medium with inclusions of noncanonical shape. *Int. J. Multiscale Comput. Enging.* **10**:261–279.
- [100] Buryachenko VA, Brun M (2012b) Thermoelastic effective properties and stress concentrator factors of composites reinforced by heterogeneities of noncanonical shape. *Mechanics of Materials*, **53**:91–110.
- [101] Buryachenko VA, Brun M (2013) Iteration method in linear elasticity of random structure composites containing heterogeneities of noncanonical shape. *Int. J. Solids and Structures*, **50**:1130–1140.
- [102] Buryachenko VA, Rammerstorfer FG (1998a) Micromechanics and nonlocal effects in graded random structure matrix composites. In: Bahei-El-Din YA, Dvorak GJ (eds) *IUTAM Symp. on Transformation Problems in Composite and Active Materials*. Kluwer, Dordrecht, 197–206
- [103] Capriz G (1989) *Continua with Microstructure*. Springer, Berlin Heidelberg New York.
- [104] Chen C, Wu L, Fu J, Xin C, Liu W., Duan H. (2024) A micromechanical scheme with nonlinear concentration functions by physics-guided neural network. *J. Mech. Phys. Solids*, **188**: 105681
- [105] Chen HS, Acrivos A (1978b) The effective elastic moduli of composite materials containing spherical inclusions at non-dilute concentrations. *Int J Solids Struct*, **14**:349–364
- [106] Chen KH, Chen JT, Kao JH (2008) Regularized meshless method for antiplane shear problems with multiple inclusions. *Int. J. Numer. Meth. Engng*, **73**:1251–1273.
- [107] Chen Q, Xiao C, Yang Z, Tabet J, Chen X. (2024) Deep neural network homogenization of multiphysics behavior for periodic piezoelectric composites *Composites: Part A*, **186**: 108421
- [108] Chen T, Dvorak GJ, Yu CC (2007) Size-dependent elastic properties of unidirectional nano-composites with interface stresses. *Acta Mechan*, **188**:39–54
- [109] Chen T, Dvorak GJ, Yu CC (2007) Solids containing spherical nano-inclusions with interface stresses effective properties and thermal-mechanical connections. *Int. J. Solids and Structures*, **44**:941–955.
- [110] Chen, X., Gunzburger, M. (2011) Continuous and discontinuous finite element methods for a peridynamics model of mechanics. *Computer Methods in Applied Mechanics and Engineering*, **200**, 1237–1250.
- [111] Chen Z, Jafarzadeh S, Zhao J, Bobaru F. (2021) A coupled mechano-chemical peridynamic model for pit-to-crack transition in stress-corrosion cracking, *J. Mechanics Physics Solids* **146**: 104203.
- [112] Cheng Z-Q, Liu H, Tan W. (2024) Advanced computational modeling of composite materials. *Engng Fract. Mechanics*, **305**: 110120
- [113] Chiu, S.N., Stoyan, D., Kendall, W.S., Mecke, J. (2013) *Stochastic Geometry and its Applications*. Third Edition. J. Wiley & Sons, Chichester, NY.

- [114] Coclite GM, Dipierro S, Maddalena F, Valdinoci E (2022a) Wellposedness of a nonlinear peridynamic model. *Nonlinearity*, **32**(1), *arXiv:1804.00273v1*
- [115] Coclite GM, Dipierro S, Fanizza G, Maddalena F, Valdinoci E (2022b) Dispersive effects in a scalar nonlocal wave equation inspired by peridynamics *Nonlinearity*, **35**(11), *arXiv:2105.01558v2*
- [116] Cosserat E, Cosserat F (1909) *Théorie des corps déformables*. A. Hermann et Fils, Paris.
- [117] Cuomo S, Schiano V, Cola D, Giampaolo F, Rozza G, Raissi M, Piccialli F. (2022) Machine learning through physics-informed neural networks: where we are and what's next. *J. Scientific Computing*, **92**:88 (62pp)
- [118] Dahal B, Seleson P, Trageser J. (2023) The Evolution of the Peridynamics Co-Authorship Network *J. Peridynamics Nonlocal Modeling*, **5**: 311–355
- [119] Decklever J, Spanos P. Nanocomposite material properties estimation and fracture analysis via peridynamics and Monte Carlo simulation. (2016) *Probab Eng Mech*, tenbf 44(SI):77–88
- [120] D'Elia M, Du Q, Glusa C, Gunzburger M, Tian X, Zhou Z (2020) Numerical methods for nonlocal and fractional models. *Acta Numerica*, **29**, 1 - 124
- [121] D'Elia M, Du Q, Gunzburger M. (2017) Recent progress in mathematical and computational aspects of peridynamics *Handbook of Nonlocal Continuum Mechanics for Materials and Structures*. Springer International Publishing.
- [122] D'Elia, M., Xingjie Li, X., Seleson, P., Tian, X., Yu, Y. (2022) A review of Local-to-Nonlocal coupling methods in nonlocal diffusion and nonlocal mechanics. *Journal of Peridynamics and Nonlocal Modeling*, **4**, 1–50
- [123] Desai S. (2024) A novel equation of motion to predict elastoplastic deformation of 1 D stochastic bars *J. Peridyn. Nonlocal Modeling*, **6**: 468–504
- [124] Diana V. (2023) Anisotropic continuum molecular models: a unified framework based on pair potentials for elasticity, fracture and diffusion type problems. *Archives Comput. Methods in Engng*, **30**:1305–1344
- [125] Diana V, Bacigalupo A, Lepidi M, Gambarotta L. (2022). Anisotropic peridynamics for homogenized microstructured materials. *Comput. Meth. Applied Mech. Engng*, **392**: 114704.
- [126] Diehl P, Prudhomme S, Levesque M. (2019) A review of benchmark experiments for the validation of peridynamics models. *J. Perid. Nonlocal Modeling*, **1**: 14–35.
- [127] Difonzo FV, Lopez L, Pellegrino SF. (2024) Physics informed neural networks for an inverse problem in peridynamic models. *Engineering with Computers* <https://doi.org/10.1007/s00366-024-01957-5>
- [128] Dimola N, Coclite A, Fanizza G, Politi T (2022) Bond-based peridynamics, a survey prospecting nonlocal theories of fluid-dynamics. *Advances in Continuous and Discrete Models*, 2022:60 (27pp.)
- [129] Ding W, Semperlotti F. (2024) Two-dimensional nonlocal Eshelby's inclusion theory: eigenstress-driven formulation and applications. *Proc. R. Soc.*, **A 480**: 20230842
- [130] Dinzart F, Sabar H (2017) New micromechanical modeling of the elastic behavior of composite materials with ellipsoidal reinforcements and imperfect interfaces. *Int.l J. of Solids and Structures*, **108**:254-262
- [131] Dinzart F, Sabar H. (2019) Electroelastic ellipsoidal inclusion with imperfect interface and its application to piezoelectric composite materials *Int. J. Solids Structures*, **136–137**, 241–249
- [132] Dipasquale D, Sarego G, Prapamonthon P, Yooyen S, Shojaei A. (2022) A stress tensor-based failure criterion for ordinary state-based peridynamic models. *J. Appl. Computat. Mechanics*, **8**, 617–628
- [133] Diyaroglu C, Oterkus E, Madenci E, Rabczuk T, Silliq A (2016) Peridynamic modeling of composite laminates under explosive loading. *Composite Structures*, 144: 14-23

- [134] Diyaroglu C, Madenci E, Phan N (2019a) Peridynamic homogenization of microstructures with orthotropic constituents in a finite element framework. *Composite Structures*, 227:111334
- [135] Diyaroglu C, Madenci E, Stewart RJ, Zobi SS (2019b) Combined peridynamic and finite element analyses for failure prediction in periodic and partially periodic perforated structures *Composite Structures*, 227:111481
- [136] Dorduncu M, Ren H, Zhuang X, Silling S, Madenci E, Rabczuk T. (2024) A review of peridynamic theory and nonlocal operators along with their computer implementations. *Computers and Structures*, **299**: 107395
- [137] Dorgan RJ, Voyiadjis GZ (2006) A mixed finite element implementation of a gradient-enhanced coupled damage-plasticity model. *Int. J. Damage Mechanics*, **15**:201-235
- [138] Drugan WJ (2000) Micromechanics-based variational estimations for a higher-order nonlocal constitutive equation and optimal choice of effective moduli for elastic composites. *J Mech Phys Solids*, **48**:1359-1387
- [139] Drugan WJ (2003) Two exact micromechanics-based nonlocal constitutive equations for random linear elastic composite materials. *J Mech Phys Solids*, **51**:1745-1772
- [140] Drugan WJ, Willis JR (1996) A micromechanics-based nonlocal constitutive equation and estimates of representative volume elements for elastic composites. *J Mech Phys Solids*, **44**:497-524
- [141] (1992) Dvorak G. Transformation field analysis of inelastic composite materials. *Proc R Soc Lond A*. **437**, 311-327.
- [142] Dvorak, G.J. *Micromechanics of Composite Materials*. Dordrecht: Springer, 2013.
- [143] Dvorak GJ, Benveniste Y (1992a) On the thermomechanics of composites with imperfectly bonded interfaces and damage. *Int J Solids Struct*, **29**:2907-2919
- [144] Du Q, Engquist B, Tian X. (2020) Multiscale modeling, homogenization and nonlocal effects: Mathematical and computational issues. *Contemporary mathematics*, **754**, 115-140.
- [145] Du Q, Gunzburger M, Lehoucq RB, Zhou, K (2013) Analysis of the volume-constrained peridynamic Navier equation of linear elasticity. *J. Elast.*, 113: 193-217.
- [146] Du Q, Lipton R, Mengesha T. (2016) Multiscale analysis of linear evolution equations with applications to nonlocal models for heterogeneous media. *ESAIM: Mathematical Modelling and Numerical Analysis*, **50**, 1425-1455.
- [147] Duan H, Wang J, Huang Z. (2022) Micromechanics of composites with interface effects *Acta Mech. Sin.*, **38**: 222025
- [148] Dunn ML, Taya M (1993) Micromechanics predictions of the effective electroelastic moduli of piezoelectric composites. *Int J Solids Struct*, **30**:161-175
- [149] Dunn ML, Taya M (1993) An analysis of piezoelectric composite materials containing ellipsoidal inhomogeneities. *Proc R Soc Lond: A***443**: 265-287
- [150] Duan HL, Wang J, Huang ZP, Karahaloo BL (2005) Eshelby formalism for nano-inhomogeneities. *Proc Roy Soc Lond Ser*, **A461**:3335-3353
- [151] Dumont , Serpilli M, Rizzoni R, Lebon FC (2020) Numerical validation of multiphysics imperfect interfaces models. *Frontiers in Materials*, **2020**, **7**:158 (14 pages)
- [152] Echlin MP, Lenthe WC, Pollock TM (2014) Three-dimensional sampling of material structure for property modeling and design. *Integ.Mater. Manuf. Innov.*, **3**:1-14
- [153] Edelen DGB, Laws N (1971) On the thermodynamics of systems with nonlocality. *Arch. Ration. Mech. Anal.*, **43**:36-44

- [154] Emmrich, E., Weckner, O., 2006. The peridynamic equation of motion in non-local elasticity theory. In: C. A. Mota Soares *et al.* (eds.), *III European Conference on Computational Mechanics. Solids, Structures, and Coupled Problems in Engineering*. Springer, Dordrecht
- [155] Emmrich, E., Weckner, O., 2007a. Analysis and numerical approximation of an integro-differential equation modeling non-local effects in linear elasticity. *Math. Mech. Solids*, **12**, 363–384.
- [156] Emmrich, E., Weckner, O., 2007b. On the well-posedness of the linear peridynamic model and its convergence towards the Navier equation of linear elasticity. *Commun. Math. Sci.* **5**, 851–864.
- [157] Eghbalpoor R, Sheidaei A. (2024) A peridynamic-informed deep learning model for brittle damage prediction *Theoret. Appl. Fracture Mech.*, **131**: 104457
- [158] Eriksson, K. and Stenström, C. Homogenization of the 1D peri-static/dynamic bar with triangular micromodulus. *Journal of Peridynamics and Nonlocal Modeling*, 2021; **3**: 85–112.
- [159] Eringen AC (1964) Simple microfluids. *Int. J. Eng. Sci.*, **2**:205–217
- [160] Eringen AC (1966) A unified theory of thermomechanical materials. *Int. J. Eng. Sci.*, **4**:179–202
- [161] Eringen AC (1968) Mechanics of micromorphic continua. In: Kröner E (ed), *Mechan of Generalized Continua*. Springer-Verlag, Berlin, 18–35
- [162] Eringen AC (1999) *Microcontinuum Field Theories I. Foundations and Solids*. Springer-Verlag, Berlin
- [163] Eringen AC (2002) *Nonlocal Continuum Field Theories*. Springer-Verlag, New York
- [164] Eshelby, J.D., 1957. The determination of the elastic field of an ellipsoidal inclusion, and related problems. *Proc. Roy. Soc. Lond.*, **A 241**, 376–396.
- [165] Eskin GI (1981) *Boundary Value Problems for Elliptic Pseudodifferential Equations*. American Mathematical Society, Providence, RI
- [166] Fan Y, D’Elia M, Yu Y, Najm HN, Silling S. (2023) Bayesian nonlocal operator regression: A data-driven learning framework of nonlocal models with uncertainty quantification. *J. Engig Mech.*, **149**, 04023049.
- [167] Fan Y, Tian X, Yang X, Li C, Webster C, Yu Y. (2022) An asymptotically compatible probabilistic collocation method for randomly heterogeneous nonlocal problems. *J. Comput. Physics*, **465**: 111376
- [168] Fan Y, You H, Tian X, Yang X, Li C, Prakash N. (2022) A meshfree peridynamic model for brittle fracture in randomly heterogeneous materials *Comput. Meth. Appl. Mech. and Engng*, **399**: 115340
- [169] Fan Y, You H, Yu Y. (2024) OBMeshfree: An optimization-based meshfree solver for nonlocal diffusion and peridynamics models *J. Peridyn. Nonlocal Modeling*, **6**: 4–32
- [170] Faroughi SA, Pawar NM, Fernandes C, Raissi M, Das S, Kalantari NK, Kourosh Mahjour S. (2024) Physics-guided, physics-informed, and physics-encoded neural networks and operators in scientific computing: Fluid and solid mechanics *J. Computing and Information Science*, **24**: 040802
- [171] Fasshauer GE (2016) Meshfree methods, *Handbook of Theoretical and Computational Nanotechnology*, M. Rieth and W. Schommers (eds.), American Scientific Publishers, **2** 33–97
- [172] Fassi-Fehri O, Hihi A, Berveiller M (1989) Multiple site self-consistent scheme. *Int J Engng Sci*, **27**:495–502
- [173] Ferreira BP, Pires FM, Bessa MA (2021) Adaptive clustering-based reduced-order modeling framework: fast and accurate modeling of localized history-dependent phenomena *arXiv preprint arXiv*, 2109.11897
- [174] Fish J (2014) *Practical Multiscaling*. Chichester: John Wiley & Sons.

- [175] Forest S, Sab K (2012) Stress gradient continuum theory. *Mechanics Research Communications*, **40**:16–25
- [176] Foster JT, Silling SA, Chen W. (2011) An energy-based failure criterion for use with peridynamic states. *Int. J. Multiscale Comput. Enging*, 9: 675–687
- [177] Francqueville F, Gilormini P, Diani J (2019) Representative volume elements for the simulation of isotropic composites highly filled with monosized spheres - *Int. J. Solids and Structures*, **158**:277–286
- [178] Frank X, Lampoh K, Deleune J-Y. (2023) From stress concentrations between inclusions to probability of breakage: A two-dimensional peridynamic study of particle-embedded materials *Physics Review*, **E108**: 034903
- [179] Firooz S, Chatzigeorgiou G, Meraghni F, Javili A (2020) Bounds on size effects in composites via homogenization accounting for general interfaces *Continuum Mech. Thermodynamics*, **32**:173–206
- [180] Firooz S, Javili A (2019) Understanding the role of general interfaces in the overall behavior of composites and size effects. *Comput. Materials Science*, **162**:245–254
- [181] Galadima Y, Oterkus E, Oterkus S (2019) Two-dimensional Implementation of the coarsening method for linear peridynamics. *AIMS Mater Sci* 6: 252–275
- [182] Galadima YK, Xia W, Oterkus E, Oterkus S (2023) A computational homogenization framework for non-ordinary state-based peridynamics *Engineering with Computers* **39**: 461–487
- [183] Galadima YK, Xia W, Oterkus E, Oterkus S (2023) Peridynamic computational homogenization theory for materials with evolving microstructure and damage. *Engineering with Computers* **39:39**: 2945–2957
- [184] Galadima Y K, Oterkus S, Oterkus E, Amin I, El-Aassar AH, Shawky H. (2023) A nonlocal method to compute effective properties of viscoelastic composite materials based on peridynamic computational homogenization theory *Composite Structures*, **319**, 117147.
- [185] Galadima YK, Oterkus S, Oterkus E, Amin I, El-Aassar A-H, Shawky H. (2024) Effect of phase contrast and inclusion shape on the effective response of viscoelastic composites using peridynamic computational homogenization theory. *Mwch. Advanced Mater. Structures*. tenbd 31, 155–163
- [186] Gao XL, Ma HM (2010) Strain gradient solution for Eshelby’s ellipsoidal inclusion problem. *Proc. R. Soc.* **A466**:2425–2446
- [187] Galli M, Cugnoni J, Botsis J (2012) Numerical and statistical estimates of the representative volume element of elastoplastic random composites. *Eur. J. Mech. A/Solids*, **33**:31–38
- [188] Geers, MGD, Kouznetsova, VG, Brekelmans, WAM. (2010) Multi-scale computational homogenization: Trends and challenges. *J. Comput. Applied Mathematics*; **234**: 2175-2182.
- [189] Ghajari M, Iannucci L, Curtis P (2014) A peridynamic material model for the analysis of dynamic crack propagation in orthotropic media. *Comput Meth Appl Mech Engrg*, 276: 431–452
- [190] Ghosh, S. *Micromechanical Analysis and Multi-Scale Modeling Using the Voronoi Cell Finite Element Method (Computational Mechanics and Applied Analysis)*. Boca Raton: CRC Press, 2011.
- [191] Gibson L, Ashby M (1998) *Cellular Solids*. Cambridge University Press, Cambridge, UK
- [192] Gilormini P, Brechet Y (1999) Syntheses: mechanical properties of heterogeneous media: Which material for which model? Which model for which material? *Modelling Simul Mater Sci Engng*, **7**:805–816
- [193] Goodfellow I, Bengio Y, Courville A (2016) *Deep learning*. MIT Press, Cambridge, MA

- [194] Goswami S, Bora A, Yu Y, Karniadakis GE. (2022) Physics-Informed Neural Operators, arXiv preprint arXiv:2207.05748.
- [195] Graham-Brady LL, Siragy EF, Baxter SC (2003) Analysis of heterogeneous composites based on moving-window techniques. *J Engng Mech*, **129**:1054–1064
- [196] Green AE, Rivlin R S (1964a) Simple force and stress multipoles. *Arch. Ration. Mech. Anal.*, **16**:325–353
- [197] Green AE, Rivlin R S (1964b) Multipolar continuum mechanics. *Arch. Ration. Mech. Anal.*, **17**:113–147
- [198] Gu GX, Chen CT, Buehler MJ. (2018) De novo composite design based on machine learning algorithm. *Extreme Mechanics Letters*, **18**: 19–28
- [199] Gu ST, He QC, Pensée V (2015) Homogenization of fibrous piezoelectric composites with general imperfect interfaces under anti-plane mechanical and in-plane electrical loadings. *Mechanics Materials*, **88**:12–29
- [200] Gutkin MY (2006) Elastic behavior of defects in nanomaterials I. Models for infinite and semi-infinite media. *Rev. Adv. Mater. Sci.* **13**:125–161.
- [201] Gurtin ME, Murdoch AI (1975) A continuum theory of elastic material surfaces. *Archive for Rational Mechanics and Analysis*, **59**:291—323.
- [202] Gurtin ME, Weissmuller J, Larche F (1998) The general theory of curved deformable interfaces in solids at equilibrium. *Philos. Mag.* **A 78**:1093—1109
- [203] Ha, Y.D., Bobaru, F. (2010) Studies of dynamic crack propagation and crack branching with peridynamics, *Int. J. Fract.* **162**, 229–244
- [204] Haghghat E, Bekar AC, Madenci E, Juanes R. (2021) A nonlocal physics-informed deep learning framework using the peridynamic differential operator. *Comput. Methods Appl. Mech. Engrg.* **385**: 114012
- [205] Haghghata E, Raissi M, Moure A, Gomez H, Juanes R. (2021) A physics-informed deep learning framework for inversion and surrogate modeling in solid mechanics *Comput. Methods Appl. Mech. Engrg.*, **379**: 113741
- [206] Han, F., Lubineau, G. and Azdoud, Y., (2016) Adaptive coupling between damage mechanics and peridynamics: a route for objective simulation of material degradation up to complete failure. *J. Mechanics Physics of Solids*, **94**, 453–472
- [207] Han, X, Gao, J, Fleming, M, Chenghai, X, Xie, W, Meng, S, Liu, WK. (2020) Efficient multiscale modeling for woven composites based on self-consistent clustering analysis. *Comput Methods Appl Mech Eng*, **364**: 112929.
- [208] Han X, Huang K, Zheng T, Zhou J, Liu H, Li Z, Zhang L, Guo L. (2025) An ANN-based concurrent multiscale damage evolution model for hierarchical fiber-reinforced composites *Compos. Science Technol.*, **259**: 110910
- [209] Harandi A, Moeineddin A, Kaliske M, Reese S. (2024) Mixed formulation of physics-informed neural networks for thermo-mechanically coupled systems and heterogeneous domains. *Int J Numer Methods Eng*, **125**: e7388
- [210] Harper LT, Qian C, Turner TA, Li S, Warrior NA (2012) Representative volume elements for discontinuous carbon fiber composites—Part 2 Determining the critical size. *Compos. Sci. Technol.*, **72**:204–210
- [211] Hashin Z (1991a) Thermoelastic properties of particulate composites with imperfect interface. *J Mech Phys Solids*, **39**:745–762
- [212] Hashin Z (1991b) The spherical inclusion with imperfect interface. *J. Appl. Mech.*, **58**:444–449
- [213] Hashin Z (2002) Thin interphase imperfect interface in elasticity with application to coated fiber composites. *J. Mech. Phys. Solids.*, **50**:2509—2537
- [214] He, C, Gao, J, Li, H, Ge, J, Chen, Y, Liu, J, Fang, D. A (2020) data-driven self-consistent clustering analysis for the progressive damage behavior of 3D braided composites. *Compos Struct* **249**: 112471.

- [215] He LH, Li ZR (2006) Impact of surface stress on stress concentration *Int. J. Solids Struct.*, **43**:6208–6219
- [216] Hill R (1963) Elastic properties of reinforced solids: some theoretical principles. *J Mech Phys Solids*, 11:357–372
- [217] Hill, R. (1965) A self-consistent mechanics of composite materials. *J. Mech. Phys. Solids* **13**, 212–222
- [218] Hobbs M, Rappel H, Dodwell T. (2024) A probabilistic peridynamic framework with an application to the study of the statistical size effect. *Applied Math. Modelling*, **128**, 137–153
- [219] Hori M, Kubo J (1998) Analysis of probabilistic distribution and range of average stress in each phase of heterogeneous materials. *J Mech Phys Solids*, **46**:537–556
- [220] Hsiao GC, Wendland WL (2008) *Boundary Integral Equations*. Springer-Verlag, Berlin
- [221] Hu H, Qi L, Chao X. (2024) Physics-informed Neural Networks (PINN) for computational solid mechanics: Numerical frameworks and applications Author links open overlay panel. *Thin-Walled Structures*: 112495
- [222] Hu, W., Ha, Y.D., Bobaru, F., (2010) *Numerical integration in peridynamics*, Tech. Rep., University of Nebraska-Lincoln
- [223] Hu W, Ha YD, Bobaru F (2011) Modeling dynamic fracture and damage in a fiber-reinforced composite lamina with peridynamics. *Int J Multiscale Comput Eng.* 9: 707–726
- [224] Hu, W., Ha, Y.D., Bobaru, F. (2012a) Peridynamic model for dynamic fracture in unidirectional fiber-reinforced composites. *Comput. Methods Appl. Mech. Engrg.*, **217**—**220**, 247—261.
- [225] Hu, W., Ha, Y.D., Bobaru, F., Silling, S.A., (2012b) The formulation and computation of the nonlocal J-integral in bond-based peridynamics. *Int. J. Fract.*, **176**, 195–206.
- [226] Hu Y-L, Yu Y, Wang H (2014) Peridynamic analytical method for progressive damage in notched composite laminates. *Composite Structures*, 108: 801—810
- [227] Hu YL, Wang JY, Madenci E, Mu Z, Yu Y. (2022) Peridynamic micromechanical model for damage mechanisms in composites. *Composite Structures*, **301**, 116182
- [228] Hu Z, Daryakenari NA, Shen Q, Kawaguchi K, Karniadakis GE. (2024) State-space models are accurate and efficient neural operators for dynamical systems. *arXiv:2409.03231*
- [229] Huang JH, Furuhashi R, Mura T (1993) Frictional sliding inclusions. *J Mech Phys Solids*, **41**:247–265
- [230] Huang O, Saha S, Guo J, Liu WK. (2023) An introduction to kernel and operator learning methods for homogenization by self-consistent clustering analysis *Computational Mechanics*, **72**, 195–219
- [231] Hütter G (2017) Homogenization of a Cauchy continuum towards a micromorphic continuum. *J. Mech. Phys. Solid.* **99**:394–408
- [232] Ibach H (1997) The role of surface stress in reconstruction, epitaxial growth and stabilization of mesoscopic structures. *Surf Sci Rep*, **29**(5-6):193–263
- [233] Isakari S, Asakura T, Haraguchi Y, Yano Y, Kakami A. (2017) Performance evaluation and thermography of solid-propellant microthrusters with laser-based throttling. *Aerospace Science Technology*, **71**: 99–108.
- [234] Isiet M, Mišković I, Mišković S. (2021) Review of peridynamic modeling of material failure and damage due to impact. *Int. J. Impact Engng*, **147**, 103740
- [235] Izadi R, Das R, Fantuzzi N, Trovalusci P. (2024) Fracture properties of green nanofibrous network with random and aligned fiber distribution: a hierarchical molecular dynamics and peridynamics approach. -Available at SSRN, 4790967

- [236] Jafarzadeh S, Mousavi M, Larios A, Bobaru F (2022) A general and fast convolution-based method for peridynamics: Applications to elasticity and brittle fracture. *Comp. Meth. Appl. Mech. Enging*, **392**: 114666
- [237] Jafarzadeh S, Mousavi M, Wang L, Bobaru F. (2024) PeriFast/Dynamics: A MATLAB code for explicit fast convolution-based peridynamic analysis of deformation and fracture. *Journal of Peridynamics and Nonlocal Modeling*, **6**, 33–61
- [238] Jafarzadeh S, Silling S, Liu N, Zhang Z, Yu Y. (2024) Peridynamic neural operators: a data-driven nonlocal constitutive model for complex material responses. *arXiv preprint arXiv:2401.06070*
- [239] Jafarzadeh S, Silling S, Zhang L, Ross C, Lee CH, Rahman SM, Wang S, Yu Y. (2024) Heterogeneous peridynamic neural operators: discover biotissue constitutive law and microstructure from digital image correlation measurements. *ArXiv preprint arXiv:2403.18597*.
- [240] Javili A, Morasata R, Oterkus E (2019) Peridynamics review. *Mathematics Mechanics of Solids*, **24**: 3714–3739
- [241] Jenabidehkordi A, Abadi R, Rabczuk T. (2020) Computational modeling of meso-scale fracture in polymer matrix composites employing peridynamics *Composite Structures*, **253**, 112740
- [242] Jin H, Zhang E, Espinosa HD. (2023) Recent advances and applications of machine learning in experimental solid mechanics: A review *Appl. Mech. Rev.*, **75**(6): 061001 (24 pages)
- [243] Jirasek M, Rolshoven S (2003) Comparison of integral-type nonlocal plasticity models for strain-softening materials. *Int. Engng Science* **41**:1553–1602.
- [244] Ju JW, Tseng KH (1992) A three-dimensional micromechanical theory for brittle solids with interacting microcracks. *Int J Damage Mech*, **1**:102–131
- [245] Ju JW, Tseng KH (1995) Improved two-dimensional micromechanical theory for brittle solids with randomly located interacting microcracks. *Int. J. Damage Mechanics* **4**:23–57
- [246] Kachanov M, Sevostianov I (2018) *Micromechanics of materials, with applications*. Springer International. Cham
- [247] Kafka OL, Yu C, Shakoor M, Liu Z, Wagner GJ, Liu WK. (2018) Data-driven mechanistic modeling of the influence of microstructure on high-cycle fatigue life of nickel-titanium. *JOM*: 1–5.
- [248] Kanaun SK (1977) Self-consistent field approximation for an elastic composite medium. *Zhurnal Prikladnoi i Tehnich Fiziki*, **18**(2):160–169 (In Russian. Engl Transl. *J Appl Mech Techn Phys*, **18**:274–282)
- [249] Kanaun SK, Levin VM (1994) Effective field method on mechanics of matrix composite materials. In: Markov KZ (ed), *Advances in Math Modelling of Composite Materials*. World Scientific, Singapore, 1–58
- [250] Kanaun KK, Levin VM (2008) *Self-Consistent Methods for Composites*. Vol. 1, 2, Springer, Dordrecht
- [251] Kanit T, Forest S, Galliet I, Mounoury V, Jeulin D (2003) Determination of the size of the representative volume element for random composites: statistical and numerical approach. *Int J Solids Struct*, **40**:3647–3679
- [252] Karniadakis GE, Kevrekidis IG, Lu L, Perdikaris P, Wang S, Yang L. (2021) Physics-informed machine learning. *Nature Reviews Physics*, <https://doi.org/10.1038/s42254-021-00314-5>
- [253] Khoroshun, L.P., 1978. Random functions theory in problems on the macroscopic characteristics of microinhomogeneous media. *Priklad Mekh*, **14**(2), pp. 3–17 (In Russian. Engl Transl. *Soviet Appl Mech*, **14**, pp. 113–124)
- [254] Khoroshun L (1996) On a mathematical model for inhomogeneous deformation of composites. *Priklad Mekh*, **32**(5):22–29 (In Russian. Engl Transl. *Int Appl Mech*, **32**:341–348)

- [255] Khoroshun LP, Dorodnykh TI (2004) The effective piezoelectric properties of polycrystals with the trigonal symmetry. *Acta Mechan*, **169**:203–219
- [256] Kilic B (2008) *Peridynamic theory for progressive failure prediction in homogeneous and heterogeneous materials*. Ph.D. Thesis, Dep. Mechan. Engng, The University of Arizona, 1–262
- [257] Kilic B, Madenci E (2010) Peridynamic theory for thermomechanical analysis. *IEEE Trans Adv Packag*, **33**: 97–105
- [258] Kilic B, Madenci E. (2010) An adaptive dynamic relaxation method for quasi-static simulations using the peridynamic theory. *Theor. Applied Fract. Mech.* **53**(3), 194–204.
- [259] Kim D, Lee J. (2024) A review of physics informed neural networks for multiscale analysis and inverse problems. *Multiscale Science and Engineering*, **6**: 1–11
- [260] Kingma DP, Ba J (2014) Adam: A method for stochastic optimization. *arXiv:1412.6980*
- [261] Kleinert H (1989) *Gauge Fields in Condensed Matter*, vol. 2. World Scientific, ISBN 9971-50-210-0
- [262] Kouznetsova VG, Brekelmans WAM, Baaijens FPT (2001) An approach to micro-macro modeling of heterogeneous materials, *Comput. Mech.* **27**: 37–48
- [263] Kouznetsova V, Geers M, Brekelmans W. (2004) Size of a representative volume element in a second-order computational homogenization framework. *Int. J. Multiscale Comput. Eng.*, **2**: 575–598
- [264] Kouznetsova V, Geers M, Brekelmans W. (2004) Multi-scale second-order computational homogenization of multi-phase materials: a nested finite element solution strategy. **Comput. Methods Appl. Mech. Eng.**, **193**: 5525–5550
- [265] Kröner E (1967) Elasticity theory of materials with long-range cohesive forces. *Int J Solid Struct*, **3**:731–742
- [266] Kröner E (1968) Interrelations between various branches of continuum mechanics. In Kröner, E. (Ed.) *Mechanics of generalized continua*. Springer-Verlag, Berlin/Heidelberg, 330–340
- [267] Kröner E (1970) The problem of non-locality in the mechanics of solids Review of present status. In Simmons J, de Wit R, Bullough R (Eds.), *Fundamental Aspects of Dislocation Theory*. Nat. Bur. Stand. (US), Washington, **II**:729–736
- [268] Kröner E (1974) On the physics and mathematics of self-stresses. In Zeman, J.L. and Ziegler, F. *Topics in Applied Continuum Mechanics*. Springer-Verlag, Wien, 22–38
- [269] Kröner E (1986) Statistical modeling. In: Gittus J, Zarka J (eds), *Modeling Small Deformations of Polycrystals*. Elsevier, London/NY, 229–291.
- [270] Kröner E, Datta BK (1966) Nichtlokal Elastostatik Ableitung aus der Gittertheorie. *Z. Phys.*, **196**:203–211
- [271] Kröner E, Datta BK (1970) Non-local theory of elasticity for a finite inhomogeneous medium—a derivation from lattice theory. In: Simmons J, de Wit R, Bullough R (eds), *Fundamental Aspects of Dislocation Theory*. Nat Bur Stand (US), Washington, 737–746
- [272] Krumhansl JA (1965) Generalized continuum field representation for lattice vibrations. In Wallis, R. F. (Ed.) *Lattice dynamics*. Pergamon, London, 627–634
- [273] Kumasaka H, Hirashima K-I (1996) Stress distributions around circular inclusion in infinite plane for nonlocal elasticity (Matrix and circular inclusion have the same nonlocal coefficients). *JSME Int. Journal*, **A39**:192–196
- [274] Kunin IA (1966) Theory of elasticity with spatial dispersion. One-dimensional complex structure. *Prikl. Mat. Mekh.*, **30**:866–874 (In Russian. Engl Transl. *J. Appl. Mathematics and Mechanics* **30**:1025–1034)

- [275] Kunin IA (1967) Inhomogeneous elastic medium with nonlocal interaction. *Zhurn. Prikl. Mekhan. Tekhn. Fiziki*, **8**:60–66 (In Russian. Engl Transl. *J. Appl. Mech. Techn. Phys.*, **8**:41–44)
- [276] Kunin IA (1983) *Elastic Media with Microstructure*. Springer-Verlag, Berlin, **2**
- [277] Kunin IA (1984) On foundations of the theory of elastic media with microstructure *Int J Solids Struct*, **22**:969–978
- [278] Kunin IA, Waisman AM (1970) On problems of the non-local theory of elasticity. In: Simmons J, de Wit R, Bullough R (eds) *Fundamental Aspects of Dislocation Theory*. Nat Bur Stand (US), Washington, 747–757
- [279] Kushch V (2020) *Micromechanics of Composites Multipole Expansion Approach*. Amsterdam Butterworth-Heinemann.
- [280] Kupradze VD, Aleksidze MA (1964) The method of functional equations for the approximate solution of certain boundary value problems. *Z. Vychisl Matemat Fiz.*, **4**:683–715
- [281] Kröner E. (1967) Elasticity theory of materials with long range cohesive forces. *Int. J. Solids Struct.* **3**, 731–742
- [282] Kumara H, Yadav N. (2023) Deep learning algorithms for solving differential equations: a survey. *J. Experimental & Theoret. Artificial Intelligence*: <https://doi.org/10.1080/0952813X.2023.212356>
- [283] Lahellec N, Michel J C, Moulinec H., Suquet P (2003) Analysis of inhomogeneous materials at large strains using fast Fourier transforms. *IUTAM Symposium on Computational Mechanics of Solid Materials at Large Strains* (Berlin: Springer) pp. 247–58
- [284] Lam D, Yang F, Chong A, Wang J, Tong P (2003). Experiments and theory in strain gradient elasticity. *J. Mech. Phys. Solids.*, **51**:1477–1508
- [285] Lanthaler S, Li Z, Stuart AM. (2024) Nonlocal and nonlinearity imply universality in operator learning. arXiv:2304.13221v2
- [286] Laurien M, Javili A, Steinmann P.(2023) Peridynamic modeling of nonlocal degrading interfaces in composites. *Forces in Mechanics*, **10**: 100124.
- [287] Lax M (1952) Multiple scattering of waves II. The effective fields dense systems. *Phys. Rev.* **85**: 621–629.
- [288] Lazar M, Agiasofitou E, Po G (2020) Three-dimensional nonlocal anisotropic elasticity a generalized continuum theory of Ångström-mechanics *Acta Mechanica*, **231**:743–781
- [289] Lazar M, Po G (2018) On Mindlin’s isotropic strain gradient elasticity Green tensors, regularization, and operator-split. *J. Micromech. Molecular Physics*, **3**:1840008 (39 pages)
- [290] Le, B., Yvonnet, J., and He, Q.-C., “Computational homogenization of nonlinear elastic materials using neural networks,” *Intern. J.r Num. Methods Engng*, **104**: 1061–1084
- [291] Le QV, Chan WK, Schwartz J. (2014) A two-dimensional ordinary, state-based peridynamic model for linearly elastic solids. *Int. J. Numerical Methods Engng* **98**, 547–561.
- [292] Lee J, Han M (2020) Three-dimensional volume integral equation method for solving isotropic/anisotropic inhomogeneity problems *Mathematics*, **8**:1866 (26 pages)
- [293] Lefik M, Boso D, Schrefler B. (2009) Artificial neural networks in numerical modeling of composites. *Comput. Meth. Appl. Mechanics Engng*, **198**, No. 21-26: 1785–1804
- [294] Lehoucq RB, Silling SA (2008) Force flux and the peridynamic stress tensor. *J. Mech. Phys. Solids*, **56**: 1566—1577.

- [295] Levin VM, Valdiviezo-Mijangos O, Sabina GJ (2011) Propagation of electroacoustic axial shear waves in a piezoelectric medium reinforced by continuous fibers. *Int. J. Engng Science*, **49**:1232–1243.
- [296] Li F, Yang X, Gao W, Liu W. (2023) A single-layer peridynamic model for failure analysis of composite laminates. *Materials Today Communications*, **37**, 106988
- [297] Li H, Kafka OL, Gao J, Yu C, Nie Y, Zhang L, Tajdari M, Tang S, Guo X, *et al.* (2019) Clustering discretization methods for generation of material performance databases in machine learning and design optimization. *Comput Mech*, **64**: 281–305.
- [298] Li, J., Li, S., Lai, X., Liu, L. (2022) Peridynamic stress is the static first Piola–Kirchhoff Virial stress. *Int. J. Solids and Structures*, **241**, 111478.
- [299] Li J, Wang Q, Li X, Ju L, Zhang Y. (2022) Homogenization of periodic microstructure based on representative volume element using improved bond-based peridynamics *Engng Analysis Boundary Elements*, **143**: 152–162
- [300] Li JY (2000) Magneto-electroelastic multi-inclusion and inhomogeneity problems and their applications in composite materials. *Int J Engng Sci*, **38**:1993–2011
- [301] Li JY (2004) The effective pyroelectric and thermal expansion coefficients of ferroelectric ceramics. *Mechan Mater* **36**:949-958
- [302] Li JY, Dunn ML (1999) Analysis of microstructural fields in heterogeneous piezoelectric solids. *Int J Engng Sci*, **37**:665–685
- [303] Li M, Wang B, Hu J, Li G, Ding P, Ji C. (2024) Artificial neural network-based homogenization model for predicting multiscale thermo-mechanical properties of woven composites *Int. J. Solids Struct.*, **301**: 112965
- [304] Li S, Jin Y, Huang X, Zhai L. (2020) An extended bond-based peridynamic approach for analysis on fracture in brittle materials. *Math. Problems Engineering*, ID 9568015, 1–12.
- [305] Li X, Gu X, Xia X, Madenci E, Chen X, Zhang Q. (2022) Effect of water-cement ratio and size on tensile damage in hardened cement paste: Insight from peridynamic simulations. *Construction Building Materials*, **356**: 129256
- [306] Li Z, Kovachki N, Azzadenesheli K, Liu B, Bhattacharya K, Stuart A, Anandkumar, A. (2003) Neural operator: Graph kernel network for partial differential equations, arXiv preprint arXiv:2003.03485.
- [307] Liang X, Wang L, Xu J, Wang J. (2021) The boundary element method of peridynamics *Int. J. Numerical Methods Engng*, **122**, 5558–5593.
- [308] Lin Z, Gu E, Huang S, Wang L. (2025) An Efficient PINN-Based Calibration Method for Mesoscale Peridynamic Concrete Models *Structural Control and Health Monitoring*. <https://doi.org/10.1155/stc/6641629>: 6641629, 15 pages
- [309] Littlewood DJ, Parks ML, Foster JT, Mitchell JA. (2024) The Peridigm mesh-free peridynamics code *J. Peridynamics Nonlocal Modeling*, **6**, 118–148
- [310] Littlewood, D.J., Silling, S.A., Mitchell, J.A., Seleson, P.D., Bond, S.D., Parks, M.L., Turner, D.Z., Burnett, D.J., Ostien, J., Gunzburger, M. (2015) *Strong local-nonlocal coupling for integrated fracture modeling*. Technical report SAND2015-7998, Sandia National Laboratories, Albuquerque, NM.
- [311] Liu M, Li H, Zhou, Zhang H, Huang G. (2024) Development of machine learning methods for mechanical problems associated with fibre composite materials: A review. *Composites Commun.* tenbf 49: 101988
- [312] Liu W, Hong J-W. (2012) Discretized peridynamics for brittle and ductile solids. *Int. J. Numer. Meth. Engng*, **89**: 1028–1046
- [313] Liu X, Tian S, Tao F, Du H, Yu W. (2020) How machine learning can help the design and analysis of composite materials and structures? arXiv preprint arXiv:2010.09438

- [314] Liu YL, Mukherjee S, Nishimura N, Schanz M, Ye W, Sutradhar A, Pan E, Dumont NA, Frangi A, Saez A. (2011) Recent advances and emerging applications of the boundary element method. *Applied Mechanics Reviews*, **64**, 031001 (38 pages)
- [315] Liu Z, Bessa MA, Liu WK (2016) Self-consistent clustering analysis: an efficient multi-scale scheme for inelastic heterogeneous materials. *Comput Methods Appl Mech Eng.*, **306**: 319–41.
- [316] Liu Z, Kafka OL, Yu C, Liu WK. (2018) Data-driven self-consistent clustering analysis of heterogeneous materials with crystal plasticity. In: *Advances in Computational Plasticity*, 221–242.
- [317] Liu, Z., Wei, H., Huang, T., and Wu, C. (2020) Intelligent multiscale simulation based on process-guided composite database. *arXiv preprint arXiv:2003.09491*
- [318] Lu J, Nie Y. (2022) A reduced-order fast reproducing kernel collocation method for nonlocal models with inhomogeneous volume constraints. *Computers & Mathematics Applications*. **121**: 52–61.
- [319] Lu J, Yang M, Nie Y. (2022) Convergence analysis of Jacobi spectral collocation methods for weakly singular nonlocal diffusion equations with volume constraints. *Applied Mathematics Computation*. **431**: 127345.
- [320] Luciano R, Willis JR (2001) Non-local effective relations for fibre-reinforced composites loaded by configuration-dependent body forces. *J Mech Phys Solids*, **49**:2705–2717
- [321] Ma H, Hu G, Wei Y, Liang L (2018) Inclusion problem in second gradient elasticity. *Int. J. Engineering Science*, **132**:60–78
- [322] Macek RW, Silling SA (2007) Peridynamics via finite element analysis *Finite Elements in Analysis and Design*, **43**: 1169–1178
- [323] Madenci E, Barut A, Futch M. (2016) Peridynamic differential operator and its applications. *Comput. Methods Appl. Mech. Engrg.* **304**, 408–451
- [324] Madenci E, Barut A, Phan ND (2017) Peridynamic unit cell homogenization, 58th AIAA/ASCE/AHS/ASC Structures, Structural Dynamics, and Materials Conference, AIAA SciTech Forum, (AIAA 2017-1138)
- [325] Madenci E, Barut A, Phan N. (2018) Peridynamic unit cell homogenization for thermoelastic properties of heterogeneous microstructures with defects. *Composite Structures*, **188**: 104-115.
- [326] Madenci E, Dorduncu M, Gu X. (2019) Peridynamic least squares minimization. *Comput. Methods Appl. Mech. Engrg.*, **348**, 846–874.
- [327] Madenci E, Guven I. (2015) *The Finite Element Method and Applications in Engineering Using ANSYS*. Springer, NY
- [328] Madenci E, Oterkus E (2014) *Peridynamic Theory and Its Applications*. Springer, NY
- [329] Madenci E, Oterkus S (2016) Ordinary state-based peridynamics for plastic deformation according to von Mises yield criteria with isotropic hardening. *J. Mech. Phys. Solids*, **86**: 192–219
- [330] Madenci E, Yaghoobi A, Barut A, Phan N (2021) Peridynamic modeling of compression after impact damage in composite laminates. *J Peridyn Nonlocal Model*, **3**: 327–347
- [331] Madenci E, Yaghoobi A, Barut A, Phan N (2023) Peridynamics for failure prediction in variable angle tow composites *Archive of Applied Mechanics*, **93**: 93–107
- [332] Malyarenko A, Ostoja-Starzewski M. (2019) *Tensor-Valued Random Fields for Continuum Physics*, Cambridge University Press, Cambridge, UK
- [333] Maranganti R, Sharma P (2007) Strain field calculation in embedded quantum dots and wires. *J. Comput. Theoret. Nanoscience*, **4**:715–738

- [334] Matouš K, Geers MGD, Kouznetsova VG, Gillman A (2017) A review of predictive nonlinear theories for multiscale modeling of heterogeneous materials. *J. Comput. Physics*, **330**: 192–220
- [335] Maugin GA (1988) *Continuum Mechanics of Electromagnetic Solids*. North-Holland, Amsterdam
- [336] Maugin GA (1998) On the structure of the theory of polar elasticity. *Philos. Trans. R. Soc. Lond.*, **A356**:1367–1395
- [337] Maugin GA (2017) *Non-Classical Continuum Mechanics. A Dictionary*. Springer Nature, Singapore
- [338] Maxwell JC (1873) *A Treatise on Electricity and Magnetism*, Dover, New York (1954). (Republication of 3rd edition of 1892.)
- [339] Mehrmashhadi J, Chen Z, Zhao J, Bobaru F. (2019) A stochastically homogenized peridynamic model for intertidally fracture in fiber-reinforced composites *Composites Science Technology*, **182**: 107770
- [340] Mengesha T, Du Q. (2014) The bond-based peridynamic system with Dirichlet-type volume constraint. *Proc. R. Soc. Edinburgh*, **A 144**: 161–186
- [341] McCoy JJ (1979) On the calculation of bulk properties of heterogeneous materials. *Q Appl Math*, **36**:137–149
- [342] Mikata Y (2012) Analytical solutions of peristatic and peridynamic problems for a 1D infinite rod. *Int. J. Solids and Structures*, **49**: 2887–2897
- [343] Mikata Y (2023) Analytical solutions of peristatics and peridynamics for 3D isotropic materials. *Eur J Mech A/Solids*, **101**: 104978
- [344] Miehe C, Koch A (2002) Computational micro-to-macro transition of discretized microstructures undergoing small strain. *Arch. Appl. Mech.* **72**: 300–317
- [345] Miller RE, Shenoy VB (2000) Size-dependent elastic properties of nanosized structural elements. *Nanotechnology*, **11**:139–147
- [346] Mindlin RD (1964) Micro-structure in linear elasticity. *Arch. Rational Mech. Anal.*, **16**:51–78
- [347] Mindlin RD, Eshel NN (1968) On the first strain gradient theories in linear elasticity. *Int. J. Solids Structures*, **4**:109–124
- [348] Mitchell JA (2011) A nonlocal, ordinary, state-based plasticity model for peridynamics. *Sandia National Laboratories*, Albuquerque SAND2011-3166.
- [349] Moës N., Belytschko T. (2002) Extended finite element method for cohesive crack growth *Engineering Fracture Mechanics*, **69**: 813–833
- [350] Mori T, Tanaka K. (1973) Average stress in matrix and average elastic energy of materials with misfitting inclusions. *Acta Metall.* **21**: 571–574
- [351] Mousavi F, Jafarzadeh S, Bobaru F (2021) An ordinary state-based peridynamic elastoplastic 2D model consistent with J2 plasticity. *Int. J. Solids Structures*, **229**, 111146
- [352] Moumen AE, Kanit T, Imad A (2021) Numerical evaluation of the representative volume element for random composites. *European Journal of Mechanics / A Solids*, **86**:104181
- [353] Mukherjee S, Liu Y (2013) The boundary element method *Int. J. Computational Meth.*, **10**:1350037 (91 pages).
- [354] Mura T. (1987) *Micromechanics of Defects in Solids (Mechanics of Elastic and Inelastic Solids)* 2nd edn Berlin: Springer
- [355] Nemat-Nasser S, Hori M (1993) *Micromechanics: Overall Properties of Heterogeneous Materials*. Elsevier, North-Holland.
- [356] Needleman A (1990) An analysis of decohesion along an imperfect interface. *Int. J. Fract.*, **42**:21–40

- [357] Ning L, Cai Z, Dong H, Liu Y, Wang W. (2023) A peridynamic-informed neural network for continuum elastic displacement characterization *Comput. Methods Appl. Mech. Engrg.*, **407**: 115909
- [358] Nguyen CT, Oterkus S, Oterkus E (2021) An energy-based peridynamic model for fatigue cracking *Engineering Fracture Mechanics*, **241**: 107373
- [359] Nowak M, Mulewska K, Azarov A, Ustrzycka A, *et al.* (2023) A peridynamic elastoplastic damage model for ion-irradiated materials. *Int. J. Mechanical Sciences* **237**: 107806.
- [360] O'Brian RW (1979) A method for the calculation of the effective transport properties of suspensions of interacting particles. *J Fluid Mech*, **91**: 17–39
- [361] Ongaro G, Bertani R, Galvanetto U, Pontefisso A, Zaccariotto M. (2022) A multiscale peridynamic framework for modeling mechanical properties of polymer-based nanocomposites. *Engng Fract. Mechanics*, **274**: 108751
- [362] Ongaro G, Seleson P, Galvanetto U, Ni T, Zaccariotto M. (2021) Overall equilibrium in the coupling of peridynamics and classical continuum mechanics *Comput. Meth. Appl. Mech. Engrng*, **381**: 113515
- [363] Ongaro G, Shojaei A, Mossaiby F, Hermann A, Cyron CJ, Trovalusci P. (2023) Multi-adaptive spatial discretization of bond-based peridynamics. *Int J Fract*, **244**: 1–24
- [364] Ortiz M, Pandolfi A (1999) Finite-deformation irreversible cohesive element for three-dimensional crack-propagation analysis. *Int. J. Numer. Methods Eng.*, **44**:1267–1282
- [365] Ostoja-Starzewski M, Kale S, Karimi P, Malyarenko A, Raghavan B, Ranganathan SI, Zhang J (2016) Scaling to RVE in random media. *tenit Adv. Appl. Mech.*, **49**:111–211
- [366] Oterkus E, Oterkus S. (2024) Recent advances in peridynamic theory: A review *AIMS Materials Science*, **11**: 515–546
- [367] Othmani Y, Delannay L, Doghri I (2011) Equivalent inclusion solution adapted to particle debonding with a non-linear cohesive law. *Int. J. Solids Struct.*, **48**:3326–3335
- [368] Oterkus, S., Madenci, E., Agwai, A. (2014). Fully coupled peridynamic thermomechanics. *J. Mech. Phys. Solids*, **64**: 1–23.
- [369] Pan Y, Wu P, Fan S, Peng X, Chen Z. (2024) Peridynamic simulation of fatigue crack growth in porous materials. *Engng Fracture Mech.*, **300**: 109984.
- [370] Parks ML, Seleson P, Plimpton SJ, Silling SA, Lehoucq RB. (2011) *Peridynamics with LAMMPS: A user guide v0.3 beta*, SAND Report 2011–8523, Sandia National Laboratories, Albuquerque, NM, and Livermore, CA
- [371] Parnell WJ. (2016) The Eshelby, Hill, moment and concentration tensors for ellipsoidal inhomogeneities in the Newtonian potential problem and linear elastostatics *J Elast*, **125**: 231–294.
- [372] Parton VZ, Kudryavtsev BA (1988) *Electromagnetic Elasticity of Piezoelectric and Electrically Conductive Bodies*. Nauka, Moscow
- [373] Paszke A, Gross S, Massa F et al (2019) PyTorch: an imperative style, high-performance deep learning library. *Adv Neural Inf Process Syst*, **32**:8024–8035
- [374] Po G, Admal NG, Lazar M (2019) The Green tensor of Mindlin's anisotropic first strain gradient elasticity *Materials Theory*, **3** 3 (16 pages)
- [375] Polizzotto C (2001) Nonlocal elasticity and related variational principles. *Int. J. Solids Structures*, **38**:7359–7380
- [376] Polizzotto C (2015) A unifying variational framework for stress gradient and strain gradient elasticity theories. *European Journal of Mechanics, A/Solids*, **49**:430–440
- [377] Ponte Castañeda P, Suquet P (1998) Nonlinear composites. *Adv. Appl. Mech.*, **34**: 171–302

- [378] Povstenko YZ (1993) Theoretical investigation of phenomena caused by heterogeneous surface tension in solids. *J. Mech. Phys. Solids*, **41**:1499–1514
- [379] Qi J, Li C, Tie Y, Zheng Y, Cui Z, Duan Y. (2024) A peridynamic-based homogenization method to compute effective properties of periodic microstructure *Computational Particle Mechanics*. <https://doi.org/10.1007/s40571-023-00698-4>
- [380] Qin Q, Yang Q-S (2008) *Macro-Micro Theory on Multifield Coupling Behavior of Heterogeneous Materials*. Springer, Berlin
- [381] Quintanilla J, Torquato S (1997) Microstructure functions for a model of statistically inhomogeneous random media. *Phys Rev*, **E55**: 1558–1565
- [382] Raissi M, Perdikaris P, Karniadakis GE. (2019) Physics-informed neural networks: A deep learning framework for solving forward and inverse problems involving nonlinear partial differential equations. *J. Comput. Phys.*, **378**: 686–707
- [383] Rayleigh L. (1892) On the influence of obstacles arranged in rectangular order upon the properties of a medium. *Philosophical Magazine*, **34**: 481–502.
- [384] Ren, B., Wu, C., Askari, E. (2017) A 3D discontinuous Galerkin finite element method with the bond-based peridynamics model for dynamic brittle failure analysis. *International Journal of Impact Engineering*, **99**: 14–25
- [385] Ren B, Wu CT, Seleson S, Zeng D, Nishi M, Pasetto M (2022) An FEM-Based Peridynamic Model for Failure Analysis of Unidirectional Fiber-Reinforced Laminates *J. Peridynamics and Nonlocal Modeling*, **4**: 139–158
- [386] Ren H, Zhuang X, Rabczuk T. (2017) Dual-horizon peridynamics: A stable solution to varying horizons *Comput. Methods Appl. Mech. Engrg.*, **318**, 762–782
- [387] Ren X, Lyu X. (2024) Mixed form-based physics-informed neural networks for performance evaluation of two-phase random materials *Engng Appl. Artificial Intelligence*, **127**: 107250
- [388] Rogula D (1982) Nonlocal theory of material media. *CISM Courses and Lectures*, **268**. Springer-Verlag, Vienna, New York
- [389] Sab K, Legoll F, Forest S (2016). Stress gradient elasticity theory existence and uniqueness of solution. *J. Elast.*, **123**:179–201
- [390] Sab K, Nedjar B (2005) Periodization of random media and representative volume element size for linear composites. *C R Mecanique*, **333**:187–195
- [391] Sarego G, Le QV, Bobaru F, Zaccariotto M, Galvanetto U. (2016) Linearized state-based peridynamics for 2-D problems *Int. J. Numer. Meth. Engng*, **108**: 1174–1197
- [392] Saroukhani S, Vafadari R, Andersson R, Larsson F, Runesson K (2015) On statistical strain and stress energy bounds from homogenization and virtual testing. *Europ. J. Mechanics A/Solids*, **51**:77–95
- [393] Scabbia F, Zaccariotto M, Galvanetto U. (2023) A new surface node method to accurately model the mechanical behavior of the boundary in 3D state-based peridynamics. *J. Peridyn. Nonloc. Modeling*, **5**: 521–555
- [394] Scabbia F, Zaccariotto M, Galvanetto U. (2023) Accurate computation of partial volumes in 3D peridynamics *Engng with Computers*, **39**: 959–991
- [395] Scabbia F, Zaccariotto M, Galvanetto U. (2024) A general ordinary state-based peridynamic formulation for anisotropic materials. *Comput. Methods Appl. Mech. Engrg.* **427**: 117059
- [396] Scott JM, Mengesha T. (2020) Asymptotic analysis of a coupled system of non-local equations with oscillatory coefficients *Multiscale Modeling & Simulation*, **18**: 1137/19M1288085
- [397] Sejnoha, M, Zeman, J. *Micromechanics in Practice*. Southampton, UK: WIT Press, 2013.

- [398] Seleson P, Du Q, Parks M. (2016) On the consistency between nearest-neighbor peridynamic discretizations and discretized classical elasticity models. *Comp. Meth. Applied Mech. Engrg.*, **11**, 698–722. 2016.
- [399] Seleson P, Gunzburger M, Parks ML (2013) Interface problems in nonlocal diffusion and sharp transitions between local and nonlocal domains. *Comput. Methods Appl. Mech. Engrg.*, **266**: 185-204
- [400] Seleson P, Littlewood DJ. (2016) Convergence studies in mesh-free peridynamic simulations. *Comput. Mathematics with Applications*, **71**: 2432–2448
- [401] Seleson P, Parks ML. (2011) On the role of the influence function in the peridynamic theory. *Int. J. Multiscale Comput. Eng.*, **9**: 689–706
- [402] Seleson P, Pasetto M, John J, Trageser J, Reeve ST. (2024) PDMATLAB2D: A peridynamics MATLAB two-dimensional code. *J. Peridyn. Nonl. Modeling*, **6**:149–205
- [403] Selvaraj J, Said BE. (2023) Multiscale modeling of strongly heterogeneous materials using geometry-informed clustering *Int. J. Solids Struct.*, **280**: 112369
- [404] Sevostianov I, Mogilevskaya SC, Kushch VI (2019) Maxwell’s methodology of estimating effective properties Alive and well. *Int. J. Engineering Science*, **140**:35–88
- [405] Shaat M, Ghavanloob E, Fazlzadehb SA (2020) Review on nonlocal continuum mechanics Physics, material applicability, and mathematics. *Mechanics of Materials*, **150**:103587
- [406] Sharma A, Mukhopadhyay T, Rangappa SM, Siengchin S, Kushvaha V. (2022) Advances in computational intelligence of polymer composite materials: machine learning assisted modeling, analysis and design *Archives Comput. Methods Engrg.*, **29**, 3341–3385
- [407] Sharma P, Dasgupta A (2002) Average elastic field and scale-dependent overall properties of heterogeneous micropolar materials containing spherical and cylindrical inhomogeneities. *Phys. Rev.*, **B 66**:224110, 1–10
- [408] Sharma P, Ganti S (2004) Size-dependent Eshelby-s tensor for embedded nano-inclusions incorporating surface/interface energies. *J Appl Mech*, **71**:663–671
- [409] Sharma, P. and Wheeler, L.T, (2007) Size-dependent elastic state of ellipsoidal nano-inclusions incorporating surface/interface tension. *J. Applied Mechanics*, **74**:447–454
- [410] Shenoy VB (2002) Size-dependent rigidities of nanosized torsional elements. *Int. J. Solids Struct.*, **39**:4039–4052
- [411] Shermergor TD. (1977) *The Theory of Elasticity of Microinhomogeneous Media*. Nauka, Moscow (In Russian)
- [412] Shermergor TD, Yakovlev VB (1993) Concentration of coupled electrical mechanical fields on a crystallite surface in textured quartz. *Izv Acad Sci Russ Phys Solid Earth*, (English edition) **2**:89–94
- [413] Silling S. (2000) Reformulation of elasticity theory for discontinuities and long-range forces. *J. Mech. Physics of Solids* **48**: 175–209
- [414] Silling S. (2010) Linearized theory of peridynamic states. *Journal of Elasticity*, **99**: 85–111
- [415] Silling .S (2011) A coarsening method for linear peridynamics. *Int. J. Multiscale Computational Engrg*, **9**: 609–622
- [416] Silling, S.A. 2014. Origin and effect of nonlocality in a composite. *J. Mechanics of Materials and Structures*, **9**, 245–258.
- [417] Silling S. (2020) Propagation of a stress pulse in a heterogeneous elastic bar. *Sandia Report SAND2020-8197*, Sandia National Laboratories.
- [418] Silling SA, Askari E. (2005) A meshfree method based on the peridynamic model of solid mechanics. *Comput. Struct.* **83**: 1526–153

- [419] Silling SA, Epton M, Weckner O, Xu J, Askari E (2007) Peridynamic states and constitutive modeling. *J. Elasticity*, **88**: 151–184
- [420] Silling SA, D’Elia M, Yu Y, You H, Fermen-Coker M. (2023) Peridynamic model for single-layer graphene obtained from coarse-grained bond forces. *J. Perid. Nonlocal Modeling*, **5**: 183–204.
- [421] Silling SA, Jafarzadeh S, Yu Y. (2024) Peridynamic models for random media found by coarse-graining *J. Peridynamics and Nonlocal Modeling*, **6**
- [422] Silling SA, Lehoucq RB. (2008) Convergence of peridynamics to classical elasticity theory, *J. Elasticity*, **93**: 13–37.
- [423] Silling SA, Lehoucq RB. (2010) Peridynamic theory of solid mechanics. *Adv. Appl. Mech.*, **44**: 73–168
- [424] Silling SA, Zimmermann M, Abeyaratne R (2003) Deformation of a peridynamic bar. *J. Elasticity*, **73**: 173–190.
- [425] Smyshlyaev VP, Cherednichenko KD (2000) A rigorous derivation of strain gradient effects in the overall behavior of periodic heterogeneous media. *J Mech Phys Solids*, **48**:1325–1357
- [426] Smyshlyaev VP, Fleck NA (1994) Bounds and estimates for linear composites with strain gradient effects. *J Mech Phys Solids*, **42** 1851–1882
- [427] Sobczyk K, Trebicki J, Movchan AB (2007) Characterization of random microstructural stresses and fracture estimation *European Journal of Mechanics-A/Solids*, **26**:573–591
- [428] Solyaev Y, Lurie S, Ustenko A (2020) On the relations between direct and energy-based homogenization approaches in second gradient elasticity. In Abali BE, Giorgio I (Eds.) *Developments and Novel Approaches in Biomechanics and Metamaterials*, Springer Nature, Switzerland AG, 443–457
- [429] Song Y, Li S, Li Y. (2023) Peridynamic modeling and simulation of thermo mechanical fracture in inhomogeneous ice. *Engineering with Computers*, **39**: 575–606
- [430] Steigmann DJ, Ogden RW (1999) Elastic surface-substrate interactions. *Proc. R. Soc. Lond.*, **A455**, 437–474
- [431] Steinbach O (2008) *Numerical Approximation Methods for Elliptic Boundary Value Problems. Finite and Boundary Elements*. Springer, NY
- [432] Sun W, Fish J (2021) Coupling of non-ordinary state-based peridynamics and finite element method for fracture propagation in saturated porous media. *Int J Numer Anal Methods Geomech.*, **45**: 1260–1281
- [433] Sun W, Fish J, Zhang G (2020) Superposition of non-ordinary state-based peridynamics and finite element method for material failure simulations. *Meccanica*, **55**: 681–699
- [434] Talamadupula KK, Povolny SJ, Prakash N, Seidel GD. (2020) Mesoscale strain and damage sensing in nanocomposite bonded energetic materials under low-velocity impact with frictional heating via peridynamics. *Modelling Simul. Mater. Sci. Eng.* **28**: 085011
- [435] Tan H, Huang Y, Liu C, Inglis HM, Ravichandran G, Geubelle PH (2007) The uniaxial tension of particle-reinforced composite materials with nonlinear interface debonding. *Int. J. Solids Struct.* **44**:1809–1822
- [436] Tan H, Huang Y, Liu C, Ravichandran G, Paulino GH (2007) Constitutive behaviors of composites with interface debonding the extended Mori–Tanaka method for uniaxial tension. *Int. J. Fract.*, **146**:139–148
- [437] Tang, S, Zhang, L, Liu, WK. From virtual clustering analysis to self-consistent clustering analysis: a mathematical study. *Comput Mech.* 2018; **62**: 1443–1460.
- [438] Temizer I, Wu T, Wriggers P (2013) On the optimality of the window method in computational homogenization. *Int. J. Eng. Sci.*, **64**:66–73

- [439] Terada K, Kikuchi N (2001) A class of general algorithms for multi-scale analyses of heterogeneous media, *Comput. Methods Appl. Mech. Eng.* **190**: 5247—5464
- [440] Tian H. (2024) Tensor-involved peridynamics: A unified framework for isotropic and anisotropic materials. *arXiv:2410.10175v2*
- [441] Tian, X., Du, Q. (2015) Nonconforming discontinuous Galerkin methods for nonlocal variational problems. *SIAM Journal on Numerical Analysis*, **53**, 762–781.
- [442] Torquato, S. 2002. *Random Heterogeneous Materials: Microstructure and Macroscopic Properties*. Springer-Verlag, New York, Berlin.
- [443] Tran VP (2016) *Modélisation à plusieurs échelles d'un milieu continu hétérogène aléatoire*. PhD Thesis. Université Paris-Est, Paris
- [444] Tran VP, Brisard S, Guilleminot J, Sab, K (2018) Mori–Tanaka estimates of the effective elastic properties of stress-gradient composites *Int. J. Solids Structures*, **146**:55–68
- [445] Trovalusci P (2014) Molecular approaches for multifield continua origins and current developments. In: T. Sadowsky and P. Trovalusci, editors, *Multiscale Modeling of Complex Materials phenomenological, theoretical and computational aspects*, **556** CISM Courses and Lectures, 211–278. Springer, Berlin
- [446] Voyiadjis GZ (Ed.) (2019) *Handbook of Nonlocal Continuum Mechanics for Materials and Structures*. Springer, NY
- [447] Voyiadjis GZ, Song CR (2020) *Gradient-enhanced Continuum Plasticity*. Elsevier, Amsterdam
- [448] Wang H, Wu L, Guo J, Yu C, Li Y, Wu Y. (2024) Three-dimensional modeling and analysis of anisotropic materials with quasi-static deformation and dynamic fracture in non-ordinary state-based peridynamics. *Appl. Math. Model.*, **125**: 625–648
- [449] Wang H, Wu L, Huang D, Chen J, Guo J, Yu C, Li Y, Wu Y. (2024) A machine-learning-based peridynamic surrogate model for characterizing deformation and failure of materials and structures *Engineering with Computers*, <https://doi.org/10.1007/s00366-024-02014-x>
- [450] Wang J, Huang Z, Duan H, Yu S, Feng X, Wang G, Zhang W, Wang T (2011) Surface stress effect of nanostructured materials. *Acta Mechanica Sinica*, **24**:53–82
- [451] Wang L, Xu J, Wang J. (2017) Static and dynamic Green's functions in peridynamics. *J. Elasticity*, **126**: 95–125
- [452] Wang L, Xu J, Wang J, Karihaloo BL. (2020) Nonlocal thermo-elastic constitutive relation of fibre-reinforced composites. *Acta Mechanica Sinica*, **36**: 176–187
- [453] Wang QZ, Hu YL, Yu Y, Wu D, Yao ZY. (2024) A peridynamic differential operator modeling approach for ceramic matrix composite microstructure with uniform or non-uniform discretization. *Compos. Struct.* **344**: 118282
- [454] Wang X, Yin Z-Y. (2024) Interpretable physics-encoded finite element network to handle concentration features and multi-material heterogeneity in hyperelasticity. *Comput. Meth. Applied Mech. Engng*, **431**: 117268
- [455] Wang Y, Wu W. (2023) A bond-level energy-based peridynamics for mixed-mode fracture in rocks. *Comput. Methods Appl. Mech. Engrg.*, **414**: 116169
- [456] Wang Y, Zhou X, Wang Y, Shou Y. (2018) A 3-D conjugated bond-pair-based peridynamic formulation for initiation and propagation of cracks in brittle solids *Int. J. Solids Structures*, **134**: 89–115
- [457] Weckner O, Abeyaratne R (2005) The effect of long-range forces on the dynamics of a bar. *J. Mech. Physics of Solids* **53**: 705–728
- [458] Weckner O, Brunk G, Epton MA, Silling SA, Askari E. (2009) Green's functions in nonlocal three-dimensional linear elasticity. *Proc. R. Soc.*, **A 465**: 3463–3487

- [459] Weckner O, Emmrich E. 2005 Numerical simulation of the dynamics of a non-local, inhomogeneous, infinite bar. *J. Comp. Appl. Mech.*, **6**, 311–319
- [460] Wen Z, Hou C, Zhao M, Wan X. (2023) A peridynamic model for non-Fourier heat transfer in orthotropic plate with uninsulated cracks. *Applied Mathematical Modelling*, **115**: 706–723
- [461] Weng GJ (1992) Explicit evaluation of Willis' bounds with ellipsoidal inclusions *Int. J. Engng Science*, **30**: 83–92
- [462] Wildman RA, O'Grady JT, Gazonas GA. (2017) A hybrid multiscale finite element/peridynamics method. *Int J Fract.*, **207**: 41–53
- [463] Willis JR (1977) Variational and related methods for the overall properties and selfconsistent estimates for the overall properties. *J Mech Phys Solids*, **25**, 85–202
- [464] Willis JR. (1980) A polarization approach to the scattering of elastic waves – I. Scattering by a single inclusion. II. Multiple scattering from inclusions. *J. Mech. Physics of Solids*, **28**, 287–327.
- [465] Willis JR. (1981) Variational and related methods for the overall properties of composites. *Advances in Applied Mechanics*, **21**: 1–78
- [466] Wu P, Chen Z. (2023) Peridynamic electromechanical modeling of damaging and cracking in conductive composites: A stochastically homogenized approach *Composite Structures*, **305**: 116528
- [467] Wu P, Yang F, Chen Z, Bobaru F. (2021) Stochastically homogenized peridynamic model for dynamic fracture analysis of concrete. *Eng Fract Mech*, 107863.
- [468] Xia, W., Galadima, Y.K., Oterkus, E. and Oterkus, S., 2019, Representative volume element homogenization of a composite material by using bond-based peridynamics *J. Compos. Biodegradable Polymers*, **7**: 51-56.
- [469] Xia W, Oterkus E, Oterkus S. (2020) Peridynamic modeling of periodic microstructured materials. *Procedia Structural Integrity*, **28**: 820–828
- [470] Xia W, Oterkus E, Oterkus S. (2021) 3-dimensional bond-based peridynamic representative volume element homogenization. *Physical Mesomechanics*, **24**: 45-51.
- [471] Xia W, Oterkus E, Oterkus S. (2021) Ordinary state-based peridynamic homogenization of periodic micro-structured materials *Theoret. Applied Fract. Mech.*, **113**, 102960.
- [472] Xu J, Askari A, Weckner O, Silling SA (2008) Peridynamic analysis of impact damage in composite laminates. *J. Aerospace Engineering*, **21**: 187–194
- [473] Xu J, Yang Z, Wang Z, Wang X, Li Y, Zhang J. (2024) Peridynamic simulation for the damage patterns of glass considering the influence of rate-dependence and pre-defects. *Engng Fracture Mechanics*, **291**: 109539
- [474] Xu X, D'Elia M, Foster JT (2021) A machine-learning framework for peridynamic material models with physical constraints. *Computer Meth Appl. Mech. Engng* **386**: 114062
- [475] Xu X, Foster JT. (2020) Deriving peridynamic influence functions for one-dimensional elastic materials with periodic microstructure. *J. Peridyn. Nonlocal Modeling*, **2**: 337–351
- [476] Xun F, Hu G, Huang Z (2004) Effective in plane moduli of composites with a micropolar matrix and coated fibers *Int. J. Solids Structures*, **41**:247–265
- [477] Yang C, Zhu F, Zhao J. (2024) A multi-horizon fully coupled thermo-mechanical peridynamics *J. Mech. Phys. Solids*, **191**: 105758
- [478] Yang X, Gao W, Liu W, Zhang X. (2024) Coupling four-parameters bond-based peridynamic and finite elements for damage analysis of composite structures *Theor. Appl. Fracture Mech.*, **129**: 104230
- [479] Yang Y, Ragnvaldsen O, Bai Y, Yi M, Xu BX. (2019) 3D non-isothermal phase-field simulation of microstructure evolution during selective laser sintering. *Npj Comput Mater*, **5**: 81 (12 pages).

- [480] Yang Z, Shen S, Guan X, He X, Cui J. (2024) Multiscale analysis-based peridynamic simulation of fracture in porous media. *Front. Struct. Civ. Eng.* **18**: 1–13
- [481] Yang Z, Zheng S, Han F, Cui, J. (2023) An efficient peridynamics-based statistical multiscale method for fracture in composite structures. *Int. J. Mech. Sciences*, **259**: 108611
- [482] Yang Z, Zheng S, Han F, Guand X, Zhange J. (2023) An adaptive coupling approach of local and non-local micromechanics *J. Comput. Physics*, **489**, 112277
- [483] Yilbas, B.S. (2013) *Laser Drilling-Practical Applications*. Springer: Heidelberg, Germany.
- [484] Yin B, Huang J, Sun W. (2024) Peridynamics-fueled convolutional neural network for predicting mechanical constitutive behaviors of fiber reinforced composites *Comp. Meth. Applied Mech. Engng*, **431**: 117309
- [485] You H, Xu X, Yu Y, Silling S, D’Elia M, Foster J. (2023) Towards a unified nonlocal, peridynamics framework for the coarse-graining of molecular dynamics data with fractures. *Applied Mathematics Mechanics*, **44**: 1125–1150.
- [486] You H, Yu Y, Silling S, D’Elia M (2020) Data-driven learning of nonlocal models: from high-fidelity simulations to constitutive laws. *arXiv:2012.04157*
- [487] You H, Yu Y, Silling S, D’Eliac M. (2022) A data-driven peridynamic continuum model for upscaling molecular dynamics. *Comput. Meth. Appl. Mechanics Engng.*, **389**: 114400.
- [488] You H, Yu Y, Silling S, D’Eliac M. (2024) Nonlocal operator learning for homogenized models: from high-fidelity simulations to constitutive laws. *J. Peridynamics Nonlocal Modeling*, <https://doi.org/10.1007/s42102-024-00119-x>
- [489] You H, Yu Y, Trask N, Gulian M, D’Elia M (2021) Data-driven learning of robust nonlocal physics from high-fidelity synthetic data. *Computer Methods Applied Mech. Engineering*, **374**: 113553
- [490] You H, Zhang Q, Ross C, Lee C-H, Hsu M-C, Yu Y. (2022) A physics-guided neural operator learning approach to model biological tissues from digital image correlation measurements. *J. Biomechanical Engng*, **144**, 121012
- [491] You H, Zhang Q, Ross CJ, Lee CH, Yu Y. (2022) Learning deep implicit Fourier neural operators (IFNOs) with applications to heterogeneous material modeling *Com.r Meth. Appl. Mech. Engng.*, **398**: 115296
- [492] Yu C, Kafka OL, Liu WK. (2019) Self-consistent clustering analysis for multiscale modeling at finite strains. *Comput Methods Appl Mech Eng.*, **349**: 339–359
- [493] Yu X-L, Zhou X-P. (2024) A nonlocal energy-informed neural network for peridynamic correspondence material models. *Engng Anal. Boundary Elements*, **160**, 273–297
- [494] Yu X-L, Zhou X-P. (2024) A nonlocal energy-informed neural network based on peridynamics for elastic solids with discontinuities *Computational Mechanics*, **73**: 233–255
- [495] Yu Y, Bargas FF, You H, Parks ML, Bittencourt ML, Karniadakis GE. (2018) A partitioned coupling framework for peridynamics and classical theory: analysis and simulations. *Comput. Meth. Appl. Mech. Engineering*, **340**: 905–931
- [496] Zaccariotto M, Mudric T, Tomasi D, Shojaei A, Galvanetto U. (2018) Coupling of FEM meshes with peridynamic grids. *Comput. Meth. Applied Mech. Engineering*, **330**: 471–497.
- [497] Zaoui A. (2002) Continuum micromechanics: survey. *J. Engng Mech., ASCE*, **128**: 808–816
- [498] Zhan JM, Yao XH, Zhang XQ. (2021) Study on predicting the mechanical properties and fracturing behaviors of particle reinforced metal matrix composites by non-local approach. *Mech. Materials*, **155**: 103790

- [499] Zhang J, Han F, Yang Z, Cui J. (2023) Coupling of an atomistic model and bond-based peridynamic model using an extended Arlequin framework. *Comput. Meth. Appl. Mech. Engineering*, **403**: 115663.
- [500] Zhang L, Tang, S, Yu C, Zhu X, Liu WK. (2019) Fast calculation of interaction tensors in clustering-based homogenization. *Comput Mech*, **64**: 351–364.
- [501] Zhang S, Nie Y. (2023) Localized Chebyshev and MLS collocation methods for solving 2D steady state nonlocal diffusion and peridynamic equations. *Math. Computers in Simulation*. **206**: 264–285
- [502] Zhang X, Gunzburger M, Ju L. (2016a) Nodal-type collocation methods for hypersingular integral equations and nonlocal diffusion problems. *Comput. Meth. Appl. Mech. Engrg.*, **299**: 401–420
- [503] Zhang X, Gunzburger M, Ju L. (2016b) Quadrature rules for finite element approximations of 1D nonlocal problems. *J. Comp. Phys.*, **310**: 213–236.
- [504] Zhang X, Sharma P (2005) Inclusions and inhomogeneities in strain gradient elasticity with couple stresses and related problems. *Int. J. Solids Struct.* **42**:3833–3851
- [505] Zhang Y, Qiao P. (2021) A fully-discrete peridynamic modeling approach for tensile fracture of fiber-reinforced cementitious composites. *Eng Fract Mech*, **242**: 107454
- [506] Zhao S, Zhang Q, Miao Y, Zhang W, Zhao X, Xu W. (2024) Sub-homogeneous peridynamic model for fracture and failure analysis of roadway surrounding rock. *Computer Modeling Engineering & Sciences*, **139**: no. 3
- [507] Zheng Q-S, Zhao Z-H (2004) Green's function and Eshelby's fields in couple-stress elasticity *Int. J. Multiscale Comput. Engrg.* **2**:15–27
- [508] Zhong J, Han F, Du Z, Guo X. (2024) Multi-time-step coupling of peridynamics and classical continuum mechanics for dynamic brittle fracture *Engng Fract. Mechanics*, **307**: 110264
- [509] Zhong Z, Meguid SA (1997) On the elastic field of a spherical inhomogeneity with an imperfectly bonded interface. *J. Elast.*, **46**:91–113
- [510] Zhou K, Hoh HJ, Wang X, Keer LM, Pang JHL, Song B, Wang QJ. (2013) A review of recent works on inclusions *Mechanics of Materials*, **60**: 144–158.
- [511] Zhou S, Li A, Wang B (2016) A reformulation of constitutive relations in the strain gradient elasticity theory for isotropic materials. *Int. J. Solids Struct.*, **80**:28–37
- [512] Zhou XP, Wang YT. (2021) State-of-the-art review on the progressive failure characteristics of geomaterials in peridynamic theory. *J. Eng. Mech.*, **147**: 03120001
- [513] Zhou X-P, Yu X-L. (2024) Transfer learning enhanced nonlocal energy-informed neural network for quasi-static fracture in rock-like materials. *Comput. Methods Appl. Mech. Engrg.* <https://doi.org/10.1016/j.cma.2024.117226>
- [514] Zohdi TI, Wriggers P. (2008) *Introduction to Computational Micromechanics*. Berlin: Springer.